Topographic Control of Order-Disorder Phase Transitions in a Quasi-2D Granular System

James Downs

University of Nottingham

A thesis submitted for the degree of

Doctor of Philosophy

March 2023

Abstract

The focus of current research in two-dimensional phase transitions has shifted towards non-equilibrium systems such as active matter and fluid dynamics. However, unlike in equilibrium systems, we lack a complete framework to describe their behaviour. Although previous work has shown that some basic concepts from statistical mechanics can be applied to non-equilibrium systems, the extent to which they can be applied remains unclear.

One intriguing problem in equilibrium systems is the two-dimensional hard-disc liquid-to-crystal phase transition. The nature of this phase transition differs from that in three-dimensions and was, until recently, a matter of much debate. Extending this debate, two-dimensional granular systems have also been studied to investigate the applicability of hard-disc model descriptions to non-equilibrium systems. Granular systems are convenient for manipulation and offer easy observations at the particle level and therefore represent an ideal test case for these investigations.

In this thesis, I present an investigation of the order-disorder phase transition in a 2D driven granular system. Previous research has shown that these systems undergo a continuous two-step phase transition. We explore a mechanism for changing the nature of this transition from continuous to first-order by introducing a triangular lattice of dimples milled into the surface. The change in phase transition behaviour, for the system we focus on for much of this thesis, enables further study of other behaviours from equilibrium physics, such as hysteresis, surface tension and wetting.

The phase behaviour of our system was studied on these dimpled surfaces for three different spacings. One of these spacings produced first-order like behaviour and was focussed on for much of the thesis.

We also investigated how changing the geometry and the inelasticity at the boundary affects the wetting of different phases. This allowed us to spatially control the coexisting liquid and solid phases. Our findings showed behaviour similar to wetting in equilibrium systems. Furthermore, I present a quantitative study confirming the first-order nature of the phase transition in this system. While doing this, I demonstrate evidence of coexistence, hysteresis and surface tension which are all ideas that are commonly associated with first-order phase transitions in equilibrium systems.

Inspired by the hydrophobic effect observed in equilibrium systems, a similar effect called the orderphobic effect was recently proposed. This is where disorder-inducing intruders placed in an ordered solid experience a force of attraction. The authors suggest that this effect should be general to any system that experiences a first-order order-disorder phase transition. Since our results showed the necessary pre-prerequisites for observing such an effect, we investigated whether such a force could be observed. Although our attempts to reproduce this effect in our non-equilibrium system were inconclusive, we believe the results are promising for future investigation.

Finally, I present a more detailed investigation into how changing the spacing of the dimpled lattice changes the nature of the transitions for a broader range of spacings. Our results indicate that different phases form depending on the lattice spacing. We also discuss how the equilibrium ideas of stability can be applied to the system using spacings that display a combination of different phases.

Acknowledgements

I've thoroughly enjoyed my time as a PhD student at The University of Nottingham. Here, I take the opportunity to thank some of the people that have helped me succeed these last four years.

First of all, I would like to thank Dr. Mike Smith for being an amazing supervisor who is always available to help me with my research. I'd also like to thank Dr. Mike Swift for useful discussions and reading over this Thesis. I must also thank Dr. James Sharp for reading my yearly reports and providing me a grilling in my vivas.

I would like to thank my parents for providing their support over the years. I can't forget my canoe polo teammates and coach for providing the elation of being two-time national champions as a welcome distraction to my studies. Thanks as well to my housemates and others for the amazing hiking, kayaking and skiing trips that have made many a memory. Finally, a massive thanks to my girlfriend Amy for her support over the last year - she has truly made it one of the happiest years of my life despite the stresses of writing a Thesis.

Thesis Outline

Chapter 1: Introduces the theory of phase transitions for three-dimensional systems and discusses theories, simulations and experiments that have attempted to apply these to two-dimensional systems. The chapter also discusses two-dimensional granular phase transitions and mechanisms to change the nature of the transition.

Chapter 2: Describes the experimental setup and methods that were used throughout the experiment.

Chapter 3: Presents the initial experiments that investigated using differently spaced dimple lattices to change the nature of the transition. Shows that the spacing with lattice spacing L to ball diameter D ratio of 1.2 was the most promising.

Chapter 4: Shows how we can use knowledge of the first-order transition to spatially control the wetting of the ordered crystal phase.

Chapter 5: Shows quantitative evidence that the liquid-solid phase transition of the $L/D = 1.2$ system is first order.

Chapter 6: My attempts at showing that the orderphobic force can be applied to non-equilibrium systems.

Chapter 7: Investigates how changing the spacing of the patterned surface used in Chapters 3-6 affects the phases that occur.

Chapter 8: Presents conclusions from my whole thesis and suggests future research directions.

Publications arising from this work

1. Downs, J., Smith, N., Mandadapu, K., Garrahan, J., and Smith, M. (2021). Topographic control of order in quasi-2d granular phase transitions. *Physical Review Letters*, 127(26):268002.

2. Smith, M. I., and Downs, J. G. (2021). Particletracker: a gui based particle tracking software. *Journal of Open Source Software*, 6(66):3611.

Table of Contents

List of Figures

Number *Page*

Chapter 1

Introduction

In my thesis, I will present investigations on what effect the surface structure has on two-dimensional phase transitions. I studied this using a model system of granular particles vibrated on a surface.

This chapter reviews some background of phase transitions and discusses a canonical system of hard discs. I will also discuss equilibrium experiments that were used to investigate the theory. Following this, I describe granular physics experiments, which through non-equilibrium steady states surprisingly reproduce the equilibrium behaviour of hard discs. Finally, I discuss experiments that investigate how changing different properties can change the nature of the transition which inspired our investigation of the role of surface structure.

1.1 Phase Transitions

Order-disorder transitions

In a liquid, the particles are disordered; there are no long-range correlations between the positions of particles. Whereas, in a solid, the particles are ordered and their positions are strongly correlated at all ranges. If a solid melts to become a liquid then it has undergone a transition from an ordered state to a disordered

state. This is an example of an order-disorder phase transition. Another example of an order-disorder phase transition is when a magnet transitions from the ordered ferromagnetic state to the disordered paramagnetic state upon an increase in temperature.

Order-disorder phase transitions can also occur in two-dimensional systems. Two-dimensional systems exist as a single layer of particles, often in the presence of a surface. Some examples of two-dimensional systems that undergo order-disorder phase transitions range from liquid-to-crystal phase transitions for sheets of electrons on the surface of liquid-He [Grimes and Adams, 1979] to the melting of a crystalline colloidal monolayer on the surface of water [Armstrong et al., 1989].

Since the discovery of graphene and its properties [Geim and Novoselov, 2007], research into 2D materials has skyrocketed. This interest is largely due to the many exciting potential applications of these materials, ranging from gas storage to supercapacitors [Rao et al., 2015]. To understand these materials and take advantage of their applications, a deeper knowledge of two-dimensional phase transitions is required.

Theory of phase transitions

The nature of the phase transition for two-dimensional particle systems is still an area of intense debate. Before I describe the competing theories and discuss the results of experiments we first need to understand the difference between a first-order and a continuous phase transition which I will introduce in this section.

Phases

When the temperature of a system changes, new phases of matter can appear, e.g. when a liquid system is heated it forms a gas. The transitions between these different phases are called phase transitions.

Firstly, what do we mean by a phase? A phase of matter is a region of material that is uniform throughout, assuming that the system is large enough that fluctuations can be ignored. That means that the physical properties, such as density or chemical composition must be the same throughout the phase. When a phase transition occurs it is accompanied by a change in the system's properties. These changes are abrupt for a first-order system. For example, when water freezes, it goes from water which can flow freely to ice which is a rigid material, whereas for continuous phase transitions, the changes are smoother. An important example is the ferromagnetic/paramagnetic phase transition above the Curie temperature where the magnetisation order parameter continuously changes to 1 as the externally applied field is increased.

A system doesn't have to contain only a single phase. More than one phase can coexist in the right conditions. One example of this is a propane bottle that one might use for camping. When the bottle is new, the propane is pressurised as a liquid which fills the bottle. As the propane is used, the high pressure forces the liquid propane out of the bottle where it becomes gas due to the lower external pressure. The pressure in the bottle is now reduced and there now exists a coexistence between propane in the liquid and gaseous form. At rest, the liquid propane fills the bottom of the bottle with the gaseous propane filling the top with a phase boundary separating the two phases. Anyone who has ever shaken a bottle of propane to estimate how much is left has experienced this first-hand.

Thermodynamic potential

It is useful to describe phase transitions in terms of a thermodynamic potential. The thermodynamic potential is a scalar quantity that depends on the global properties that define the thermodynamics of the system. The most stable phase of matter is the one with the lowest thermodynamic potential. If a phase's thermodynamic potential is higher than the minimum value then it is unstable and could decay into the stable phase. Different systems can be described by different thermodynamic potentials. Throughout this section, I will describe a general thermodynamic potential $\Phi(\phi)$ which depends only on a single parameter ϕ.

If $\Phi(\phi)$ of a system has only one minimum at ϕ_0 then this is the stable state. The system can lower its energy by moving ϕ towards ϕ_0. However, if $\Phi(\phi)$ has two minima, then the behaviour is more complex.

Figure 1.1 shows the thermodynamic potential $\Phi(\phi)$ at three different temperatures $T_{1,2,3}$. If we first look at $\Phi(\phi)$ for T_1 which has two minima at ϕ_1 and ϕ_2 then the minimum at ϕ_2 has a lower value of Φ than the minimum at ϕ_1, so it is the more stable state. If the system is free to change ϕ then it can lower its energy by moving ϕ towards ϕ_2, the global minimum. This is simple when the system is at a value of ϕ greater than the peak between the minima as small changes in ϕ towards ϕ_2 decrease the thermodynamic potential. However, if the system has $\phi \sim \phi_1$ then it is in the higher stable state. Small changes in ϕ towards ϕ_2 now increase the thermodynamic potential. This higher state is referred to as a metastable state as it requires a large change in ϕ to lower the thermodynamic potential.

We now need to look at what happens to $\Phi(\phi)$ as the temperature of the system evolves. At T_1 the minimum at ϕ_2 is lower. As the temperature increases through T_2 to T_3, $\Phi(\phi)$ evolves such that the lowest minimum is at ϕ_1. When the system changes from one stable minimum to another the phase changes. Phase transitions can be one of two types: a first-order phase transition where there is a discontinuity in a first derivative of Φ or a continuous transition where there is no discontinuity.

First-order

The evolution shown in Figure 1.1 is of a first-order phase transition. As the temperature increases through T_2, the system evolves abruptly between the well at ϕ_2 being the most stable to the well at ϕ_1 being more stable. As we move through T_2, it suddenly becomes more stable for the system to shift to the other state. This is accompanied by an abrupt change in the properties of the system, for example, liquid changing to a gas with an abrupt change in density.

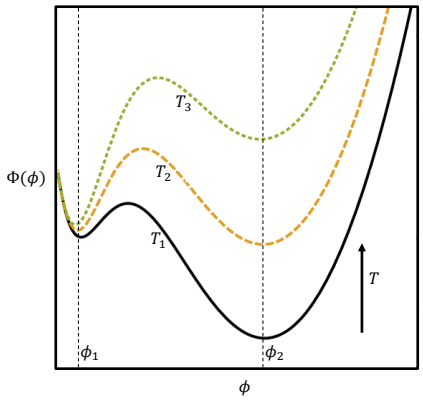

Figure 1.1: A generic thermodynamic potential Φ as a function of a control parameter ϕ at three different temperatures T_1, T_2 and T_3. ϕ_1 and ϕ_2 could represent the pressure of a liquid and gaseous phase.

If the two minima Φ_1 and Φ_2 vary with temperature at different rates then the entropy of each well is

$$S_{1,2} = -\left(\frac{\partial \Phi_{1,2}}{\partial T}\right). \tag{1.1}$$

When the system changes from one phase to another the entropy changes which gives rise to a latent heat given by

$$L_{1,2} = T_p(S_1 - S_2), \tag{1.2}$$

where T_p is the temperature of the phase transition. A simple way of considering latent heat is the energy released by a liquid as it freezes to become a solid. Latent heat is one of the characteristic properties of a first-order phase transition.

Metastability

The presence of metastable states is a characteristic property of a first-order phase transition. If we revisit Figure 1.1 and consider a system at T_1 that is in the stable state at ϕ_2, if the temperature of the system is increased rapidly to T_3 then the system will initially remain in the now metastable state at ϕ_2 despite the minimum at ϕ_1 being more stable. For the system to reach ϕ_1 it must first cross a free energy barrier. This requires thermal activation. The rate at which this happens depends on the relative size of the barrier compared to the thermal energy $k_B T$.

If the height of the barrier is given by $\Delta\Phi^*$ then the probability of a thermal fluctuation occurring that increases the thermodynamic potential by this amount is given by the Boltzmann factor which is proportional to $\exp(-\Delta\Phi^*/k_BT)$. If $\Delta\Phi^* \ll k_BT$ then the system rapidly finds its way to well 1. However, if $\Delta\Phi^* \gg k_BT$ then the metastable state can persist for a long time and appear like a stable state.

Phase coexistence

So far we've only considered global changes in ϕ to reduce the thermodynamic potential. If the value of ϕ in a system is fixed then we cannot change ϕ to lower the thermodynamic potential. Instead, the system can minimise the thermodynamic potential by separating into two-coexisting phases. The two phases with ϕ_1 and ϕ_2 divide such that the average value of ϕ is constant - this is known as the Lever rule. Consider Figure 1.2 which describes a system that has an average value of ϕ between the two minima at $\bar{\phi}$. The system can evolve to lower Φ so that a fraction of the system, a, sits in well 1 and the remainder, $(1-a)$ sits in well 2 such that the average $\bar{\phi} = a\phi_1 + (1-a)\phi_2$.

If the average value of ϕ lies between ϕ_1 and ϕ_2 then the system is unstable and can lower its thermodynamic potential by separating into two coexisting phases. This part of the line is known as the coexistence curve or the bimodal.

The ability of the system to phase separate depends on how small fluctuations in the amount of each phase change the thermodynamic potential of the system. In Figure 1.3 we look closer at the $\Phi(\phi)$ curve at T_1 from Figure 1.1. If the average value of ϕ in this system is at ϕ_b and we make a very small fluctuation along the red line then the thermodynamic potential is lowered from Φ_b to Φ'_b. As this lowering of Φ is favourable then the system is unstable to small fluctuations and will immediately phase separate. In contrast, at ϕ_a a similar fluctuation will cause the thermodynamic potential to be raised from Φ_a to Φ'_a. This unfavourable

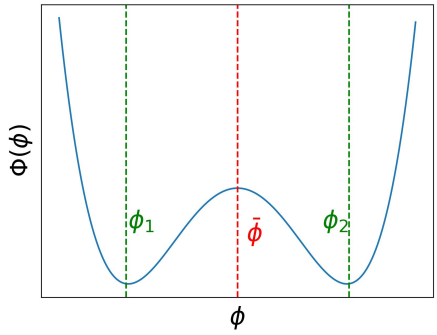

Figure 1.2: A thermodynamic potential, $\Phi(\phi)$, with two minima. If the system starts at an average value $\bar{\phi}$ then it can phase separate into two phases with $\phi = \phi_1$ and $\phi = \phi_2$ to lower the thermodynamic potential of the system.

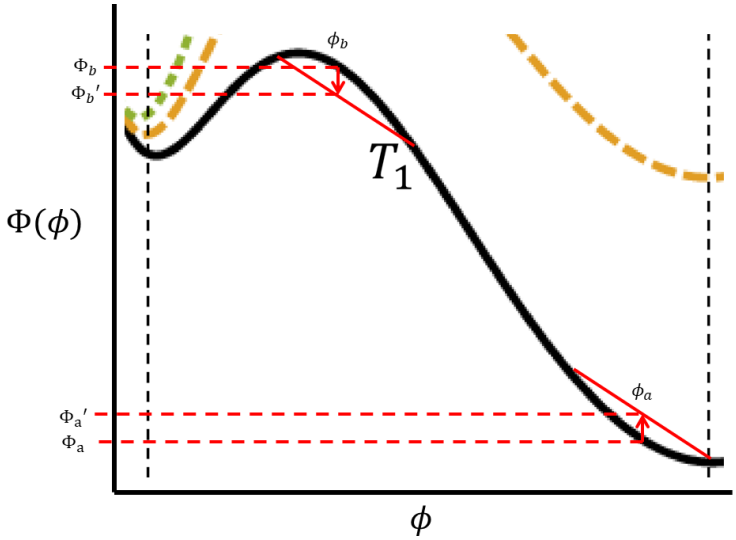

Figure 1.3: A zoomed-in portion of Figure 1.1. Shows how the free energy changes for small fluctuations in composition for points which are unstable (ϕ_b) and metastable (ϕ_a).

raising of Φ means that the system is locally stable to small fluctuations even though it is globally unstable to very large fluctuations. This means that this composition is metastable. The points along the line that are metastable are known as the spinodal.

Nucleation

If the system is quenched into a metastable state then it is stable to small fluctuations in the composition. For the system to phase separate and lower the free energy, a region of the other phase must be nucleated by a thermal fluctuation. Creating this nucleation with radius r has two effects on the free energy of the system. First, it will decrease the free energy of the system in a way proportional to its volume. Secondly, it will increase the free energy in a way proportional to its surface area due to the interfacial energy associated with its creation. This means that there is a critical radius below which these nucleations are unstable as they increase the free energy. Above the critical radius, the nucleations succeed in lowering the free energy, so are stable and can continue to grow and lower the free energy. If the energy required to create this critical nucleus is given by $\Delta\Phi^*$ then the probability of creating this nucleus can again be calculated using the Boltzmann factor by $\exp(-\Delta\Phi^*/k_BT)$.

If we take a small volume of very pure water and quickly cool it several degrees below the freezing point then the water can remain liquid - we deem it supercooled. This is because the probability to create the critical nuclei is remarkably low, so the nucleation required to drive the phase change might not happen. This type of nucleation is called homogeneous nucleation as it requires spontaneous fluctuations to nucleate the phase.

Another type of nucleation is called heterogeneous nucleation. This is where impurities in the liquid decrease the energy required to create a critical nucleus subsequently considerably increasing the probability for nucleation to occur. This is the case because the interfacial tension between the impurity and the solid phase is lower than between the liquid and solid phases which reduces the free energy penalty of creating a critical nucleus. A familiar example of this is the laser etched logo in the bottom of a lager glass which acts as a nucleation site and is designed to carefully control the amount of bubbles that form in your pint of lager.

Hysteresis

If a liquid is cooled below the solidification temperature and the solid phase has not nucleated then we can say the liquid is supercooled. It isn't until a solid is nucleated somewhere and spreads throughout the liquid that the transition occurs. If we take the system around a cycle in which the solid is heated and then cooled we would obtain two different estimates of the transition temperature. This behaviour, known as hysteresis is a characteristic of a first-order phase transition.

Continuous phase transitions

Continuous phase transitions occur when the minimum in the thermodynamic potential evolves smoothly as the temperature changes. Figure 1.4 shows that as the temperature increases from T_1 to T_2 the thermodynamic potential smoothly moves from the minimum at ϕ_1 to the minimum at ϕ_2. There isn't a point at which the minimum of the potential suddenly changes, so the properties of the system don't abruptly change at any temperature.

This means that there are a number of phenomena that exist in first-order phase transitions that don't occur for continuous phase transitions.

Firstly there is no latent heat associated with a phase transition. This is because the system's properties change continuously, so there is no jump in entropy at any given temperature.

There is also no metastability in the system. This arises due to the thermodynamic potential having only one minimum, so there is no local minimum within which a metastable state can exist. All fluctuations are unstable.

The lack of metastability also prevents the separation of the phases into coexistence. This in turn means that there is no surface tension present in a continuous phase transition.

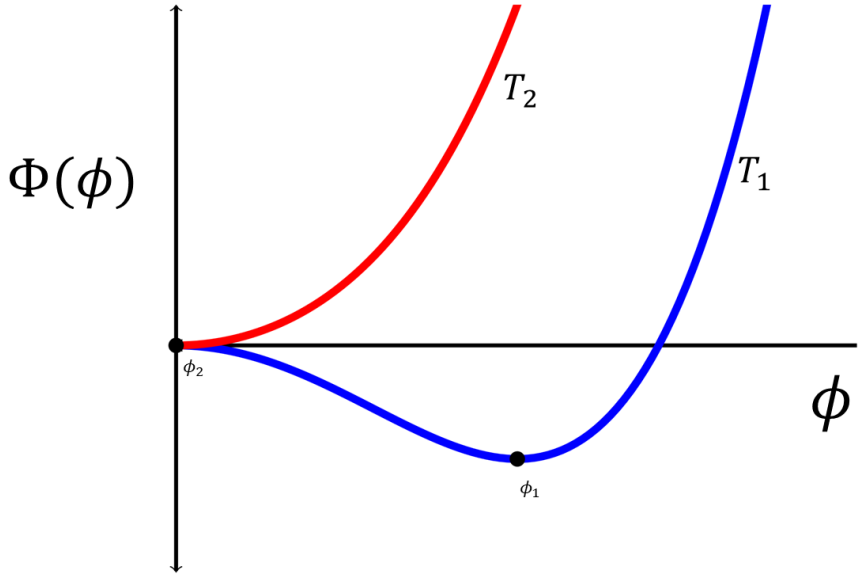

Figure 1.4: Thermodynamic potential at two temperatures for a continuous phase transition. The potential smoothly changes from the minimum at ϕ_1 being stable to the minimum at ϕ_2 being stable as the temperature increases from T_1 to T_2.

1.2 Liquid-to-crystal transition & hard spheres

The liquid-to-crystal transition in three dimensions is of fundamental importance to a wide range of applications in physics and engineering. To understand the nature of the transition theorists have used a simple model. This model strips out all the interactions between particles and the environment resulting in the so-called hard-sphere model. Hard spheres are quite simple: they interact with a potential that is zero except when the spheres overlap where the potential is infinite.

Hard sphere simulations have been shown to undergo first-order phase transitions [Alder and Wainwright, 1957] where the coexistence of liquid and solid phases was observed. However, it should be noted that temperature is not relevant in hard-sphere phase transitions. The transition between solid and liquid is driven entirely by entropy. Therefore, the phase transitions are driven by changing the packing fraction of the hard spheres - effectively changing the volume. The maximum packing fraction that can be achieved for hard spheres in 3D is 0.7404 when the spheres are packed in a close-packed structure. If, instead, the spheres are randomly packed together then the maximum packing fraction that can be achieved is ~ 0.63 [Scott and Kilgour, 1969].

It is clear that at high packing fractions, the hard spheres must be forced to take up a close-packed structure. However, it is surprising that crystals appear at packing fractions far below the values for regular or random close packing. If the transition is driven by entropy then this is surprising. Why would the close-packed crystal have higher entropy than the liquid? Surely the long-range order in a crystal reduces the entropy. It is in fact the difference between the regular and random close packing that means individual spheres in the close packing have more space locally to explore, resulting in a higher entropy.

It wasn't until later that these numerical simulations were confirmed experimentally using a system of colloidal hard spheres [Pusey and van Megen, 1986]. Their system involved a suspension of colloidal spheres which had a very short-range repulsive potential closely mimicking a hard sphere. Here the results of the 3D hard sphere model were confirmed, by the system moving from liquid to crystal through a region of coexistence as the concentration was increased. Figure 1.5a shows their system 4 days after tumbling, for increasing concentrations (labelled 2-10 from left to right). The most dilute sample (far-left) showed no observable behaviour over time which supported other work that established this should be arranged like a dense liquid. After minutes to hours, small crystallites formed homogeneously throughout samples 3-7, settling at the bottom for samples 3-5 which is representative of liquid-solid coexistence. Samples 6 and 7 remain full of small crystallites. Sample 8 crystallised heterogeneously forming much larger crystals. Samples 9 and 10 are trapped in a glassy state due to the hindered particle diffusion. Figure 1.5b shows this behaviour in a phase diagram.

This work confirms the nature of the melting transition for 3D hard spheres but the case in two dimensions remained contentious until much more recently.

1.3 Two-dimensional phase transitions

In two-dimensional particle systems, the exact nature of the melting transition has a long history, with two competing theories. The first was proposed by Kosterlitz, Thouless, Halperin, Nelson and Young (KTHNY). This theory suggests that the transition is fundamentally different to that observed in three dimensions, and

(a)

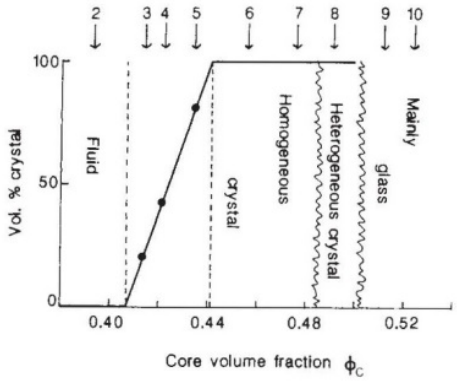

(b)

Figure 1.5: Figures from [Pusey and van Megen, 1986]. (a) Suspension of hard-sphere colloids 4 days after tumbling labelled 2-10 for increasing concentrations from left to right. (b) Phase diagram of the system shown in (a), the numbered arrows refer to the labelled images.

consists of two continuous phase transitions through an intermediate hexatic phase [Kosterlitz and Thouless, 1973, Halperin and Nelson, 1978, Young, 1979]. The second approach contains several theories that propose that the transition is first-order as in three dimensions [Hoover and Ree, 1968]. These theories, proposed between 1973 and 1985 stimulated research using simulations and experiments to understand the transition. In this section, I introduce some main competing theories and discuss the results of previous experiments and simulations.

Defining a crystal in 2D

In a two-dimensional solid, there exists (quasi)-long-range positional order and long-range orientational order. In the hexatic phase (intermediate phase between solid and liquid that will be explained shortly) there is no long-range positional order but long-range orientational order. Finally, in the liquid phase, there is no long-range positional and no long-range orientational order.

To understand this, I need to define what we mean by orientational and positional order and introduce order parameters used to describe them. The orientational order can be described by the orientational order parameter ψ_6 which is related to the angles between neighbouring particles. In a perfect crystal, one would expect the angles of all the neighbouring particles to be 60° apart. This would correspond to a perfect orientational order. The orientational order parameter is a complex vector where the magnitude defines the amount of order and its phase indicates the direction of the crystal's lattice vectors. It is calculated for particle i by

$$\psi_6^i = \frac{1}{N} \sum_{j=1}^{n} \exp i6\theta_{ij}, \tag{1.3}$$

which sums over the n nearest neighbours where θ_{ij} defines the angle between the particle i and each of its neighbours. The nearest neighbours of each particle are selected from a Delaunay triangulation (explained in more detail in Chapter 2). In the case of vacancies this method sometimes selects particles that are not nearest neighbours, so these particles are rejected using a cut-off distance. This is demonstrated in the left pane of Figure 1.6 where the red line shows the cut-off distance acting on the selected green particles.

We can also define the translational order parameter which can describe the positional order of the system. Here we consider that along some crystallographic direction, we expect particles to sit at regular intervals. So by defining a reciprocal lattice vector $\vec{G}$ we can measure how close the particle is to its expected position in that direction. Here, the magnitude of the vector has no meaning but by comparing the angles of different particles the state of the positional order of the system can be determined. It is calculated for particle j at position vector $\vec{r}_j$ by

$$\psi_T = \exp i\vec{G} \cdot \vec{r}_j. \tag{1.4}$$

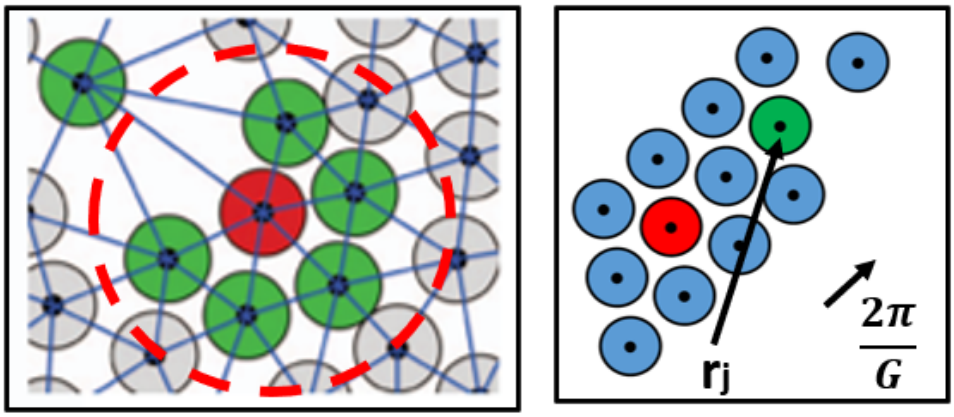

Figure 1.6: Left: representation of calculating the orientational order parameter for the red particle using its 6 green neighbours. Right: Representation of positional order for the green particle at position vector r_j. The lattice vector $2\pi/\vec{G}$ is noted.

This is demonstrated in the right pane of Figure 1.6.

KTHNY theory

Crystals have particle positions that fluctuate about fixed positions in a lattice with fixed bond angles, exhibiting both long range positional order and long range orientational order [Mermin and Wagner, 1966]. In three dimensions, increasing temperature and/or decreasing pressure causes the crystal to undergo a first order transition to become a liquid which has short range positional and orientational order. In two dimensions however, it was argued that the thermal motion of long-wavelength phonons destroys long-range order in a 2D solid [Peierls, 1935]. However, computer experiments of hard discs demonstrated a transition to a 2D ordered state which cast doubt on these results [Alder and Wainwright, 1962]. It was later proved that for Lennard-Jones power law potentials conventional crystalline long-range order in 2D is excluded, but the result was inconclusive for hard-core potentials; This is known as the Mermin-Wagner Theorem [Mermin, 1968].

This led Kosterlitz and Thouless (2016 Noble Prize winners) to develop their KT theory of melting which shows that the two-dimensional XY model melts through the dissociation of bound vortex pairs with opposite circulations [Kosterlitz and Thouless, 1973]. The KT theory was expanded for particle systems that form

triangular lattices by Halperin and Nelson and separately by Young which resulted in the complete theory being known as the KTHNY theory of two-dimensional melting [Halperin and Nelson, 1978, Young, 1979]. These particle systems are described by two different order parameters: the orientational and positional order. The two-dimensional solid is defined as having long-range orientational order but only quasi-long-range positional order - considering the restriction placed by the Mermin-Wagner theorem.

Mermin-Wagner theorem states that long-range positional order is broken up by fluctuations in the lattice. This description of long-range means that particles infinitely apart are positionally correlated. Over large finite distances, however, the particles may still be positionally correlated which is why we refer to the positional order as quasi-long-range.

In KTHNY theory the melting of the two-dimensional crystalline solid occurs in two stages. The two stages consist of the dissociation of two different topological defects, dislocations and disclinations. A topological defect refers to a localised irregularity or discontinuity in the structure or properties of a crystal structure.

A dislocation is a type of point defect which exists as a localised region of the system where the arrangement of particles is different from the region's surroundings. Specifically, in a triangular lattice, it can be considered as a missing/extra row of discs starting from the defect. The defect is defined by its Burgers vector which defines the vector which closes the path that would surround a perfect lattice. Another way of visualising a dislocation in a triangular lattice is a pair of adjacent particles which have 5 and 7 neighbours instead of 6. Figure 1.7a shows an example of a free dislocation with the annotated Burgers vector and Figure 1.7b shows a bound pair of dislocations where the Burgers vector is zero. Discs with 5 and 7 neighbours are red and blue respectively.

A disclination is when a single particle in a region of a triangular lattice has 5 or 7 neighbours instead of 6. An example of a 7 neighbour and 5 neighbour disclination can be seen in Figure 1.8

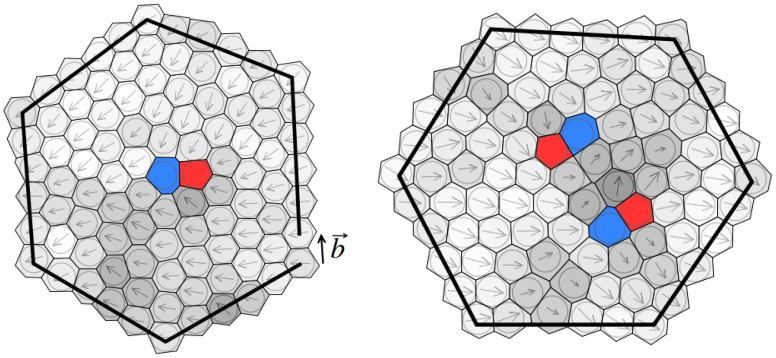

(a) (b)

Figure 1.7: Figure from [Bernard, 2011]. Dislocations in hard discs. Discs with 5 and 7 neighbours are in red and blue respectively. The arrows represent the orientational order parameter. (a) A free dislocation. A path around the defect, which would be closed in a perfect lattice, fails to close by the Burgers vector. (b) A bound pair of dislocations, a stable configuration that maintains positional order as the lattice is only locally stressed. As the system moves from the solid to the hexatic phase these bound dislocations in (b) unbind to form the free dislocations in (a).

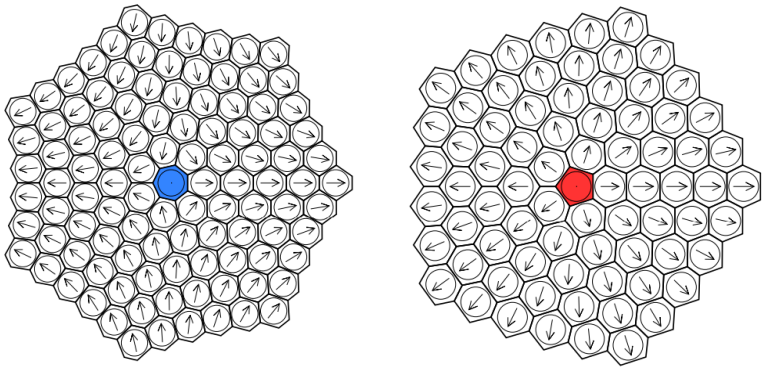

(a) (b)

Figure 1.8: Figure from [Bernard, 2011]. Disclinations in hard discs. Arrows show the local orientational order. Discs with 5 and 7 neighbours are shown in red and blue respectively. As the hexatic phase melts further to become the liquid phase free dislocations unbind to form disclinations. (a) A negative disclination where the core disc has seven neighbours. (b) A positive disclination where the core disc has 5 neighbours.

To melt the two-dimensional solid, KTHNY theory predicts two separate continuous transitions. The first involves the destruction of long-range positional order by unbinding bound dislocations (Figure 1.7b) to form free dislocations (Figure 1.7a. This leaves the system in a new phase, the hexatic phase which has quasi-long-range orientational order like a crystal , but short-range positional order like a liquid. This orientational order in the hexatic phase is then destroyed by the unbinding of free dislocations (Figure 1.7a) to form disclinations (Figure 1.8) leaving the system as a liquid with both short-range positional and orientational order.

Hard-disc evidence of two-dimensional phase transitions

The original work using molecular dynamics simulations, in 1962, by Alder and Wainwright showed evidence of a transition to a 2D ordered state in a simulation of hard discs (see Figure 1.9a) and proposed that this transition was first-order due to a loop in the density vs pressure curve as seen in Figure 1.9b [Alder and Wainwright, 1962]. This was then confirmed by Monte Carlo simulations by Hoover and Ree in 1968 [Hoover and Ree, 1968]. However, these works preceded the KTHNY theory of melting, so there was no suggestion that the transition could be continuous at the time.

After the publication of KTHNY theory, in the late 70s, there were a variety of hard disc simulations which aimed to prove whether the two-dimensional hard-disc phase transition was indeed continuous or first-order.

Initially, Monte Carlo simulations of hard discs showed evidence for first-order phase transitions by observing coexistence [Lee and Strandburg, 1992, Zollweg and Chester, 1992] and showing a lack of an intermediate hexatic phase [Weber et al., 1995]. In [Weber et al., 1995] it was claimed that the first-order phase transition for 2D hard discs was well established despite the popular KTHNY theory that opposed this conclusion. However, these small systems suffered from finite-size effects which make it difficult to distinguish between a weak first-order and a continuous transition.

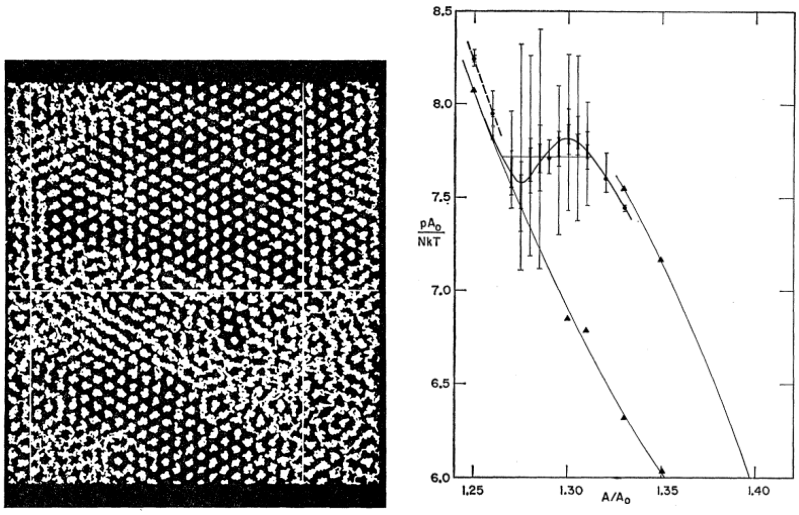

(a) (b)

Figure 1.9: Figures from [Alder and Wainwright, 1962]. (a) The traces of the centres of particles in the phase transition region showing both liquid and crystalline regions. The horizontal and vertical lines represent an arbitrary grid. (b) A plot of the reduced pressure against the reduced area. Shows a van der Waals loop which supports a first-order phase transition.

However, as simulations got larger, Monte Carlo simulations of hard discs by Jaster showed evidence of the intermediate hexatic phase and used analysis of pressure to rule out a first-order phase transition [Jaster, 2004]. Later work by Mak, showed evidence for two separate phase transitions with an intermediate hexatic phase, proving that the solid-hexatic phase transition was continuous [Mak, 2006]. One consensus that has emerged from these studies is that the 2D hard disc system is very sensitive to finite-size effects affecting the nature of the transition.

After the development of a faster Monte Carlo method [Bernard et al., 2009] Bernard et al. showed that the melting transition for 2D hard discs follows neither a first-order nor a KTHNY-like phase transition [Bernard and Krauth, 2011]. Instead, they show that the transition is a two-step transition with a continuous solid-hexatic and first-order hexatic-liquid transition. This result was later complemented by Engel et al. where they confirmed the result using three different simulation methods [Engel et al., 2013].

While the nature of the transition for two-dimensional hard discs seems to be solved, the nature of the transition can be altered through subtle changes in the inter-particle potential [Kapfer and Krauth, 2015]. This raises the question of how such theoretical understanding maps onto real-world systems.

Consequently, recent studies have explored how 2D phase transitions are influenced by factors such as polydispersity [Russo and Wilding, 2017], and interparticle potential [Kapfer and Krauth, 2015, Li and Ciamarra, 2020]. Russo et al. showed that by adding a mixture of large and small discs the hexatic phase disappeared resulting in a single first-order transition [Russo and Wilding, 2017].

Experimental studies of liquid-crystal transitions in 2D

Experiments involving equilibrium systems have played a key role in exploring the 2D liquid-to-crystal phase transition. The role of these experiments is important as it allows firstly, the confirmation of the results of simulations. They also help us to understand how the results from hard discs apply to real systems.

Many very different studies have been used to explore 2D phase transitions. One of the earliest examples was an electron-crystal to electron-liquid transition for a sheet of electrons confined at the surface of liquid helium by an electric field [Grimes and Adams, 1979]. They use an electric field to drive the electrons up and down against the He surface and determine that the electrons are in a crystal configuration when the driving causes resonance and creates standing capillary waves on the He surface. Their electron layer is an example of a nearly ideal 2D Coulomb surface as the only interaction is the repulsion between the electrons.

Monolayers of noble gases form another early example of a 2D system exhibiting a phase transition [Birgeneau et al., 1981]. These monolayers were realised by increasing the pressure of a container of noble gas in the presence of a monolayer such as graphite. As the pressure increases, the coverage of gas molecules on the substrate increases. As the coverage changes, phase transition between different adsorbed states can be observed.

These were often achieved by increasing the pressure of a noble gas in the presence of the monolayer, as the pressure increases the amount of coverage on the substrate increases and phase transitions can be observed as the pressure and therefore the monolayer coverage increases.

Several experiments have also been performed on thin liquid-crystal films [Pindak et al., 1981, Davey et al., 1984]. These systems were found to follow the KTHNY theory despite their complex phase behaviour. When the thickness of the films increases to over 4 layers the nature of the transition becomes first order [Peng et al., 2010]. However, this is stretching the description of 2D as, although it has a large aspect ratio, the system is technically 3D which is expected to be first order for hard disc systems.

Colloids were instrumental in solving the 3D hard sphere model. This proved the case again when an experiment using a quasi-two-dimensional system of colloidal hard spheres confirmed the 2D hard disc melting scenario described by [Bernard and Krauth, 2011] in which the system undergoes a first-order liquid-hexatic transition followed by a continuous hexatic-solid transition [Thorneywork et al., 2017]. They used a tilted monolayer of colloidal hard spheres in sedimentation-diffusion equilibrium to establish the phase behaviour. Figure 1.10 shows an experimental image and a schematic of their system.

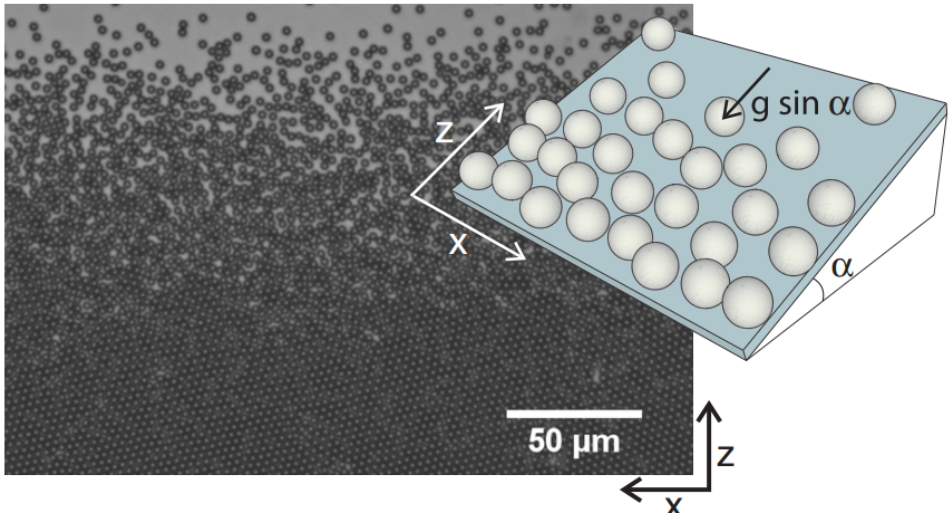

Figure 1.10: From [Thorneywork et al., 2017]. An experimental image of a 2D hard colloidal system in sedimentation-diffusion equilibrium for a tilt angle of $\alpha = 0.56°$. Inset, a schematic diagram of the experimental geometry showing the effect of tilting the sample by a small angle, α, and the resultant in-plane component of gravity.

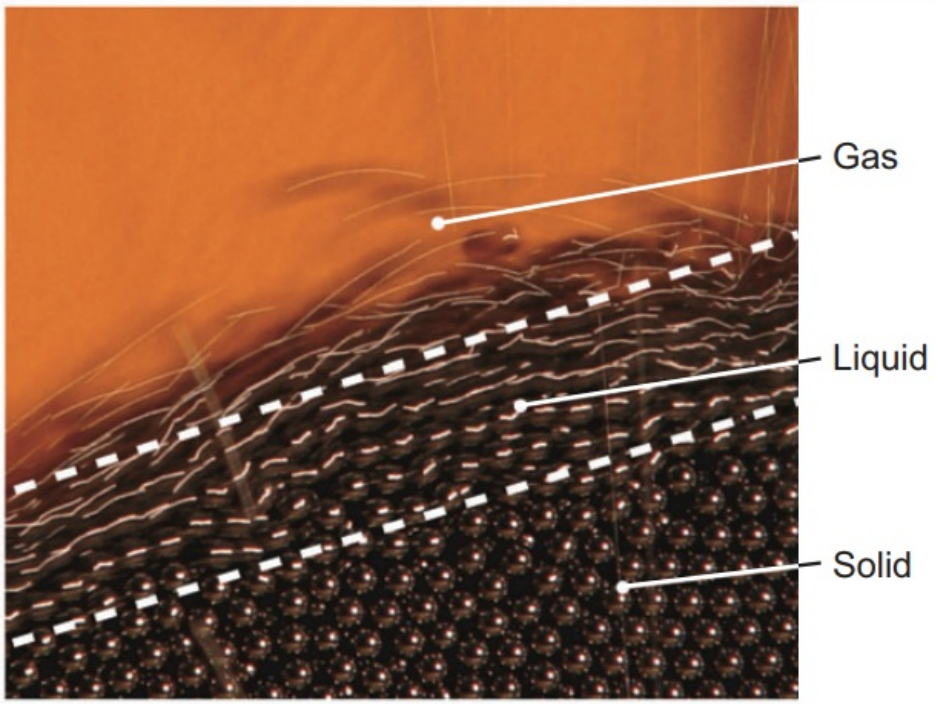

Figure 1.11: Figure from [Forterre and Pouliquen, 2008]. Solid, liquid and gas flow regimes in a tilted pile of ball bearings.

1.4 Using granular systems to study phase transitions

Granular materials are large collections of discrete macroscopic particles. The particles are large enough that they are not influenced by thermal fluctuations. Examples of granular materials range in size from small powders of various materials such as sand and snow to the largest scale such as collections of asteroids.

A simple pile of steel ball bearings can exhibit behaviour resembling the three phases of matter. When the surface below the pile of ball bearings is flat (or below the angle of repose), the material behaves like a solid and remains at rest despite the gravitational forces acting on it. When it is tilted beyond the angle of repose as can be seen in Figure 1.11 it begins to flow. The balls in the region closest to the surface do not move and behave like a solid, the balls near the top of the pile flow like a liquid and the balls that bounce above the flow act like a gas [Forterre and Pouliquen, 2008].

While granular materials can exhibit behaviour similar to the conventional equilibrium phases of matter they have some distinct differences.

Grain Size

The most obvious difference between grains and traditional molecules such as water is their size. A grain of sand, for example, is of the order 10^{18} times more massive than a water molecule. This is important as it means that the energy from thermal fluctuations is too small to have any effect.

For example, to raise a grain of sand with a mass, m of 60 µg to a height, h of 100 µm in Earth's gravity g would require $mgh = 59$ nJ of energy. If this energy were provided by temperature alone (k_BT) it would require a temperature of 4×10^{15}K. This unreasonably high temperature shows that ordinary thermodynamic descriptions cannot be used.

Conservation of Energy

Idealistic molecules, such as ideal gas molecules, undergo completely elastic collisions. Collisions between granular particles, however, are inelastic, resulting in a loss of kinetic energy.

Length scales

If we study an experiment in a 50 cm square box containing water molecules the ratio of the experiment size to the molecule size is of order 10^9. However, in a granular system of small grains with a diameter of 0.5 mm then this ratio is only of the order 10^3. This inherently means finite-size effects and system boundaries play an important role.

Grain-grain interactions

In molecular systems, the forces between molecules are typically weakly attractive at range and repulsive at their core. This long-range attractive force is important for many behaviours of typical liquids such as surface tension. Typically, in grains, these long-range forces do not exist and interactions only occur when they physically collide.

Granular steady states

One way to study the phase behaviour of granular systems is to excite the motion of the particles/grains. In this case, particles are excited by either a turbulent flow of gas [Narayan et al., 2007], moving walls [van Zon and MacKintosh, 2004], or a rough, vibrating plate [Olafsen and Urbach, 1998]. In each case, the injection of energy into the system causes the particles to move, resulting in dissipative particle-particle and particle-boundary collisions. This leads to a non-equilibrium steady state where the energy input is balanced with the energy lost from dissipation. The energy causes particles to diffuse in a manner analogous to thermal energy in molecular systems.

Quasi-two-dimensional non-equilibrium steady states can be attained by either trapping particles between a lid such that they cannot bounce over each other [Reis et al., 2006] or by carefully controlling the input energy such that gravity holds them in a single layer [Olafsen and Urbach, 1998]. The word quasi is used as the particles do move in the vertical direction but remain in a single layer. These systems provide a useful analogue of the 2D hard disc models which were previously discussed.

Granular Phase Transitions

Granular systems have been found to undergo a variety of different phase transitions. Transitions may occur as a function of the packing fraction with changes to the excitation energy provided to the particles. There are, however, some subtle features which can lead to nominally similar experiments exhibiting very different behaviour.

To illustrate this we consider the work by [Castillo et al., 2012]. They shook a quasi-2d collection of beads of diameter D in a horizontal cell. The cell has a lid which in experiment A resulted in a gap of $1.83D$ and experiment B resulted in a gap of $1.94D$. Analysis revealed that in experiment A the transition from liquid to an exotic crystal configuration was first order while in B it was continuous.

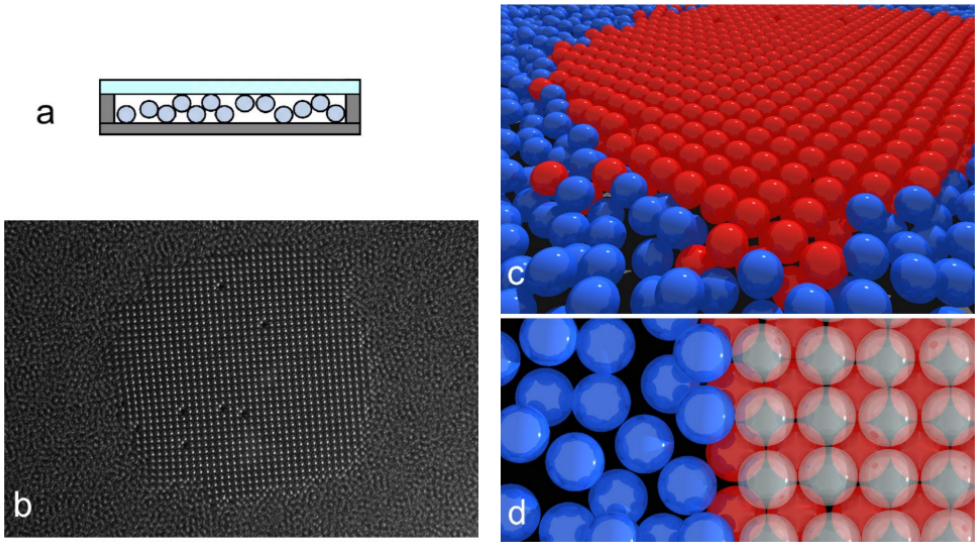

Figure 1.12: Figure from [Prevost et al., 2004]. Two-phase coexistence in the steady state of a quasi-2d collection of beads with a lid at a tightly controlled height. (a) Side view of the experimental setup. The system is shaken vertically and imaged from above. (b) Experiment: the time-averaged image of ball positions. Only the top layer of the crystal is visible. (c, d) Simulation: 3D rendering of instantaneous ball positions. In (c), balls in the crystal are coloured red, and balls in the liquid are coloured blue. In (d) a closeup of the crystal is shown with the top layer transparent.

Interestingly, the solid phase is very different to that of hard discs. In this case the solid phase forms with an increase in the excitation energy and forms as two-layer crystals with square symmetry as can be seen in a similar experiment in Figure 1.12 [Prevost et al., 2004].

The phrase ”quasi-2D” in granular physics is ubiquitously used to describe a vibrated monolayer of particles however, the definition of ”quasi” is important to avoid confusion or ambiguity. While the systems described in [Castillo et al., 2012, Prevost et al., 2004] are referred to as quasi-2d, the mechanism behind the transition relies on particles fully or partially leaving the horizontal plane of particles. Wherever the phase transition mechanism relies on the vertical motion of the particles, studies cannot be considered analogous to the 2D hard disc model.

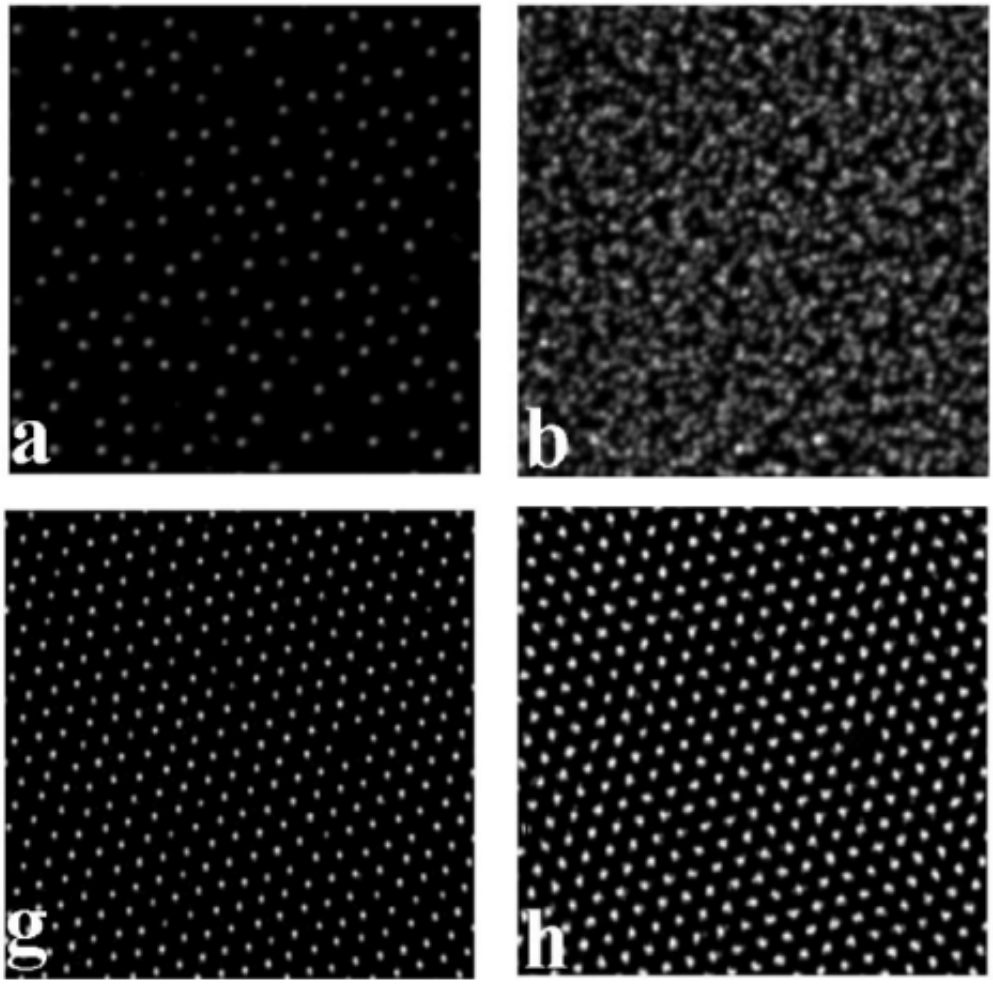

Figure 1.13: Figure edited from [Olafsen and Urbach, 1998]. Instantaneous (left column) and time-averaged (right column) photographs showing the different phases of a granular monolayer. (a, b) Shows the system in a disordered state. (g, h) Shows the system in an ordered state.

In a two-dimensional granular NESS that does not rely on the vertical motion of particles, a phase transition from states that resemble a hard-sphere liquid to an ordered state is observed as the acceleration is reduced [Olafsen and Urbach, 1998]. Their system can be seen in Figure 1.13 which shows instantaneous and time-averaged snapshots of the system in a liquid (a,b) and a solid phase (g, h).

Olafsen and Urbach then showed that the transition from a solid phase with long-range order to a liquid with only short-range order with an increase in shaking acceleration followed a continuous phase transition similar to the KTHNY scenario for hard discs [Olafsen and Urbach, 2005]. Similar melting behaviour was also observed by Reis et al. when increasing the packing fraction at constant acceleration [Reis et al., 2006]. Together these works showed that driven granular systems can be used as analogies for equilibrium systems.

Olafsen and Urbach suggested an analogy between the granular temperature (mean kinetic energy) and the thermodynamic temperature as their granular system melted from a solid to a liquid as the increasing acceleration amplitude increased the granular temperature. However, the temperature is not a relevant variable for systems of hard discs as the transition is driven entirely by changes in area fraction. This causes a conundrum if the hard disc phase transition is to be used to explain the nature of the granular transition. To overcome this they suggest that while increasing the acceleration amplitude does increase the granular temperature it is the increased space available to particles at higher accelerations that drives the transition.

The standard method for determining the presence of the hexatic phase in hard discs is by considering the area fraction that each of the translational and orientational correlation functions change from a power law to an exponential decay. This is the method used in [Olafsen and Urbach, 2005] and [Reis et al., 2006]. However, for these small granular systems the exact area fraction this occurs is difficult to determine. A novel approach by Sun et al. overcomes this by considering the susceptibility of translational and orientational order as the packing fraction increases which they use to clearly show the presence of the hexatic phase and confirm a two-step phase transition [Sun et al., 2016]. The susceptibility will be defined in more detail in Chapter 5.

Equilibrium hard spheres in a non-equilibrium steady state

The results in [Olafsen and Urbach, 1999, Reis et al., 2006, Sun et al., 2016] are very surprising. Granular systems are highly non-equilibrium due to their dissipative nature but yet they reproduce the equilibrium results. It is not clear theoretically why this should be the case. The basic assumptions of equilibrium statistical mechanics are not satisfied. One must keep in mind therefore that the study of granular systems is only a fruitful analogy to their equilibrium counterparts.

Throughout this thesis, I will also frequently use language and terminology such as heating and cooling to describe my experiments. The granular temperature, the average kinetic energy of the particles, is an analogy of the temperature in molecular systems, but is not exactly equivalent. First, it is possible for two phases in coexistence in a granular system to have different granular temperatures. This is not possible for a molecular system. Also, if the nature of the transition is similar to the hard disc model then the granular temperature might not drive the transition like temperature does in equilibrium systems.

1.5 Changing the nature of the transition

Two-dimensional granular systems have been shown to transition from liquid to solid through two continuous phase transitions [Olafsen and Urbach, 2005, Reis et al., 2006, Sun et al., 2016]. The initial aim of my PhD was to explore the orderphobic effect. The orderphobic effect describes an attractive force between two disorder inducing intruders placed in an ordered system. This effect requires a first-order order-disorder phase transition. Since in 2D it is generally expected that the liquid-crystal transition is a two-step continuous transition, we were interested in strategies to change the type of the transition.

Many studies have been performed in hard disc, equilibrium experiments and driven granular systems that explore how changing system properties can change the nature of the transition. Here, I will review some of these results which provided insight into how we might create a first-order granular system which can be used for investigations.

Methods to change the nature of the transition have been explored extensively for systems of hard discs. It was shown that in a system of hard discs the stability window of the hexatic phase is reduced as small amounts of smaller discs are introduced to the system [Russo and Wilding, 2017]. As the number of small discs is increased the hexatic phase eventually disappears completely, at a surprisingly low concentration of less than 1%. They speculate that as the number of small discs increases they migrate strongly to the liquid phase and raise the entropy of the liquid relative to the hexatic and solid phases. This in turn makes the liquid favourable over the other two phases.

In a hard polygon simulation, it was shown that the number of sides the polygon has can drastically change the nature of the transition [Anderson et al., 2017]. Hexagons, triangles and squares were all shown to follow a KTHNY-like transition with two continuous phase transitions through an intermediate hexatic phase. Pentagons and fourfold pentiles (a pentagon squashed so that it tessellates) were shown to follow a first-order phase transition from liquid to solid through a region of coexistence. Finally, any polygon with ≥ 7 sides follows the continuous solid-hexatic / first-order hexatic-liquid scenario. Figure 1.14 shows a phase diagram of this behaviour [Anderson et al., 2017].

Another study of hard discs found that introducing an attractive potential between particles induced a discontinuous transition and widened the coexistence region at the expense of the hexatic phase for low temperatures [Li and Ciamarra, 2020]. Figure 1.15 shows the phase diagram of their system for attractive hexagons, discs, squares and pentagons. Colours are used to mark the different regions where white shows coexistence between the adjacent phases. One can see that at low temperatures the hexatic phase is suppressed in favour of the solid-liquid coexistence region.

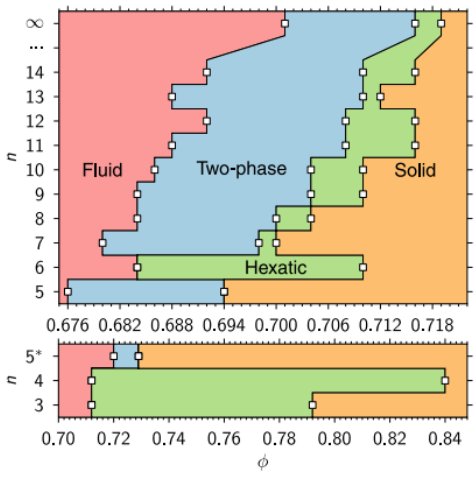

Figure 1.14: Figure from [Anderson et al., 2017]. Phase diagram of hard polygon melting behaviour for n-sided polygons. 5^* refers to the fourfold pentile which is a pentagon which is squashed such that it packs perfectly.

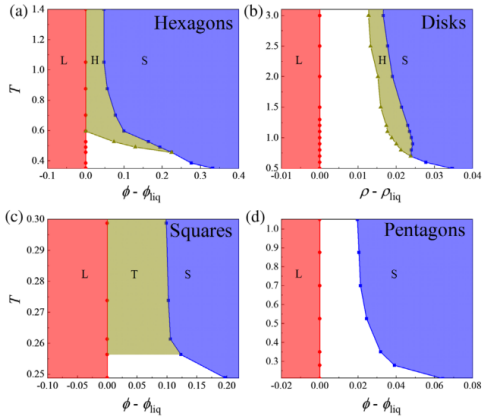

Figure 1.15: Figure from [Li and Ciamarra, 2020]. Phase diagram of attractive polygons and LJ disks. The phase diagrams for (a) hexagons, (c) squares, and (d) pentagons are plotted in the $T - \phi$-ϕ_{liquid} plane and the one for (b) disks is in $T - \rho$ - ρ_{liquid} plane, where ϕ_{liquid} (ρ_{liquid}) is the highest area fraction (number density) of the liquid phase. At each investigated temperature, the estimated phase boundaries are marked with symbols. Colours are used to distinguish the pure phases, liquid (L), solid (S), hexatic (H), and tetratic (T). Coexistence regions, including hexatic-liquid and solid-liquid coexistence, are white.

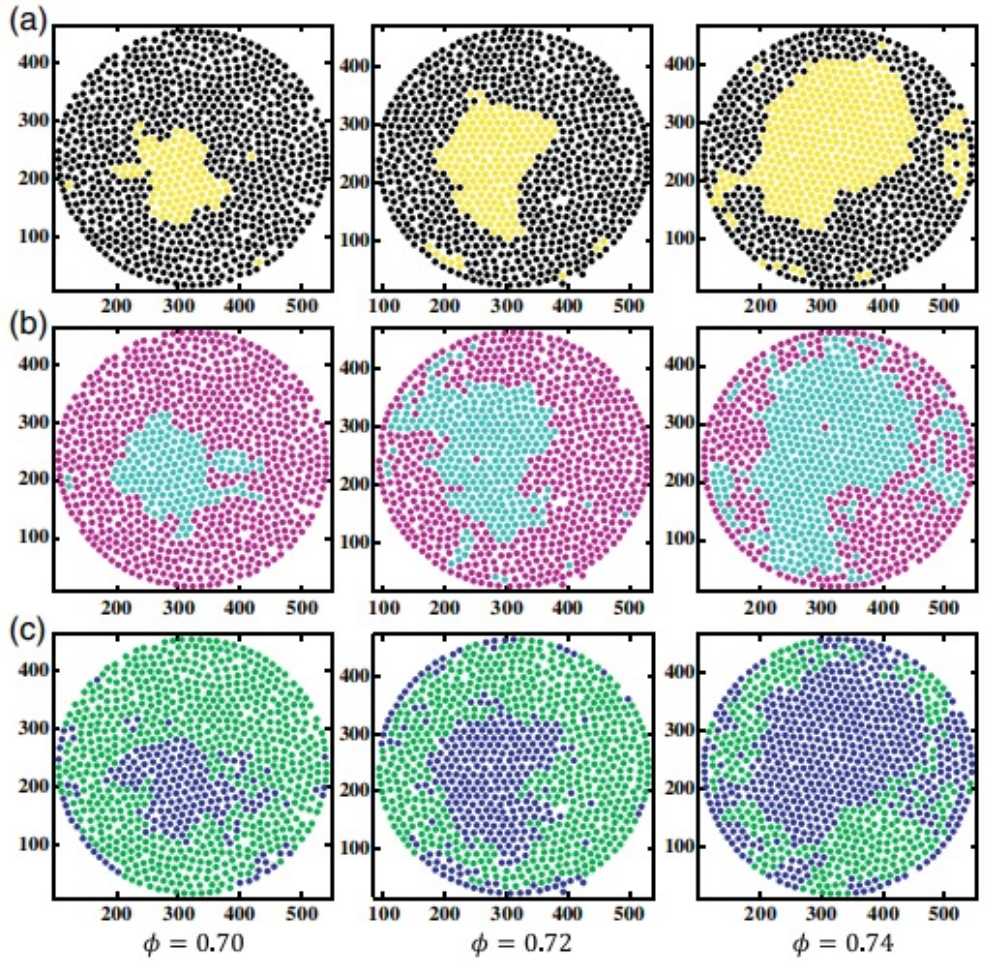

Figure 1.16: Figure from [Komatsu and Tanaka, 2015]. Liquid-solid coexistence in their rubber ball system at three area fractions. (a) Shows the magnitude of the hexatic order parameter, at a threshold of 0.6. (b) Shows the local density calculated from the Voronoi cell area, at a threshold of 9.4 mm^2. (c) Shows the displacement over 10 s at a threshold of 3.4 mm.

In a driven granular system, Komatsu et al. showed how replacing stainless steel balls, which undergo a continuous phase transition, with more dissipative rubber balls can change the transition to first-order [Komatsu and Tanaka, 2015]. In their rubber ball system, they observed a coexistence between liquid and solid phases which can be seen in Figure 1.16 which was one of the indications that the transition was first order. However, previous work in our lab was unsuccessful in reproducing this behaviour with similar dissipative particles showing no first-order characteristics [Smith, 2019].

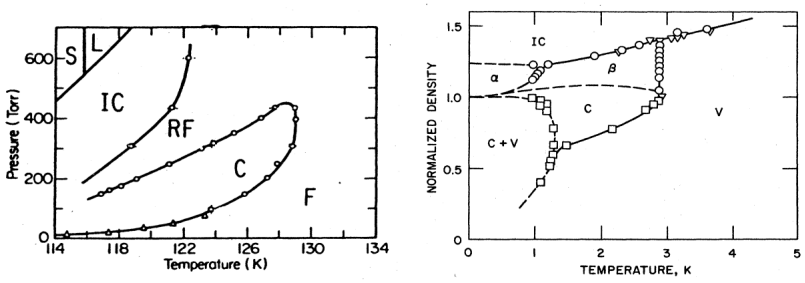

(a) (b)

Figure 1.17: Phase diagrams of noble gases adsorbed on graphite. (a) Phase diagram of near-monolayer krypton: F, fluid; C, commensurate solid; RF, re-entrant fluid; IC, incommensurate solid; S, bulk solid; L, bulk liquid. (From [Specht et al., 1984]). (b) Phase diagram of helium demonstrating several-different phases. (From [Motteler, 1985]).

External potentials and surfaces

Two-dimensional systems often interact with an external potential, e.g. a surface, or an electric or magnetic field, which can alter the nature of the observed phase transitions [Rysti et al., 2021, Miserev et al., 2021, Matvija et al., 2017]. Early two-dimensional experiments involved different noble gases adsorbed on graphite substrates [Strandburg, 1988]. The main differences in interactions arose from the mismatch of the graphite lattice spacing to the preferred spacing of the adsorbed noble gases. Many-different phases could be observed in these systems as the pressure and temperature are changed for different gases with both first-order and continuous phase transitions between phases. Phase diagrams for krypton and helium are shown in Figure 1.17.

In a similar, but very non-equilibrium manner simulations of active matter on a periodic substrate created coexistence between liquid and solid phases, which can be seen in Figure 1.18 [Reichhardt and Reichhardt, 2021].

The nucleation of colloidal crystals was also controlled using template-assisted growth which controlled the position and size of the nucleation [Mishra et al., 2016]. Mishra et al. used square Moiré patterns on PDMS films to produce structures like those in Figure 1.19a, which created the controlled crystals in Figure 1.19b. This is a great example of using a patterned substrate to control the wetting of a crystal phase.

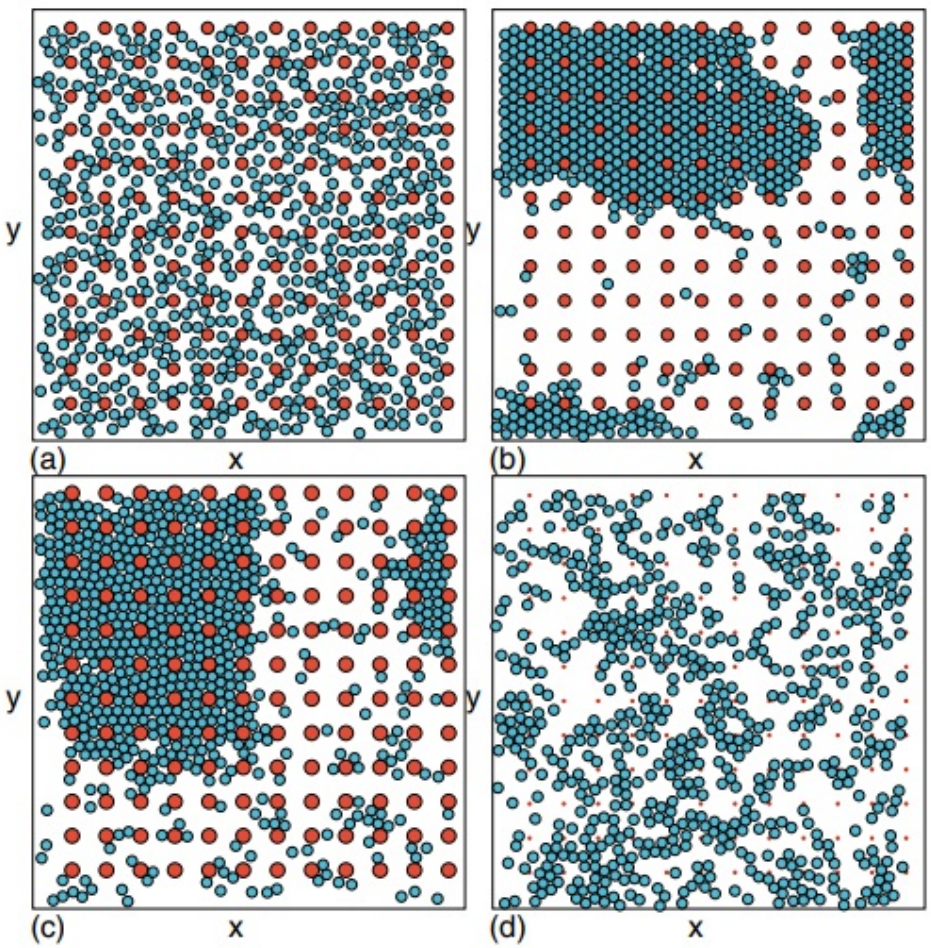

Figure 1.18: Figure from [Reichhardt and Reichhardt, 2021]. Snapshots of disc positions (blue circles) and obstacles (red circles) for their system which shows different behaviour depending on the obstacle size and spacing.

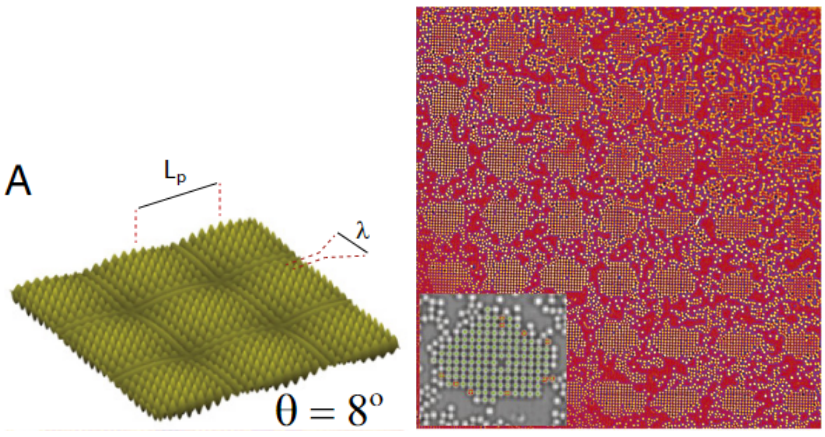

(a) (b)

Figure 1.19: Figures from [Mishra et al., 2016]. Example of using template-assisted growth to control the wetting of a colloidal crystal. (a) Optical micrograph of a square Moiré pattern used to control the wetting of colloidal crystals. (b) Representative snapshot of island growth on a square Moiré pattern which shows clear control of wetting by the pattern.

In many of these cases, it is clear that the surface results in crystalline packing. The nature of the transition is however not clear. Simulations of colloids showed that the continuous liquid-solid transition changed to first-order as the stiffness of the crystal was increased by pinning a small selection of particles in the crystal [Qi and Dijkstra, 2015].

1.6 Conclusion

Under normal circumstances, quasi-two-dimensional granular systems, in the more restrictive sense used here, have been shown to undergo a two-step continuous phase transition. However, other systems that undergo a similar continuous phase transition have shown that the nature of the transition can be changed by introducing a fixed geometry into the system. The change from two-step continuous to first-order could be caused by the new geometries preventing the creation of topological defects with 5/7 neighbours suppressing the hexatic phase. In the absence of the hexatic phase, the system would be expected to undergo a single first-order phase transition from solid to liquid.

This inspired us to use a patterned surface to try to control the nature of the two-dimensional granular phase transition.

Chapter 2

Methods

In this chapter, I will introduce the equipment and procedures used in our experiments. I will also discuss how we use image analysis to track the positions of the particles and some of the basic tools we use to characterise particles.

2.1 Equipment

My thesis explores the behaviour of phase transitions in a quasi-two-dimensional granular system. To achieve this, particles (balls of various sizes and materials) are vibrated vertically on a rough surface such that they move around horizontally. The system is only quasi-two-dimensional as the balls are free to move vertically however, the number of particles and the vibration amplitude are kept low enough so that the particles mostly sit in a single layer.

Experimental Cell

The first part of my experimental setup to note is the experimental cell. The cell consists of a baseplate with a boundary ring clamped on top of it. The baseplates and boundaries can be changed between experiments. A photo of an experimental cell with a baseplate and a boundary is shown in Figure 2.1.

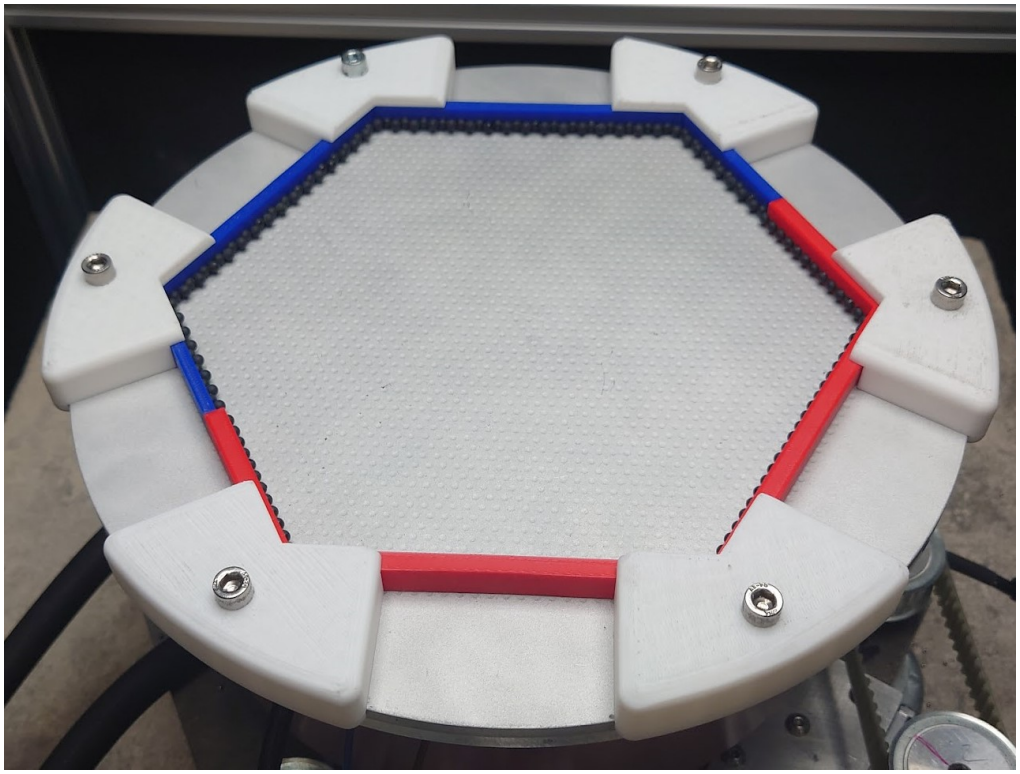

Figure 2.1: Photo of the experimental cell. The boundary (red/blue) is held in place by the white clamps. The surface of the cell is sandblasted and has a triangular lattice of dimples milled into the surface.

The baseplate is a circular aluminium plate with a diameter of 300 mm and a thickness of 10 mm. It is roughened by sandblasting the surface which helps to convert the vertical oscillations of the plate into horizontal forces on the particles. The baseplates are also milled with a triangular lattice of dimples with different spacings; this will be explained in detail in Chapter 3. One baseplate is kept flat (no dimples) to be used as a control.

Boundaries

A boundary in the shape of a regular hexagon with a flat-to-flat distance of 200 mm and thickness of 10 mm is placed on top of the aluminium plate. This is made from milled aluminium or 3D-printed PLA depending on the experiment. An aluminium boundary is shown in Figure 2.1 attached to a baseplate.

Lid

The experimental cell does not have a lid for several reasons. First, as discussed in the introduction, small variations in the lid spacing to particle diameter ratio vastly change the phase behaviour of granular systems [Castillo et al., 2012] in which square crystal phases were observed as the shaking amplitude was increased. This behaviour is far from the hard-disk model that our system aims to mimic, so I remove the lid to avoid the problem and reduce the parameter space of my experiments.

Secondly, I have no choice but to illuminate my experiments from above as the baseplates are aluminium. Introducing a lid makes it much harder to film and track the particles from above due to reflections. The rubber particles used in our experiment, chosen for their dissipative nature, were especially hard to track due to their dark colour.

Shaker

The experimental cell sits on top of a shaker. The shaker consists of an electromagnet sitting in the bottom of a cast iron bowl. A steel disc is suspended a small distance above the poles of the electromagnet on three TUFNOL cotton fabric laminate leaf springs mounted radially to the perimeter of the bowl. On top of the steel disc is a large aluminium mounting plate that is used to attach the experimental cell. A photo of the system's shaking mechanism is shown in Figure 2.2b. The shaking occurs by repeatedly pulling the steel disc towards the magnet and releasing it, allowing it to oscillate on the three leaf springs.

Experiment Base

The shaker is in turn mounted onto a large hexagonal steel block. At three corners of the block are rubber feet on adjustable legs so that the shaker can be levelled. Three feet were chosen as it ensures that all the feet are equally weighted, this is an update of the system described in [Smith, 2019] which sat on four feet in a

square and was difficult to level. The rubber feet sit directly on a large concrete block. The combination of a solid steel block and rubber feet sitting on a large concrete block all contribute towards removing unwanted vibrations from the system.

Two of the adjustable legs are controlled by heavily geared stepper motors which are controlled by an Arduino. This allows the automatic levelling of the system using feedback from a camera. It is critically important that the system is completely level.

Figure 2.2a shows an annotated photo of the equipment. The experimental cell, cast iron bowl containing the shaking mechanism, the adjustable feet and the motors that control them are annotated. Figure 2.3 shows an annotated diagram of the shaker.

Considerations

Several important considerations were taken into account when designing the equipment to ensure that the vibrations are as uniform as possible.

Redesigning the system from four legs to three legs was critical. This improvement eliminated any chance of wobbling as the feet are at the widest part of the system.

The leaf springs were carefully chosen to all be the same stiffness. A collection of 20 leaf springs were created from a single sheet of Tufnol. The stiffness of all the springs was precisely measured using a three-point-flexion test on a rheometer and three of the springs with the closest stiffness were chosen.

The baseplate of the cell was made 6 mm thick. This is thick enough so that it has negligible flex at the vibration amplitude used. This thickness was balanced against the need to minimise the weight. Too much weight on the springs would have led to unstable vibrations and potentially damage the shaker's leaf springs.

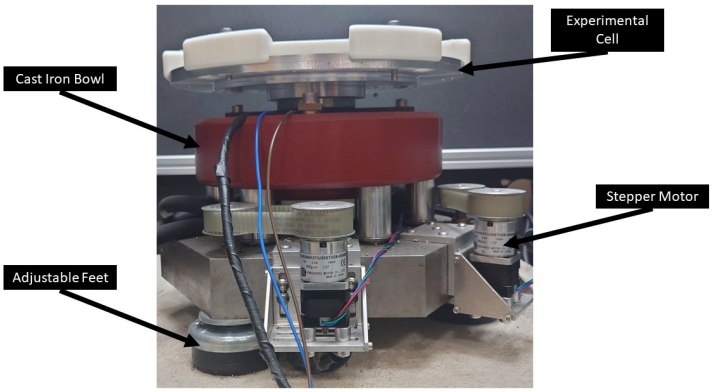

(a)

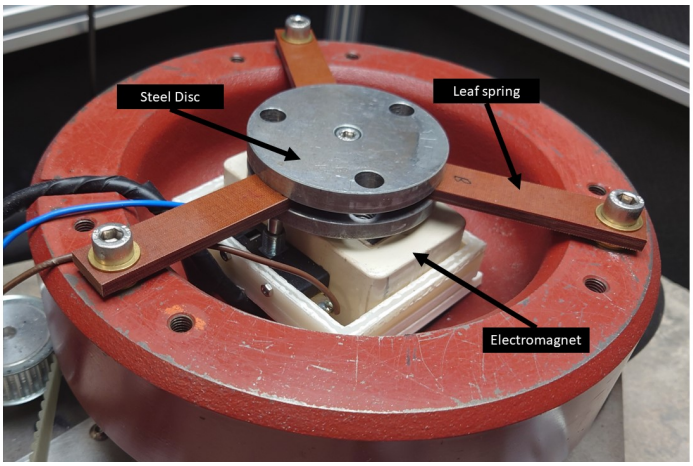

(b)

Figure 2.2: (a) Photo of the shaker from the side. (b) Photo of the inside of the shaker mechanism.

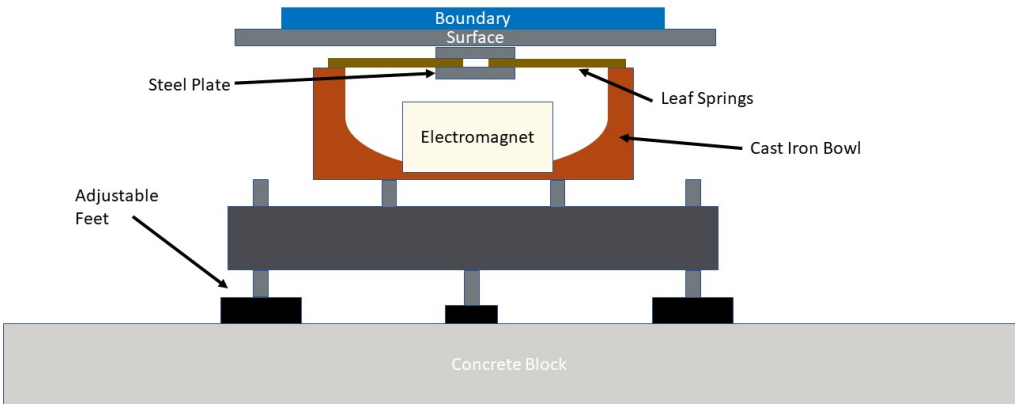

Figure 2.3: Diagram of the shaker.

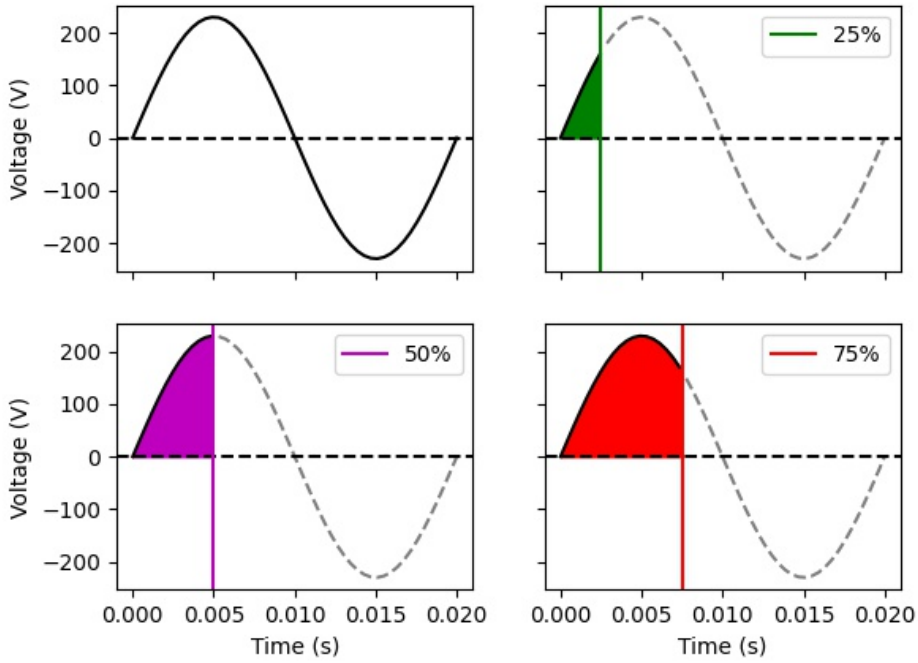

Figure 2.4: Diagram of duty cycles of 25%, 50% and 75% taken from the positive half of a sinusoidal mains voltage. The shaded regions show the times when the magnet is powered.

2.2 Operation

The electromagnet is powered by the shaker controller. The controller filters the positive half of mains AC electricity, at a frequency of 50 Hz and 230 V. This means that the electromagnet pulls down and releases the steel plate 50 times per second, causing oscillations.

The amplitude of the oscillations can be changed by altering the duty cycle of the magnet. The duty cycle is the fraction of the positive part of one period of the AC voltage supplied to the magnet, as seen in Figure 2.4 which demonstrates duty cycles of 25%, 50% and 75%. The duty cycle can be incremented by a computer to steadily increase or decrease the amplitude of oscillations.

As the amplitude of oscillations increases so does the acceleration amplitude of the experimental cell. The vibrations can be characterised by the dimensionless acceleration

$$\Gamma = A(2\pi f)^2/g, \tag{2.1}$$

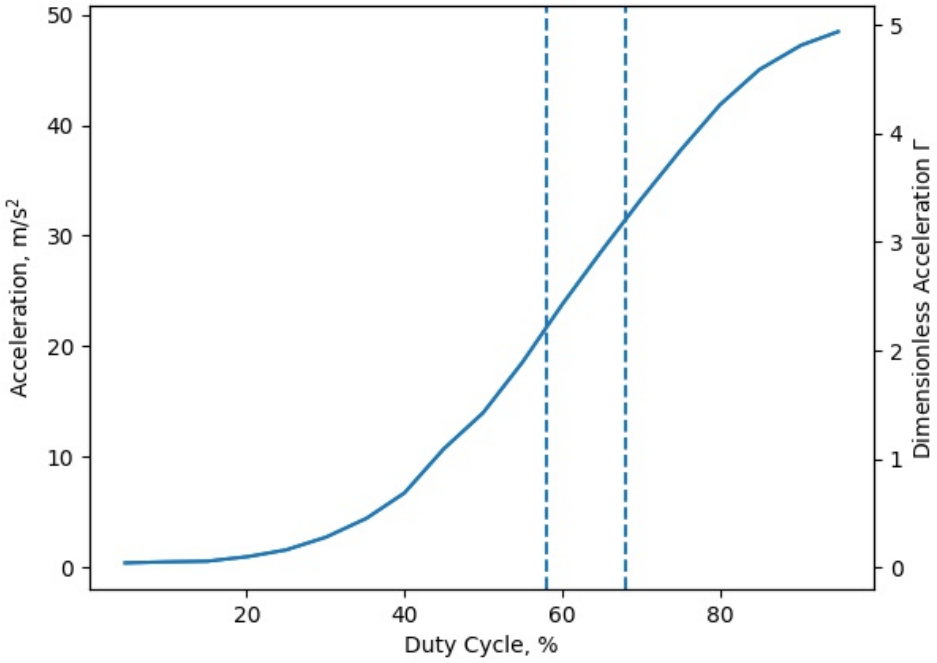

Figure 2.5: Shows how the acceleration of the plate depends on the duty cycle of the electromagnet. The acceleration is the amplitude of the acceleration measured using an accelerometer. The vertical lines show the region in which most experiments in Chapter 2 take place which is mostly linear.

where A is the amplitude of oscillations, f is the frequency of vibrations and g is the acceleration due to gravity.

The dimensionless acceleration was mapped to the duty cycle by securely attaching an accelerometer to the experimental cell and measuring the root-mean-square acceleration. The root-mean-square value was then converted to peak-to-peak values. This was repeated at six different positions around the cell to ensure that the vibrations are uniform across the cell. The average of the dimensionless acceleration plotted against the duty cycle is shown in Figure 2.5. The region in which I performed experiments is the region between duty cycles of 58% and 68% where the acceleration to duty cycle relationship is roughly linear.

Nomenclature

One caveat of granular systems is that they are out of equilibrium, so equilibrium language doesn't necessarily apply. However, after enough comparisons to equilibrium systems the term granular temperature, T_g was defined which is the average kinetic energy of the particles measured in the horizontal plane. Consequently, I will use the language of heating and cooling to describe steadily increasing and decreasing the amplitude of oscillations throughout this report which in turn influences T_g. Throughout this thesis, the granular temperature of the system is not calculated as the maximum frame rate of our camera is too low to accurately measure the velocity of particles. This is because at the frame rate of the camera, particles that are colliding in a crystal appear not to move as their positions are aliased by the frame rate of the camera. The frame rate of a camera required to measure the velocity of the particles is approximately 500 Hz. This was crudely determined using some simulations, but more work is required to be confident of the value.

2.3 Particle Tracking

Tracking the positions of particles is critical to my experiments. Being able to do so precisely is extremely important as many of the properties I will describe later are very sensitive to incorrect tracking.

As part of my development, together with my supervisor, I developed Particle-Tracker: a GUI-based particle tracking software [Smith and Downs, 2021]. This software provides a graphical interface for particle tracking and analysis for videos of two-dimensional physics experiments. It allows users, who don't necessarily have coding experience, to adjust parameters on the fly and quickly create a particle-tracking routine for their experiments. We published this software open source and have successfully used it for our experiments and provided it to undergraduates for their projects.

Filming equipment

To be able to adequately track particles they first must be uniformly illuminated. This is achieved using a large LED ceiling tile light that consists of led strips mounted on the sides of a square waveguide which scatters the light uniformly. This LED panel is mounted above the shaker.

The camera is mounted above the LED panel with a small hole cut into the centre of the panel the same size as the camera lens. The camera is placed 1.5 m above the experimental cell to remove as much lens distortion as possible while still filling the camera image with the cell as much as possible. The camera films at a 4K resolution (2160x3840 pixels) at a frame rate of 50 fps.

Finding Boundaries

Before the locations of the particles are obtained, the boundaries of the hexagonal cell need to be found. This can be achieved using the colour of the boundaries to select them. In the experiments, several boundaries are used so here I will explain how one case is found which is seen in Figure 2.6a. The images from the camera are in the BGR colourspace where three numbers from 0-255 define the amount of blue, green and red in each pixel. The images are first converted to the LAB colourspace where the three channels describe its luminosity from black (0) to white (255), its colour between green (0) and red (255) and its colour between blue (0) and yellow (255). This allows a simple selection of different coloured boundaries that is insensitive to the illumination.

With the image in the LAB colourspace, the blue-to-yellow channel of the image is thresholded. An image threshold is performed by setting all pixels below a threshold value to 0 and all pixels above a threshold value to 1. The result is a binary image which is a single-channel image where pixels have values of either 1 (white) or 0 (black). The resulting binary image is seen in Figure 2.6b.

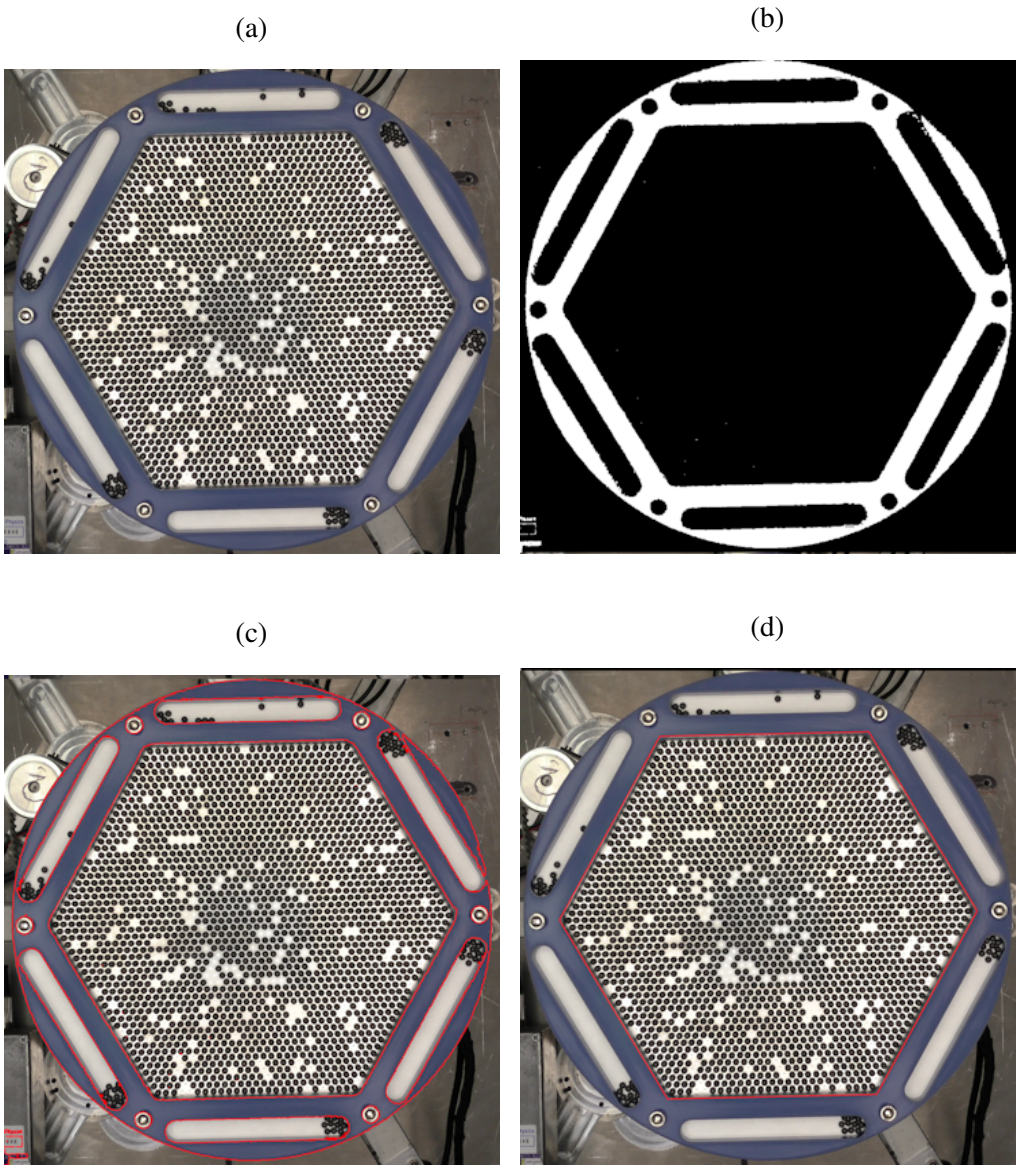

Figure 2.6: Image processing steps used to automatically locate the boundary. (a) The original image in LAB colourspace. (b) The blue-yellow channel of the image is thresholded to obtain the blue boundary. (c) Contours (red lines) are found for the thresholded image. (d) The contour with the second-largest area corresponds to the boundaries of the cell.

Contours are then found in the binary image and drawn in red in Figure 2.6c. Contours are continuous curves of equal colour or intensity. In this case, the contour with the second-largest area represents the experimental cell. A hexagon is then fitted to this contour by minimising the distance between the hexagon and the points along the contour which is shown in Figure 2.6d.

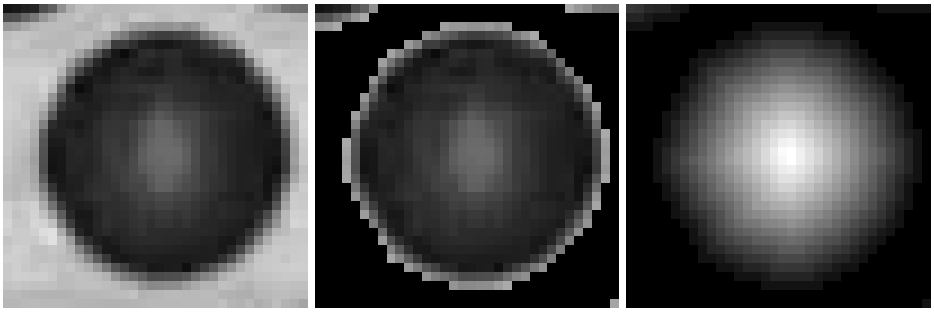

(a) (b) (c)

Figure 2.7: Shows the preprocessing steps applied to the image before tracking. (a) An original image of a particle. (b) The result of a greyscale threshold. (c) The result of a distance transform on the thresholded image.

Once the boundary of the cell is found the image is converted from BGR to grayscale. A grayscale image is a single channel image where each pixel has a value, Y from 0 (black) to 255 (white) and is generated using a simple combination of the blue, green and red colour channels by $Y = 0.114B + 0.587G + 0.299R$. The grayscale image is then masked and cropped by setting all pixels outside the hexagon to white and cropping to the vertical and horizontal bounds of the cell.

Several methods of locating the particles were used. Here I describe the method for the nitrile particles shown in Figure 2.7a which shows a bright spot in the centre of the particle and that the bright background surrounds the particle. A common simple technique, where the centres of the particles and the background have opposite intensities, is to threshold the image so that only the centres of the particles remain. This does not work for these particles as thresholding the image does not just select the centre of the particles, so a different technique is required.

First, the background of the image is set to black by finding all pixels with a grey level greater than 170, the result of which is shown in Figure 2.7b. The distance transform is then calculated which measures the distance of each pixel to the nearest black pixel. The result in Figure 2.7c is a greyscale image, where the brightest pixels correspond to pixels furthest from a black pixel in the original image which gives particles a Gaussian-like appearance.

The images containing the result of the distance transform are then passed to TrackPy's [Allan et al., 2014] locate function which provides an implementation of the Crocker Grier centroid-finding algorithm [Crocker and Grier, 1996] that identifies local brightness maxima as candidate pixel locations. A pixel is adopted as a candidate if no other pixel within a distance w is brighter. As only the brightest pixels correspond to particles, candidate pixels must also be in the upper 30th percentile of brightness for the entire image. Where necessary, once the particles are found in every frame they are linked into trajectories by TrackPy which determines which particle in a given video frame most likely corresponds to the one in the previous frame using the Crocker-Grier linking algorithm [Crocker and Grier, 1996]. The likelihoods are calculated by considering proximity and previous trajectories of the particles since the particles are visibly identical.

2.4 Recording duty cycle

When running experiments where the "temperature" is changing it is important to know exactly what the acceleration (duty cycle) is for each frame of the video. This cannot be easily recorded as when the command to the camera which starts recording is sent, a variable amount of time passes before the recording starts.

Therefore, I record the live status of the duty cycle in the audio channel of the video. To do this the microphone input of the camera is wired to an Arduino which transmits an audio signal. The frequency of the audio signal corresponds to different duty cycles. After the experiment the duty cycle of a video frame is decoded by performing a Fourier transform on the audio signal corresponding to that frame and the peak frequency, f is used to calculate the original duty cycle, D, through a simple formula:

$$D = \frac{f - 1000}{15}. \tag{2.2}$$

This equation was chosen such that the range of duty cycles used in our experiments covered the whole range of audio frequencies that the camera is sensitive to.

2.5 Levelling

Before running any experiments one of the most important steps is levelling the system. If the cell was not perfectly level then particles moved down the slope and close-packed against one of the edges. This was especially sensitive as the vibrations help the balls roll downhill against the uneven surface making it even more important that the system is totally level.

It was found that the particles in the cell were much more sensitive to the level than any spirit level we tried, therefore I tested the level by observing different behaviours in the particles. The general method was to track particles in the system and then automatically raise and lower the stepper motor-driven legs in response to the positions of the particles.

It would have been desirable to simply track the locations of all the particles and calculate their centre of mass to make adjustments however, the 4K camera that I use for recording experiments needs to have the video files manually transferred to the computer once the card is full. This means it could not be used for this automatic levelling, so a 1920×1080 webcam was used instead from which the computer could grab live frames. As this camera has a quarter as many pixels as the main camera, tracking the individual nitrile balls precisely was not possible.

Instead, different tracking methods were utilised depending on the system involved. As I will explain in Chapter 3 my system of nitrile balls forms a crystal/liquid coexistence when the system is cooled on a dimpled surface. If an orderphillic boundary (causes the crystal to wet along the edge - discussed in Chapter 4) is selected then the crystal forms around the edges of the tray, leaving a circular liquid phase somewhere in the centre. If the system is not level then this liquid phase forms on the 'uphill' side of the tray. The position of the liquid phase is recorded after several cooling cycles to determine its mean position. This mean position is then used to adjust the height of the motorised legs and these steps are repeated until the mean position is within a threshold distance of the centre of the tray.

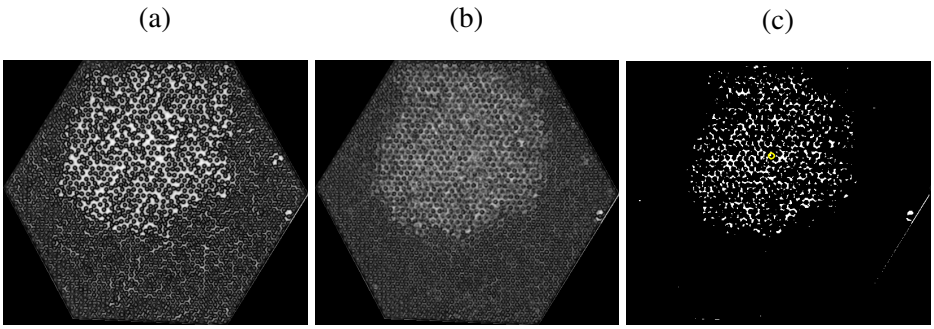

Figure 2.8: Calculating the level of the system by tracking the position of the liquid phase in a system. (a) The original image. (b) The image averaged over 20 consecutive frames. (c) The image after it has been thresholded showing the calculated centre of mass (yellow circle).

Since the individual tracking of particles was not possible the liquid phase had to be tracked differently. Instead of recording a single frame (Figure 2.8a), an average of 20 consecutive frames were used which is shown in Figure 2.8b. Since the baseplate of the image was of a higher intensity than the particles, averaging had the effect of brightening the fast-moving particles of the liquid and darkening the slow-moving particles in the crystal. The image was then thresholded and the centre of mass of the image (Figure 2.8c) was found which corresponded to the centre of the liquid phase. This position was then used to inform the motion of the motorised feet before the iterative process is restarted.

The levelling is an iterative process where each iteration required several repeats with each repeat taking roughly 100 seconds to cool the system. Consequently, it is a very slow process which was often run overnight as it could sometimes take several hours to reach a satisfactory level. The level of the system was considered satisfactory when the centre of mass of crystals from several repeated cooling ramps had an average position within 5 cm of the centre of the cell.

2.6 System stability

Another important property of the system is that the accelerations that are produced are both stable and repeatable. The system can be considered stable if the acceleration of the plate is constant when the system is at a constant duty cycle for a long time. Repeatable means that if the system is heated from a duty cycle of A to a duty cycle of B and cooled back to A then the measured acceleration, Γ, is the same for both instances of A. The system should be repeatable regardless of the cooling rates.

Initial tests of the system involved shaking the system at a constant Γ such that a system of particles was just crystalline. The system was left running for several hours and the acceleration of the system was measured by using both an accelerometer and observing the behaviour of the particles.

These initial tests, shown in Figure 2.9 found that the RMS acceleration of the system changed steadily over time when the duty cycle was kept constant. This was a problem as many of our planned experiments required precise control of the system's acceleration.

I observed that as the system was left running for a long time the electromagnet heated up considerably. This heating of the magnet was the most likely cause of the changing acceleration as it could change the strength of the magnetic field that the electromagnet produced. Residual heat from the hot magnet could also affect the material properties of the three leaf springs that support the baseplate.

To overcome the heating problem, the electromagnet was fitted with a water-cooling system which aimed to maintain the electromagnet at a constant temperature. With the cooling system in place, the temperature of the magnet decreased steadily for approximately 2 hours until the temperature became stable. After this the temperature remained constant which was measured using a temperature probe fixed to the outside of the magnet and confirmed by measuring the resistance of the electromagnet.

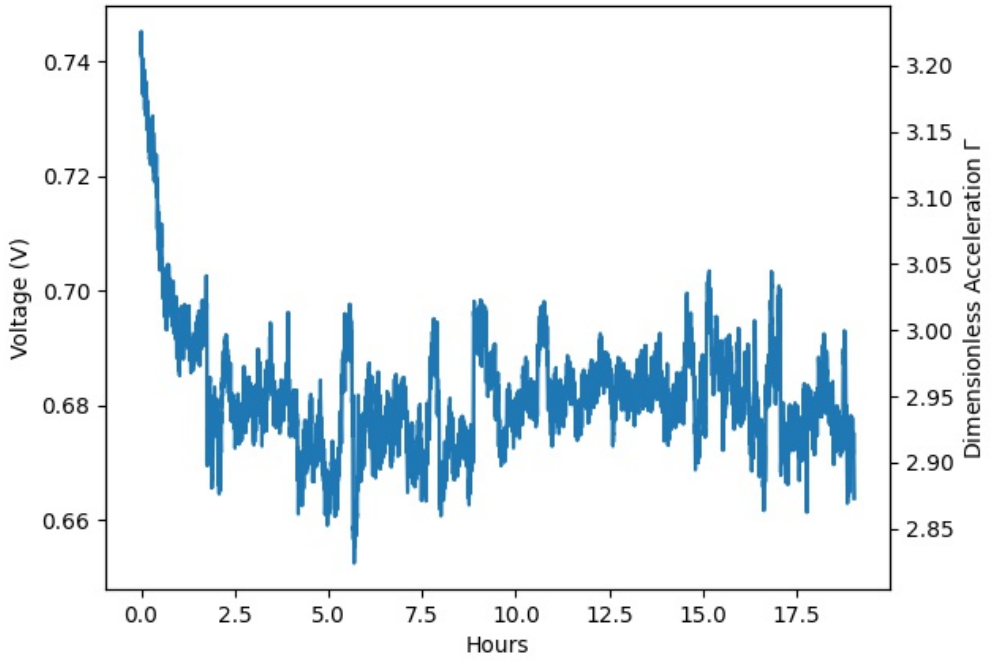

Figure 2.9: Plot showing the stability of the plate acceleration after being turned on at a duty cycle of 80%. It shows that the system becomes stable after roughly 2 hours.

Testing the steady state of the acceleration showed similar behaviour - the acceleration steadily increased for the first 45 minutes then became constant afterwards for several hours.

The system was also tested for repeatable accelerations after the system had become stable. This was achieved by heating and cooling the system between a duty cycle of 80% and 60% at different rates and measuring how the acceleration changed. This proved to be consistent across all the rates that were tested.

These investigations meant that I could be confident that the accelerations that I measured between experiments are equivalent. However, it required that the system be 'warmed up' before any experiments are performed. To achieve this I run the experiment at a duty cycle of 70% for one hour before performing any experiments.

2.7 Analysis

The solid-liquid phase transition in granular systems is often referred to as an order-disorder phase transition. Therefore, a method of measuring the order in the system is required. There are two types of order that I will measure, the orientational order and the positional order.

Orientational Order Parameter, ψ_6

The orientational order of the system is described using the global orientational order parameter Ψ_6 which is an average of the magnitude of each particle's local orientational order parameter ψ_6. The local orientational order parameter for particle j is given by

$$\psi_6^j = \frac{1}{N} \sum_{n=1}^{N} \exp 6i\theta_n, \tag{2.3}$$

which sums over the N neighbours of particle j where θ_n describes the angle of neighbouring particle n from particle j with respect to an arbitrary axis.

As ψ_6 is a complex number it has both a magnitude and a phase which both describe different properties of the particle. The magnitude of ψ_6 describes how ordered the crystal surrounding a particular particle is, having a value of 1 if the particle is located in the centre of 6 perfectly ordered particles and reducing to 0 as the ordering of the neighbours reduces. The magnitude is useful for describing the total orientational order of the system. The phase of ψ_6 describes the orientation of the crystal domain surrounding the particle. If the crystal is aligned with the horizontal axis then it has a phase of 0 whereas if the crystal is aligned 30° from this axis then it has a phase of $\pm\pi$.

The sum in Equation 2.3 is over the N neighbours of particle j. There are two different common methods of finding the neighbours of a particle. The first is to use the six nearest neighbours of the particle as this is the number of particles that a particle in a perfect crystal would be expected to have. It is also a good idea to also apply a carefully chosen cut-off distance to remove candidates that are not neighbours like in Figure 2.11.

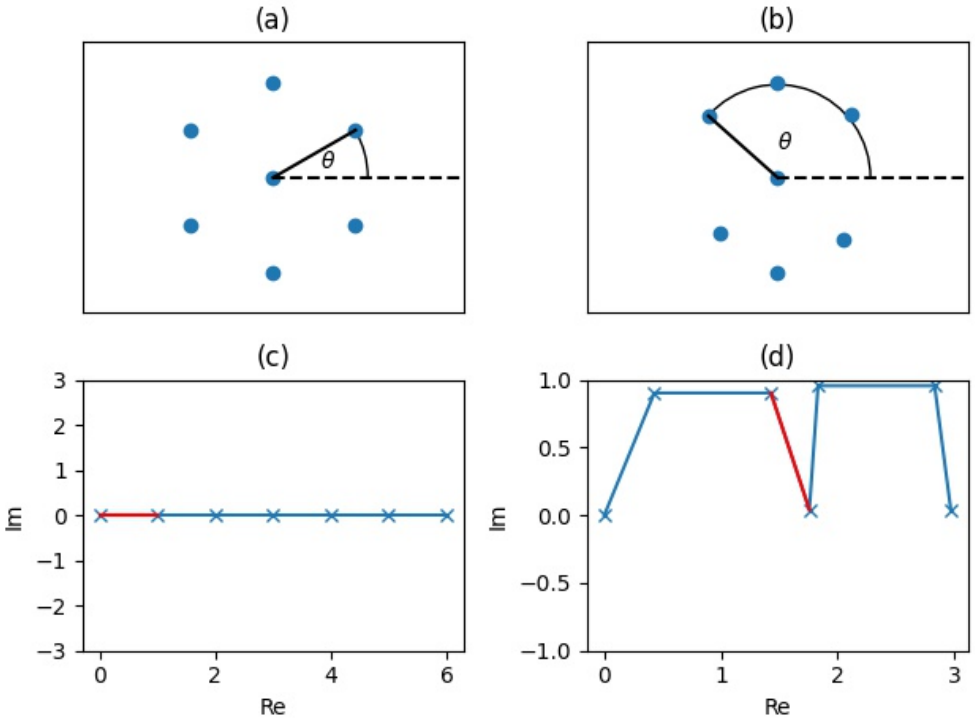

Figure 2.10: Diagrams explaining the calculation of the orientational order parameter, ψ_6. (a) Shows six perfectly ordered neighbours around a central particle. The angle noted is between the arbitrary axis and the first neighbour. (b) Shows 6 less than perfectly ordered neighbours around a central particle. The angle noted is between the arbitrary axis and the third neighbour. (c) Shows how the sum from Equation 2.3 increases as the different neighbours are considered in a perfect crystal. (d) Shows how the sum increases for an imperfect crystal. The red lines represent the increase from the particles with annotated angles.

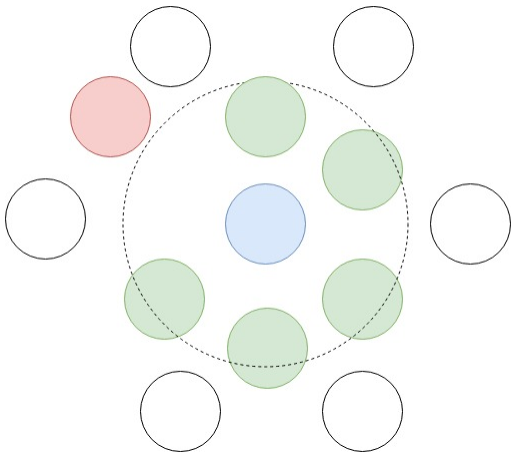

Figure 2.11: The six nearest neighbours of the blue particle are coloured. Only the green particles are included in calculations as the red particle is outside the cut-off distance - annotated by the dashed line.

.

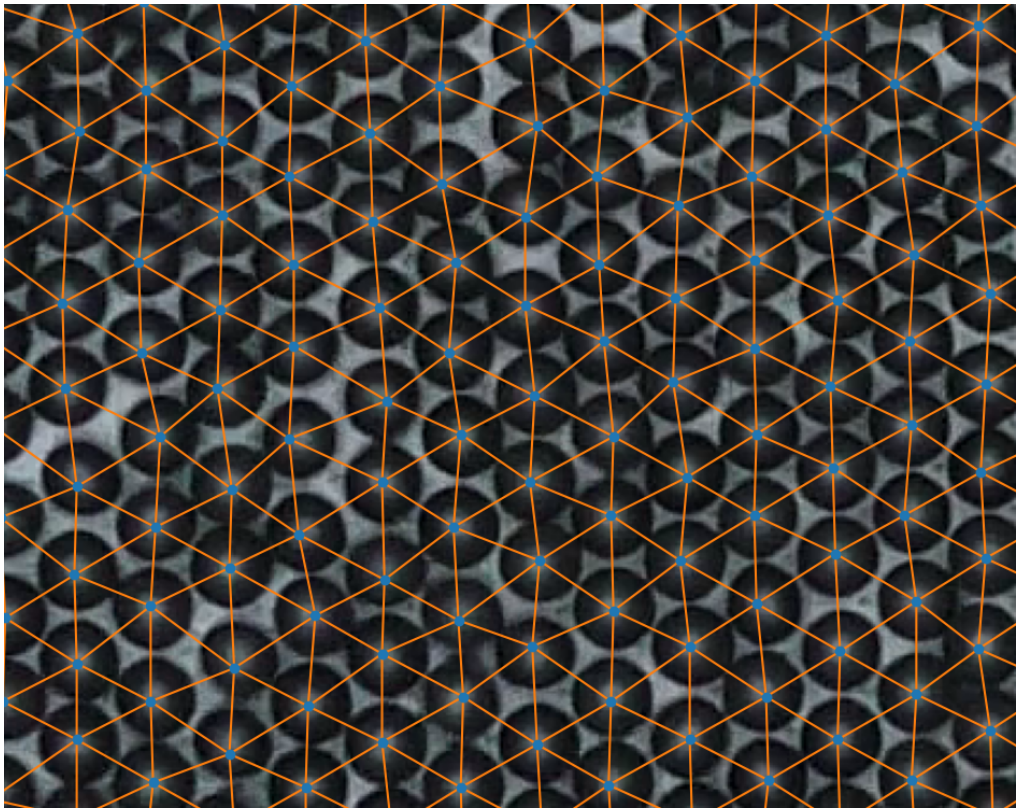

Figure 2.12: Delaunay triangulation diagrams. Blue dots mark the tracked positions of particles. Orange lines show the Delaunay triangulation.

The second is the use of the Delaunay triangulation to calculate the neighbouring particles. The Delaunay triangulation is a way of dividing a set of points into triangles in such a way that no point is inside the circumcircle of any triangle. A circumcircle is a circle that passes through all the vertices of a polygon. In other words, it creates a network of triangles that covers the entire set of points, with no gaps or overlaps. An example of a triangulation calculated on my system is shown in Figure 2.12. It is also necessary to apply a cut-off distance to remove unwanted candidates. The Delaunay triangulation can be easily calculated using a variety of scientific programming packages, for example, SciPy [Virtanen et al., 2020].

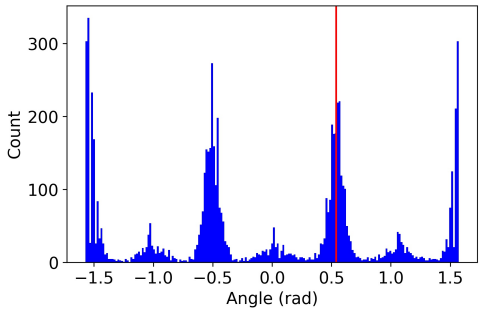

Figure 2.13: A histogram of the angles calculated from the Delaunay triangulation used for calculating the reciprocal lattice vector $\vec{G}$. The red line shows the median value ($\sim \frac{\pi}{6}$) for histogram values between $\frac{\pi}{12}$ and $\frac{3\pi}{12}$.

Positional Order Parameter, ψ_T

The other type of order that needs to be described is the positional order of the system. This can be described by the translational order parameter for particle j given by

$$\psi_T^j = e^{i\vec{G}\cdot\vec{r}_j}, \tag{2.4}$$

where $\vec{r}_j$ is the position vector of particle j and $\vec{G}$ is a primary reciprocal lattice vector.

The translational order parameter is extremely sensitive to both the length and angle of $\vec{G}$, which in an experimental system are not trivial to calculate as the orientation and spacing of the system are not automatically known.

To calculate G, a Delaunay triangulation of the particles in the solid phase is calculated which returns a list of all the vectors between neighbouring particles. A histogram of all the vector angles is then calculated which will have a peak for each of the three principal directions and is shown in Figure 2.13. The median value of data around one of the histogram peaks is taken as the angle of the lattice vector. The length of the lattice vector is taken as the median length of all the vectors. Given the angle ($\vec{a}_\theta$) and the length ($\vec{a}_r$) of the lattice vector $\vec{a}$ the reciprocal lattice vector $\vec{G}$ is then calculated where $\vec{G}_r = \frac{4\pi}{\vec{a}_r\sqrt{3}}$ and $\vec{G}_\theta = \vec{a}_\theta + \frac{\pi}{2}$.

The exact value of $\vec{G}$ is refined further by calculating ψ_T for a perfect crystal using a small range of values around the values of $\vec{G}_r$ and $\vec{G}_\theta$. The values of $\vec{G}_r$ and $\vec{G}_\theta$ that produce the smallest standard deviation in the phase of ψ_T across the system are used as the final values. This refines the values further than can be achieved using the Delaunay method.

As ψ_T is a complex exponential, it always has a length of 1 so that cannot be used to characterise the system. Therefore, the phase of ψ_T is the only useful information which can be used to determine whether two different particles are in a matching crystal. Two particles in the system will have the same phase if their separations are an exact multiple of the lattice vector. If two particles separations are $(N + \frac{1}{2})L$ where L is the lattice vector and N is any integer, then the particles then the phase of ϕ_T will differ by π between the particles.

2.8 Conclusions

In this chapter I have presented our experimental equipment and described our operation procedure. I explained how we perform our image analysis to track the position of the particles and the tools we use to characterise the orientational and positional order of the particles. I have also discussed the levelling of my system and the steps to ensure that the accelerations it produces are stable.

In the next chapter, I will introduce the dimpled surfaces used to alter the nature of the phase transition and present initial observations for a few different spacings.

Chapter 3

Initial Investigations

As outlined in Chapter 1, the 2D hard sphere system undergoes a two-step continuous phase transition through an intermediate hexatic phase [Bernard and Krauth, 2011]. However, Komatsu et al. found that introducing strongly inelastic particles changed the nature of the transition from continuous to strongly first-order [Komatsu and Tanaka, 2015]. Despite this result, previous work in our lab contradicted this finding and was unable to reproduce this effect [Smith, 2019]. This chapter explores an alternative mechanism to generate a first-order transition in a granular system.

As I discussed in the introduction two-dimensional surfaces often interact with an external potential. For example, the experiments involving noble gases deposited on graphite substrates [Birgeneau et al., 1981] and the colloidal experiments using patterning to control nucleation [Ganapathy et al., 2010, Miserev et al., 2021]. Simulations of colloids and active matter have also demonstrated how periodic structures can suppress the hexatic and lead to strong phase separation [Qi and Dijkstra, 2015, Reichhardt and Reichhardt, 2021].

A common theme in many of these studies is the idea that preventing 5/7 neighbour disclinations suppresses the hexatic phase leading to a first-order liquid-solid phase transition. We take these ideas of controlling the nature of phase transitions using an external geometry and see if these ideas can be applied to a non-equilibrium system. To achieve this, I investigate how changing the topography of the surface can change the nature of the phase transition in a quasi-two-dimensional granular system.

3.1 Surfaces

The topography of the surface was changed by introducing a triangular lattice of dimples cut into the surface which aimed to be an analogue of a surface in an equilibrium system that provided a periodic potential. We hoped that the triangular shape would prevent the formation of topological defects that drive the change KTHNY transition as the energy to create dislocations, which require adding or removing a neighbour, would be too high.

The dimples are spherical-cap-shaped and cut using a spherical ball cutter with a diameter of 10 mm and cut to a depth of 0.10 mm which results in a dimpled radius of 0.99 mm. Figure 3.1 shows the dimensions of the ball cutter and the dimple. The dimensions of the dimples were chosen such that a dilute collection of particles were all trapped by dimples when the system was slowly cooled.

With the chosen dimple dimensions three surfaces were created with lattice spacings, L, of 3.89 mm, 4.30 mm, and 4.80 mm which when compared to the diameter of the particles D had L/D ratios of 0.97, 1.08, and 1.2 respectively. These spacings were carefully chosen such that the distance from the boundary of the system to the nearest row of dimples was exactly half of the lattice spacing of the dimples as limited access to the workshop limited us to one aluminium boundary.

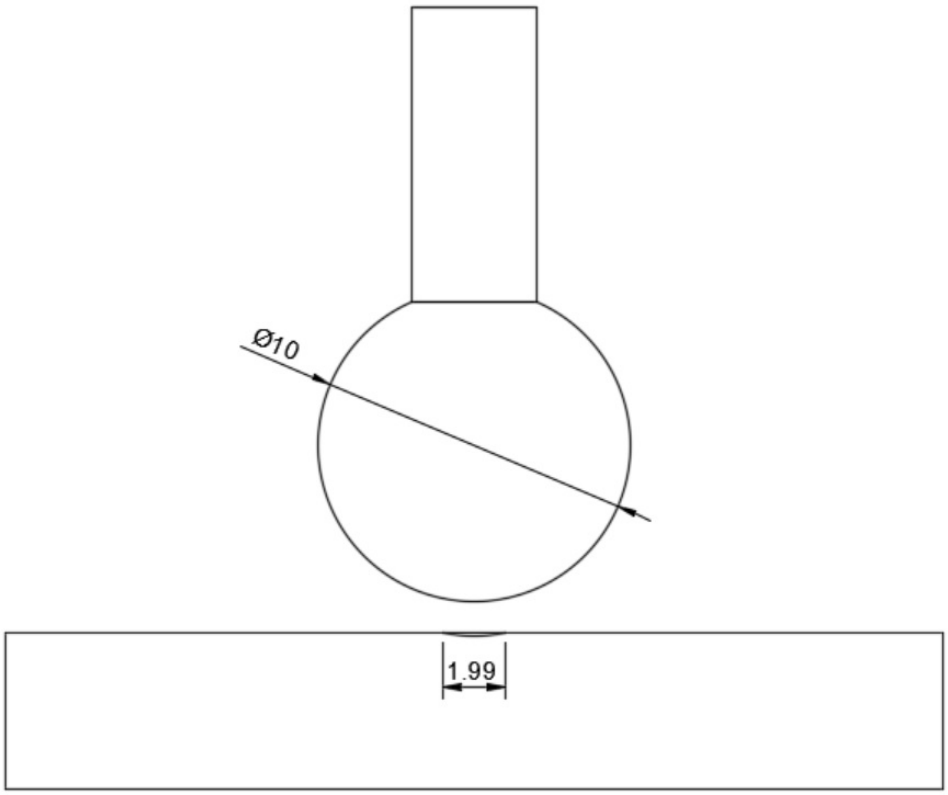

Figure 3.1: The dimensions of the ball cutter and the dimple in mm.

3.2 $L/D = 0.97$

The first surface that was tested has a spacing of 3.89 mm, smaller than the particles with a diameter of 4 mm. The system was set up with an area fraction, $\phi = 0.8$. The area fraction describes the area of the experimental cell that is filled with particles and is therefore proportional to the number of particles in the cell. Due to the spherical shape of the particles, the highest area fraction that can be achieved in two dimensions is when perfect 2D hexagonal packing occurs with an area fraction of $\phi = 0.907$. The system was cooled from a dimensionless acceleration of 2.6 to 1.3 at a slow rate of $1 \times 10^{-3}\ \mathrm{s}^{-1}$. A snapshot of the system is shown in Figure 3.2 at a dimensionless acceleration of 1.3 after being cooled. Here, the particles in the system have formed a pattern of small clusters of roughly equal size across the system. This behaviour was fascinating and was explored in more detail which will be presented in Chapter 7, however, it is not representative of a first-order phase transition from a liquid to a solid so will not be discussed further in this chapter.

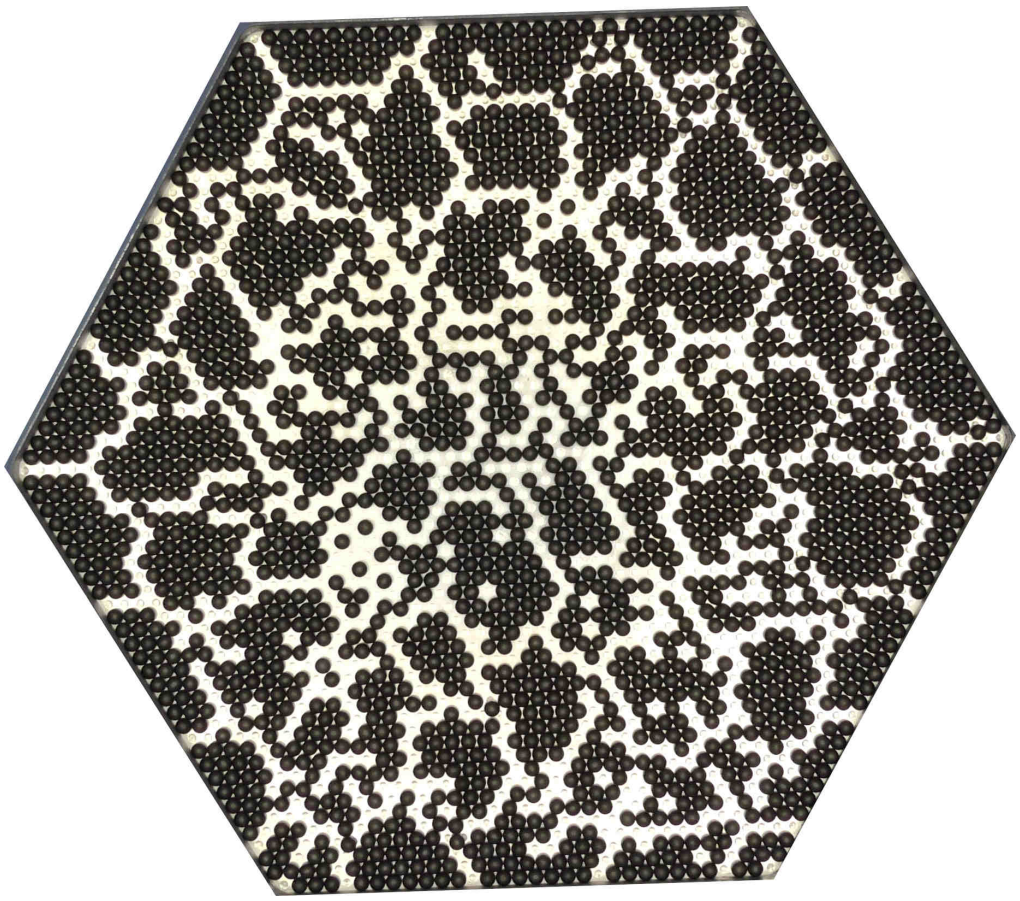

Figure 3.2: Figure showing the result of cooling on the 3.89 mm surface which corresponds to $L/D = 0.97$.

3.3 $L/D = 1.08$

The next surface that was tested has a spacing of 4.30 mm, just larger than the particles with a diameter of 4 mm. We initially thought that this spacing would have the most promise as we expected it to hold particles in a triangular lattice and prevent the dislocations and disclinations that are so critical in a continuous phase transition. Again, the system was set up with an area fraction, ϕ, of 0.8 and cooled from a dimensionless acceleration of 2.6 to 1.3 at a slow rate of 1×10^{-3} s^{-1}. This time, the system seemed to transition from a liquid to an ordered solid however, there did not seem to be any evidence of first-order behaviour. The particles seemed to homogeneously transition from a liquid to a solid without coexistence or evidence of surface tension that would be expected in a first-order transition and looked at first glance very similar to previously studied systems in our lab

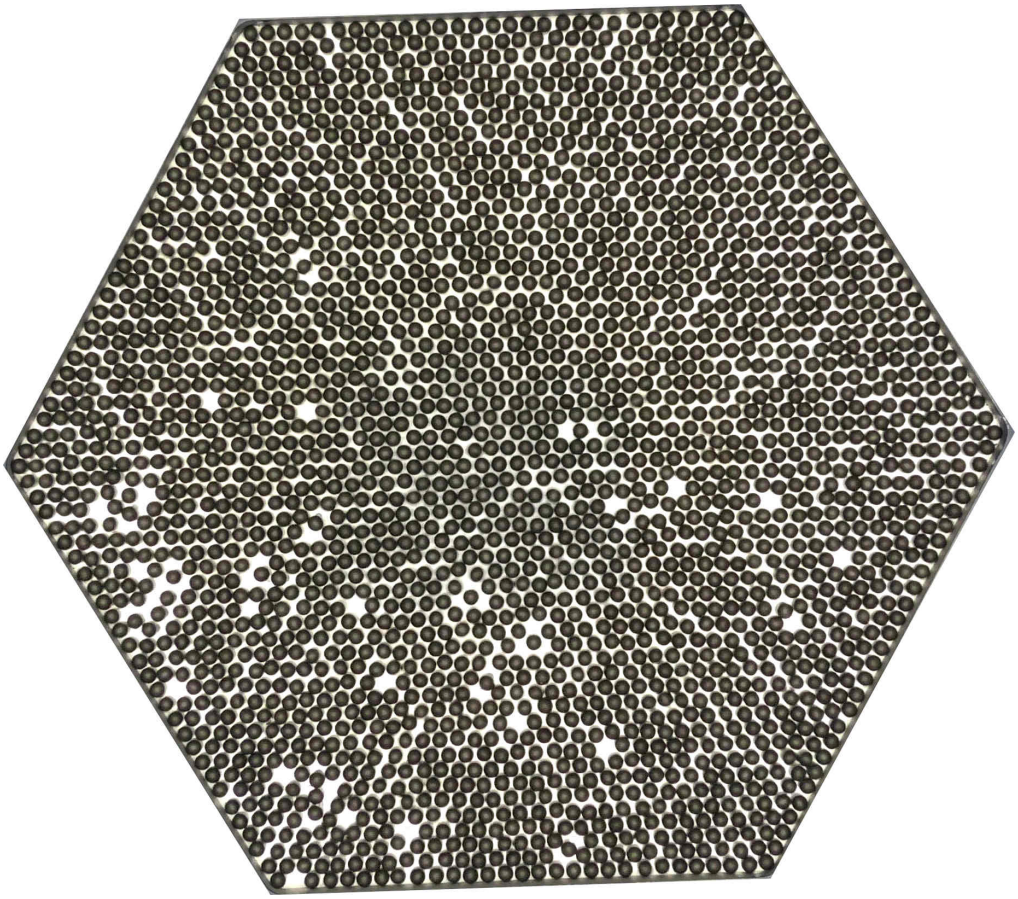

Figure 3.3: Figure showing the result of cooling on the 4.30 mm surface which has a dimple spacing, L, to particle diameter, D, ratio of $L/D = 1.08$.

that were continuous [Smith, 2019]. This occurred gradually over a range of accelerations. The snapshot in Figure 3.3 shows the result of cooling on this surface, here the system is a crystal but shows no evidence of coexistence between liquid and crystal which is critical evidence of a first-order phase transition.

3.4 $L/D = 1.2$

The final surface that was tested has a spacing of 4.80 mm, which is larger than the particles with a diameter of 4 mm. After the results of the $L/D = 1.08$ surface, this was not expected to produce a first-order phase transition as we expected the behaviour to be similar. However, the results of cooling with an area fraction, $\phi = 0.8$ from a dimensionless acceleration of 2.6 to 1.3 at a rate of 1×10^{-3} s^{-1} immediately surprised us. Initially, at high acceleration, the system was liquid but as the system cooled, small regions of crystal began to fluctuate in and out

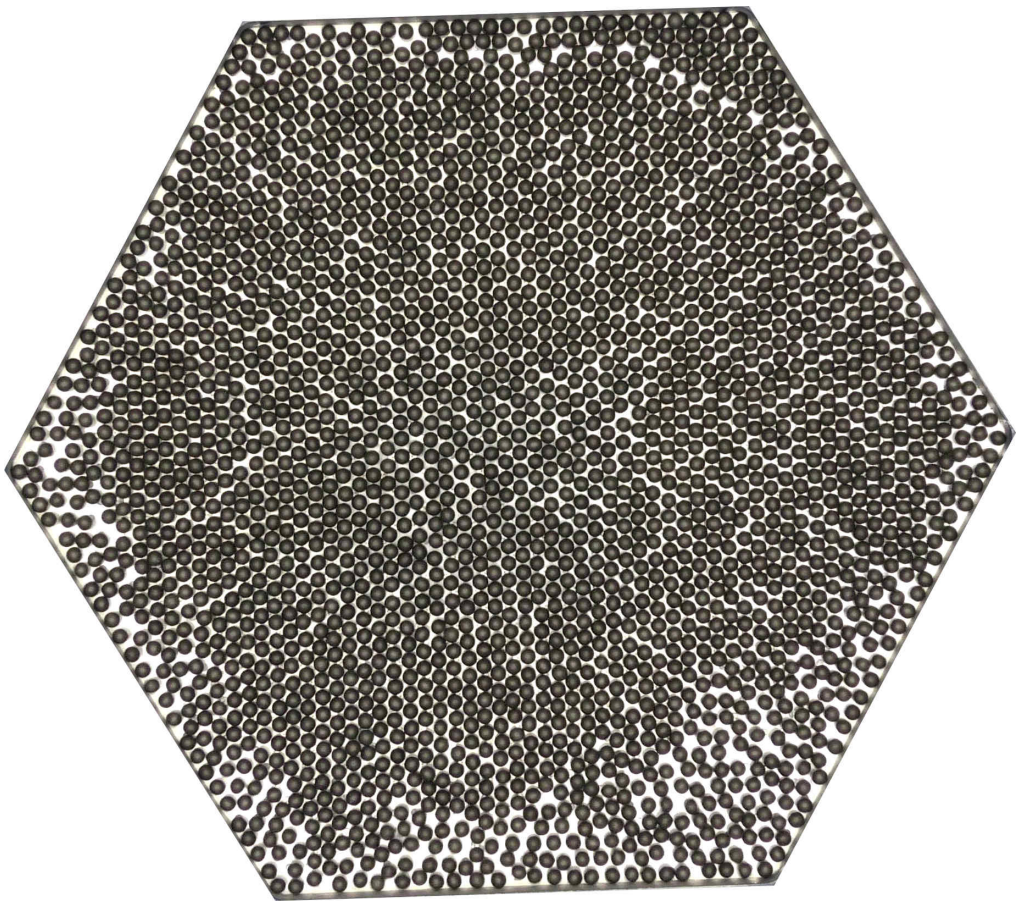

Figure 3.4: Snapshot of the system with $L/D = 1.2$ after it has cooled from $\Gamma = 2.6$ to $\Gamma = 1.3$. Here, there is clear evidence of coexistence between the liquid and solid phases, a key attribute of a first-order phase transition.

of existence until one of the crystals became stable. Once this small region of crystal, surrounded by liquid, became stable it continued to grow in a cohesive lump as the temperature of the system was further reduced. This evidence of coexistence between the liquid and solid phases is clear evidence that the phase transition between liquid and solid is first-order as coexistence is not observed in continuous phase transitions. A snapshot of the system is shown in Figure 3.4 after the system has cooled where coexistence between liquid and crystal can be observed.

We expected the dimpled surfaces to create crystals where each particle in the crystal sat in a dimple such that the crystal and the dimple pattern had the same spacing and crystal direction. However, this is not the case for this spacing. Here, the particles in the crystal are oriented 30° with respect to the dimpled lattice and have a smaller spacing such that every other particle along a crystal direction sits

in a dimple with the particles between located on the midpoint of the hexagons separating dimples. This is shown in Figure 3.5 which shows a small region of a crystal sitting on top of the dimples. I believe this occurs for a few reasons: (1) When the area fraction of particles is at 0.8, there are significantly more particles than dimples in the system which forces the particles to adopt a tighter spacing than the dimples can provide. (2) This tighter spacing is conveniently provided by packing along this rotated direction as the apothem (the distance from the centre of a hexagon to the centre of one of its edges) is 4.16 mm for this surface which is just larger than the particle's diameter. This system shows characteristics of a first-order phase transition. However, a far more sophisticated analysis will need to be employed (Chapter 5) to confirm this. Finite-size effects, the influence of the edges, and inelasticity could all be important.

3.5 Conclusion

The spacing of 4.8 mm ($L/D = 1.2$) shows strong qualitative evidence of a first-order phase transition.

The next two chapters will focus on two consequences of the first-order nature of the transition, the wetting of different phases, and the orderphobic effect. Quantitative evidence of the first-order transition for this spacing will follow later in Chapter 5 as it relies on the wetting behaviour uncovered in Chapter 4.

The nature of the phase behaviour for the other lattice spacings will be explored in much more detail in Chapter 7.

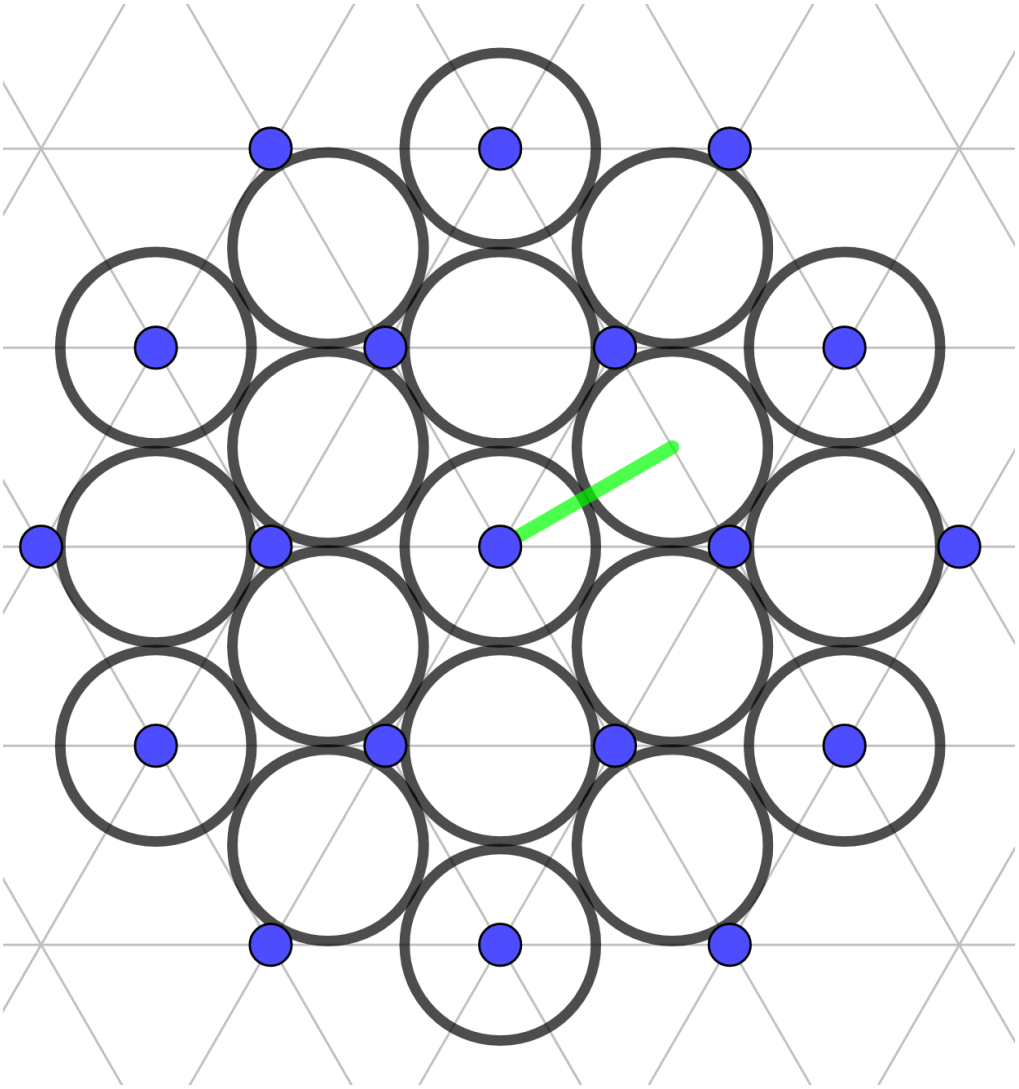

Figure 3.5: Diagram explaining the orientation of the crystal. The blue dots represent the positions of dimples on the surface. The black circles represent the positions of particles in the crystal. The crystal lattice is rotated 30° with respect to the dimple lattice. The green line marks the separation of the particles in the crystal which is equal to $\frac{\sqrt{3}}{2}L = 4.16\,\text{mm}$ when the dimple spacing, L, is 4.8 mm.

Chapter 4

Controlling Wetting of Different Phases

In the previous chapter I presented observations from three different lattice spacings that produced distinct behaviour. We focussed our efforts on the surface with $L/D = 1.2$ which produced behaviour that seemed first-order. Before providing quantitative evidence for the first-order nature of the transition in Chapter 5 I first present our investigation into the controlling the wetting of the different phases which is important preliminary work for the next chapter.

4.1 Introduction

There are some major differences between simulations and an experimental granular system that are important to consider. The most critical of these is how the boundary influences the behaviour of the system.

One consequence of boundaries in granular systems is the granular temperature profile that exists between the centre of the cell and the boundary; particles moving in the centre of the tray move faster than those at the boundary. This effect reduces as the packing fraction increases but is still a relevant concern [Smith and Smith, 2017]. Molecular dynamics simulations of granular systems have also found that introducing friction at the sidewalls can yield non-Gaussian tails in their velocity distribution and sharper peaks at zero velocity [van Zon et al., 2004].

Other effects that the boundary could cause would be the heterogeneous nucleation of crystal at a boundary that would not occur in a large system. Additionally, the finite size of a system can cause the suppression of interface effects that arise from the first-order transition [Bernard and Krauth, 2011].

To alleviate some of these concerns it is desirable to alter how the system interacts with the boundary. One way to do this is to control how the boundary is wetted by the different granular phases in the system. Here are a few examples of studies that have controlled the wetting at boundaries before I show my results.

In a granular system, Komatsu et al. showed that with a hard boundary, the solid phase sits mostly in the middle of the container without making much contact with the side walls which are mostly wetted by the liquid phase [Komatsu and Tanaka, 2015]. They suggested that this was due to the larger coefficient of restitution of a particle-boundary collision than the particle-particle one, so the hard boundary was preferentially wetted by the liquid phase with the higher granular temperature. They confirmed this behaviour by introducing a soft boundary which was slightly wetted by the solid phase. Figure 4.1 shows the particles of the liquid (black) and solid (yellow) phases with a hard (a) and soft (b) boundary which shows the wetting effects described above. This is an example of dissipation-induced wetting.

Another example of controlling the spatial phase separation is through geometry-induced wetting which has been achieved in several equilibrium systems. For example, when ice melts, disorder at a solid-wall boundary will tend to induce pre-melting by raising the interfacial energy of the solid relative to the liquid through effects such as roughness, dislocations and impurities [Dash et al., 1995]. A model of a two-dimensional soft matter system showed that when the fluid phase was confined by a linear wedge, then freezing was strongly promoted if the angle of the wedge was commensurate with the crystal lattice [Archer and Malijevský, 2016]. Figure 4.2 shows density profiles of the system under wedges of different angles where the amount of crystallisation that is promoted at the boundary depends on whether it is commensurate with the crystal lattice.

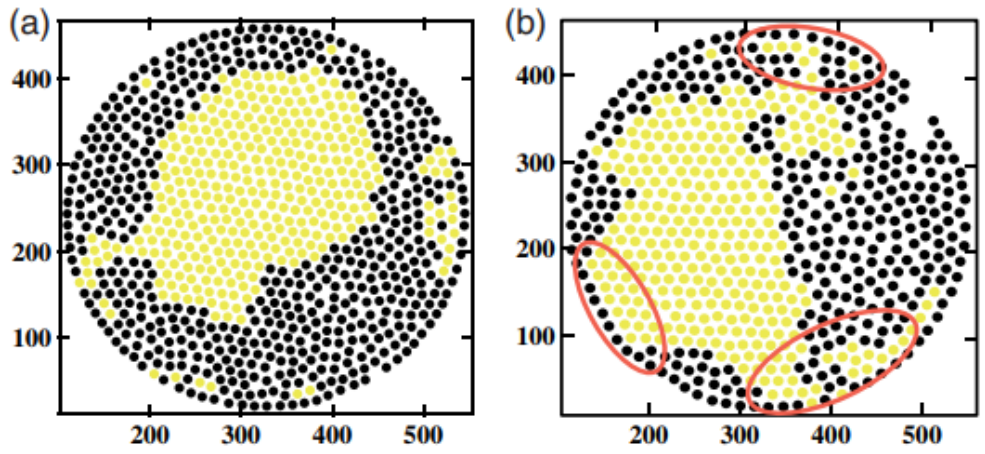

Figure 4.1: Figure from [Komatsu and Tanaka, 2015]. Effects of boundary softness on the spatial phase separation of the liquid (black) and solid (yellow) phases. (a) A hard wall that is wetted by the liquid phase. (b) A soft wall that is partially wetted by the solid phase. The circled areas in red show the regions where the soft wall is wetted by the solid phase - the single line of black particles arises because the circular boundary lowers the hexatic phase.

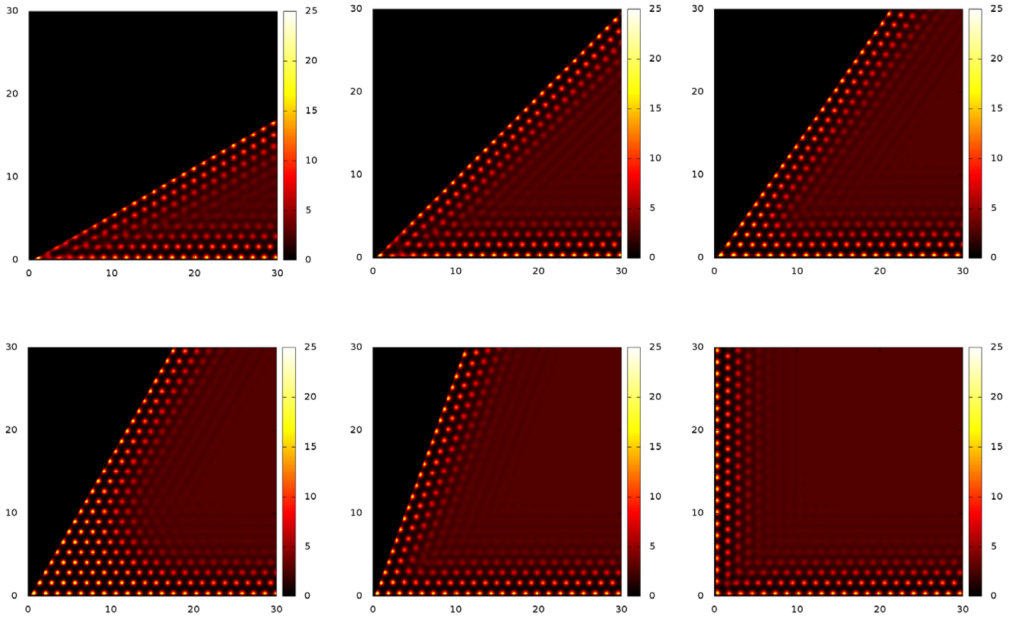

Figure 4.2: Figure from [Archer and Malijevský, 2016]. Shows how the angle of a wedge affects the amount of crystallisation that is promoted by the boundary depending on whether it is commensurate with the crystal lattice. From top left to bottom right, 30 deg, 45 deg, 55 deg, 60 deg, 70 deg, 90 deg.

In this chapter, I will show how I manipulated the shape and material of the boundaries of my experiment to control the wetting of the crystal and liquid phases.

4.2 Original Design

When the experiment was first conceived, a hexagonal aluminium boundary was used. This boundary was designed such that if the dimple spacing is L then the wall is $L/2$ from the outermost line of dimples. The aim of this was to ensure that the space between particles sitting in dimples was the same as between particles sitting in dimples and the wall. In fact, in doing this there is slightly less space between particles in the outermost dimples and the wall than there is between particles. Figure 4.3a explains this schematically. The points where the grey lines meet represent the centres of the dimples, the black circles represent the nitrile particles sitting in the dimples and the black line represents the boundary. The distance between dimples, L, is marked in orange and the distance from the centre of the particle to the wall, $L/2$, is marked in green.

This, however, turned out to be counterproductive as we saw in Figure 3.4 and explained in Figure 3.5 that the crystal phase is rotated 30° relative to the dimples. Figure 4.3b shows how particles in this rotated crystal phase sit in relation to the boundary, the distance between particles, $L\sqrt{3}/2$, is marked in orange and the distance from the centre of a particle to the wall, $L/2$, is marked in green. The walls of the boundary are now rotated 30° with respect to the crystallographic direction, this means that there is now an abundance of space between a crystal and the wall.

This had some unintended consequences when the system was cooled. The extra space means that particles tend to collect around the edges of the cell, in contact with the boundary. These particles in contact with the boundary do not mesh with the rotated crystal phase so exclude the crystal phase from a small region near the boundary. This exclusion effect can be seen in Figure 4.4 where particles have been annotated with the phase of their orientational order parameter. If we look at

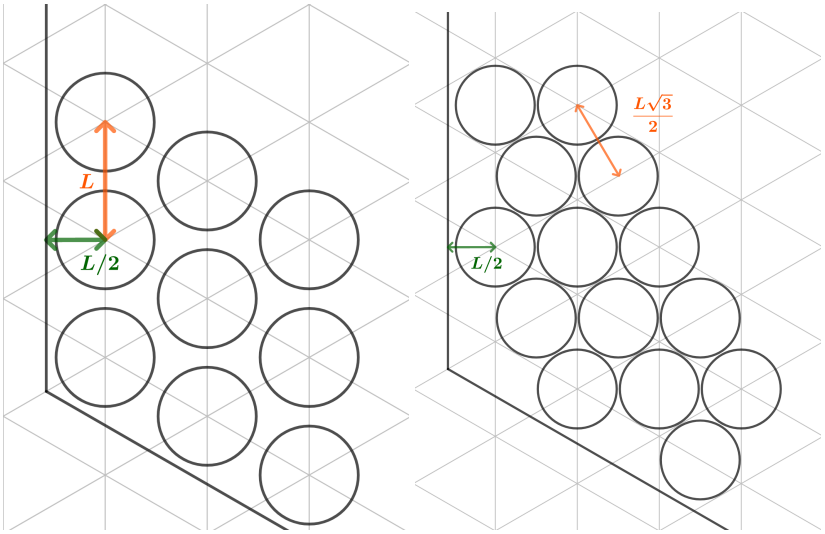

(a) (b)

Figure 4.3: Diagrams to explain the geometry of the original aluminium boundaries. The intersects of the grey lines making up the isometric grid represent the centres of the dimples. (a) Particles sat in dimples near the edge of the boundary showing the motivation for the position of the boundary before knowledge of the rotated crystal phase. (b) Particles sat in the rotated crystal phase near the edge of the boundary which shows the space between the crystal and the boundary that cannot be filled. The distance between neighbouring particles is marked in orange and between particles and the wall in green.

the top-right boundary of the system then we can see a row of cyan particles that mesh with the boundary. These particles (phase 0) cannot mesh with the crystal particles (phase $\pm\pi$) which causes a gap between these two phases, preventing the crystal from forming against the boundary.

The original boundary acted to prevent the formation of the crystal phase against its edges. I'll refer to this behaviour as orderphobic as it is preventing the wetting of the ordered phase. This illustrates that the boundary can either promote or inhibit crystal formation. I will refer to this as orderphillic/orderphobic.

This begs the question of a second type of boundary that helps the formation of the crystal phase which I will refer to as orderphillic as it attracts the ordered phase. The next sections discuss my process of creating an orderphillic boundary and using what I learn to create one that is more strongly orderphobic.

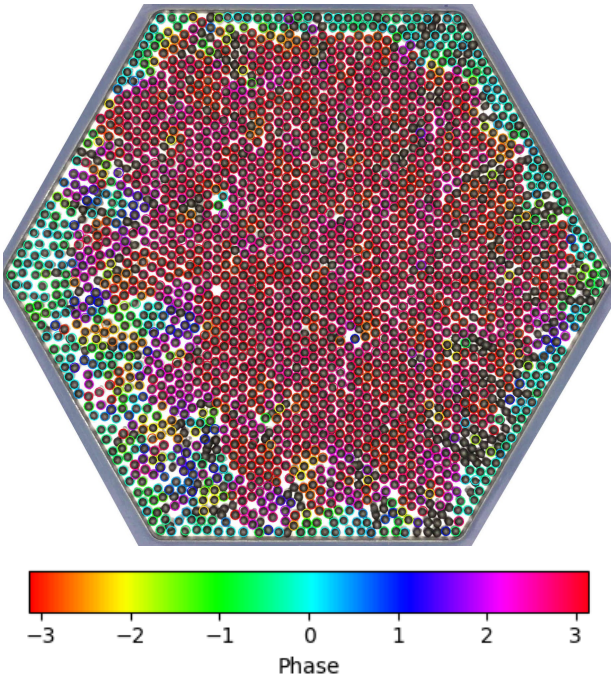

Figure 4.4: Formation of a crystal with the original aluminium boundary. The boundary is "Orderphobic" as it is wetting a crystal phase by encouraging particles to sit along its length, out of phase with the crystal in the bulk of the cell. The colour of the annotated circles represents the phase of the hexatic order parameter.

4.3 Orderphillic - Wetted by the ordered phase

In this section, I describe the iterations of boundaries that were developed in the search for an Orderphillic boundary; one that is perfectly wetted by the ordered phase.

Smooth Shims

The first method that I tried aimed to tightly control the spacing from the boundary to the crystal phase. This was achieved by creating acrylic shims that were laser-cut with a thickness $T = \frac{L}{2} + \frac{L\sqrt{3}}{4}$ such that the distance between the centre of particles in the crystal and the boundary is $\frac{L\sqrt{3}}{4}$. Figure 4.5 shows how the thickness of these shims results in a tighter fit to the crystal phase than in Figure 4.3b. The shims were fixed to the inside edges of the boundary using double-sided tape.

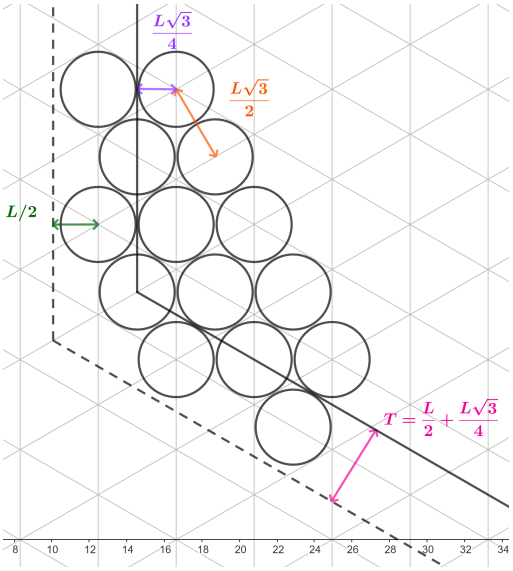

Figure 4.5: Diagram to show how shims were used to move the boundary from the dotted line to the solid line to reduce the distance from particles in the crystal to the edge of the boundary. The thickness, T, of the shims is annotated in pink and the distance to the new boundary is annotated in purple.

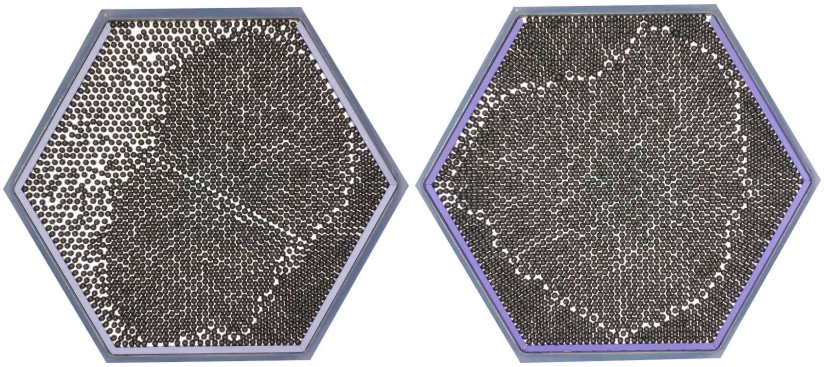

(a) (b)

Figure 4.6: Cooling of a system at two different area fractions. Five out of six of the boundaries are fitted with shims that ensure the crystal phase is tightly confined to the boundary using the geometry in Figure 4.5. The shims have not had the desired effect and have nucleated a closely packed crystal phase that is incommensurate with the central crystal phase and the underlying dimple lattice.

The system was cooled at two different area fractions of 0.76 and 0.86 from an acceleration, Γ, of 2.6 to 1.6 which is shown at $\Gamma = 1.8$ in Figure 4.6. Here, you can see that the edges of the system allow the formation of crystal against their surfaces. However, this crystal is not the same as the bulk crystal in the centre of the cell. Instead, it is a closely packed crystal that has the same orientation as the underlying dimple lattice. However, it is important to note that the spacing is incommensurate with the dimpled lattice.

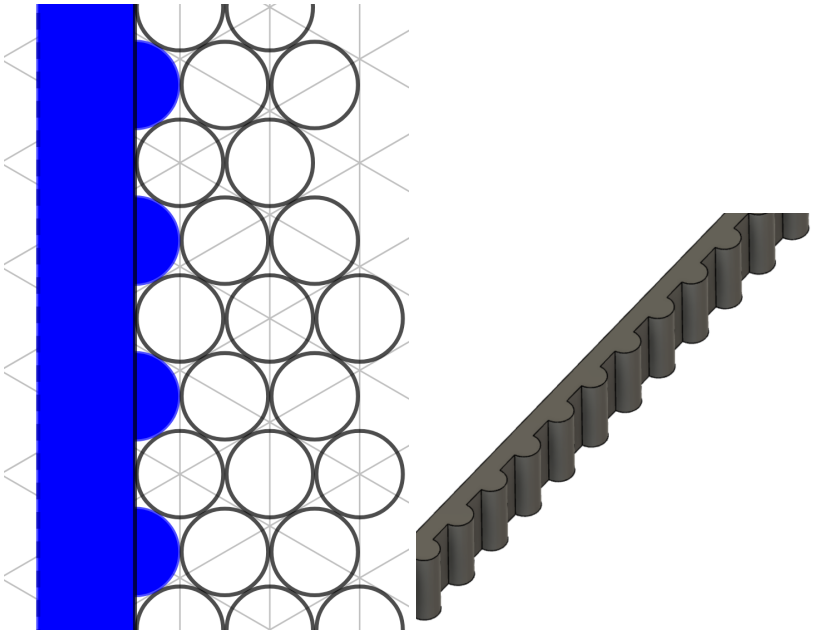

(a) (b)

Figure 4.7: The first orderphillic boundary using a convex geometry. (a) Diagram of the boundary (blue) and how it meshes with the particles (black circles) in the rotated crystal phase. Dimples are located at the crossing points of the grey isometric grid. (b) A 3D render of the boundary which is 3D printed.

While the boundary seems to be wetted by a crystal phase, it is not a phase that existed without the boundary. Perhaps this is due to the fixing method of the boundary as the plastic shims were stuck into place with double-sided tape. This meant that the walls were slightly flexible so might have reduced the coefficient of restitution between the particles and the wall which may have caused some heterogeneous nucleation of the closely packed crystal phase.

Bumpy plastic

I wanted to prevent the formation of the undesirable closely packed crystal and encourage the wetting at the boundaries of the rotated crystal that forms in the centre of the cell. To achieve this I introduced a geometry to the boundaries that was compatible with the desired crystal. Instead of the laser cut shims, 3D printed segments were created which had semi-cylindrical bumps along their inner edge which have the same radius as the particles and are positioned to align with the crystal phase. Figure 4.7 shows a diagram and render of this design.

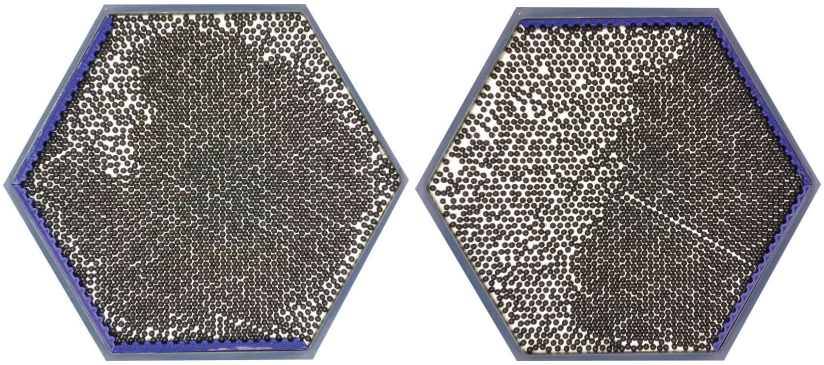

(a) (b)

Figure 4.8: Two examples of cooling trials of 3D printed segments attached on the inside edge of the boundary which aimed to be wetted by the crystal phase. (a) Semi-cylindrical bumps with equal radius to the particles in positions which are commensurate with the crystal phase. The ordered phase forms close to the boundary, but not much evidence of wetting is seen after many repeats. (b) Semi-cylindrical pockets with a radius slightly larger than the particles in the same positions that are commensurate with the crystal phase. Provides much more evidence of wetting.

The system was set up with these 3D-printed boundaries fitted on three adjacent faces of the hexagon. After many repeated cooling experiments it was clear that this was an improvement on the previous design. Now, the ordered phase is not excluded from the boundary as it was before and can form much closer to the boundary. A snapshot of the system after cooling is shown in Figure 4.8a which shows this behaviour.

An alternative design was trialled where the bumps were replaced with pockets of the same shape but slightly larger size to accommodate particles. Figure 4.9 shows a diagram of how this boundary fits with the crystal phase and a render of the 3D print. This produced much more promising results as the new boundary was wetted much more readily by the ordered phase. Figure 4.8b shows a snapshot of the system after being cooled which shows the new boundary being partially wetted by the ordered phase. It has been shown before [Komatsu and Tanaka, 2015] that the wetting of the crystal phase is encouraged by introducing inelasticity at the boundaries. I believe this improved wetting arises from particles being trapped in the pockets at these boundaries in commensurate positions. These particles effectively lower the boundary's coefficient of restitution, encouraging the wetting of the crystal phase.

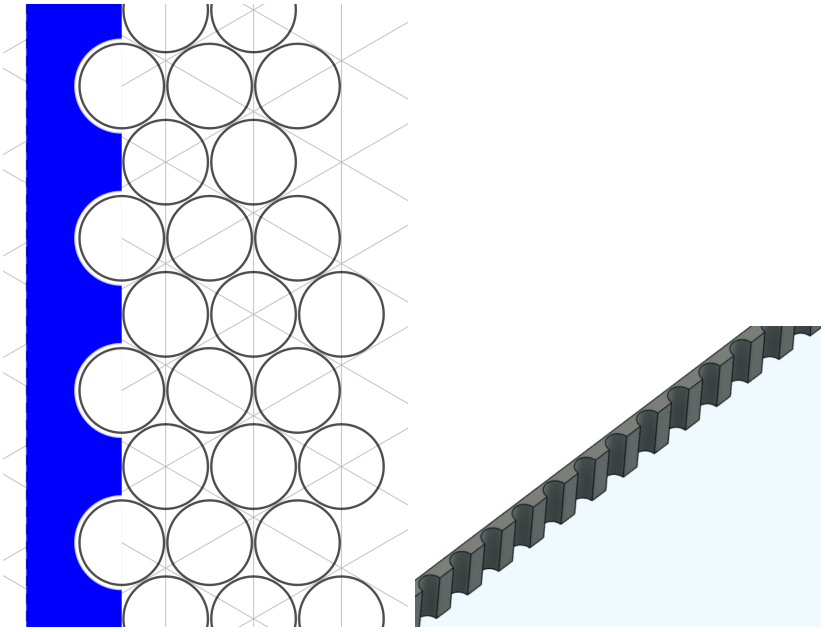

(a) (b)

Figure 4.9: The orderphillic boundary using a concave geometry. (a) Diagram of the boundary (blue) and how it meshes with the particles (black circles) in the rotated crystal phase. Dimples are located at the crossing points of the grey isometric grid. (b) A 3D render of the boundary which is 3D printed.

Final Orderphillic Boundary

There were a few weaknesses with the previous orderphillic boundary using semi-cylindrical pockets. Firstly, the wetting of the crystal phase depended on particles being trapped by the pockets. The probability of this happening was fairly low due to the tightness of the pockets. This means that as the rate of cooling was increased the wetting performance of the boundary was drastically reduced. The second problem was that the wetting performance of the boundaries was extremely sensitive to small changes in their position as it becomes mismatched with the underlying dimpled lattice. As the fixing method had minimal indexing to place it correctly and the double-sided tape used had non-zero thickness, correct placement was quite difficult.

Trapped particles improved the wetting performance of the boundary so to overcome the first problem, the boundary was printed with hemispherical holes in the same positions as the bumps in Figure 4.7. The centre of the holes was placed at a height of 3 mm to account for the estimated average height of the particles above the surface at accelerations where the wetting first occurred. Particles,

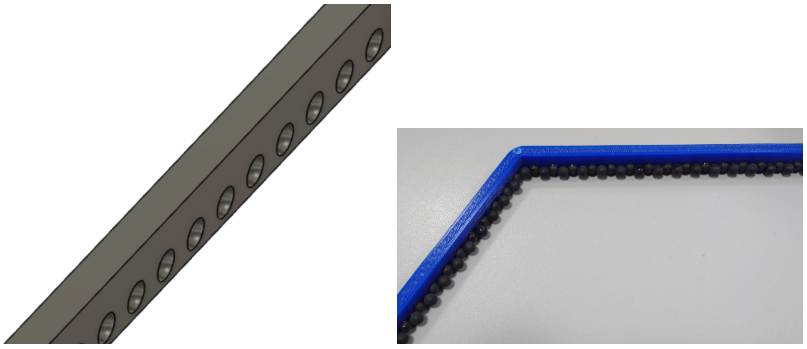

(a) (b)

Figure 4.10: The final orderphillic boundary using pockets which the experiment particles are glued into. (a) 3D render of the boundary showing the pockets for particles which are spaced to be commensurate with the rotated crystal phase. (b) A photo of a section of boundary with the particles glued in place.

like those used in the experiment, were carefully superglued into each of these holes. After initial trials with weak performance, additional particles were glued between every pair of particles, so that the whole boundary was the same material. Figure 4.10 shows a render of the 3D print showing the pockets and a photograph of the boundary with two layers of glued particles in place.

Correct positioning of the boundary also improved the crystal-wetting performance. Fitting separate segments around the boundary inhibited this. To ensure the boundary was always placed correctly, the full boundary was printed to form a single piece, so that it fits perfectly inside the existing aluminium boundary.

To test this boundary the system was initialised with $\phi = 0.82$ by heating the system to $\Gamma \sim 2.6$. At this acceleration, the entire system exhibits a disordered liquid state. The system was then slowly cooled at a rate of $\dot{\Gamma} = 0.0013\,\mathrm{s}^{-1}$. As the system cools the crystal phase sits next to the boundary and grows from the edges of the cell, leaving a disordered region in the centre of the cell. Figure 4.11 shows the system after it has cooled with the orderphillic boundary (coloured in blue) in place.

It is energetically favourable for the crystalline phase to wet the boundary. There are several possible reasons.

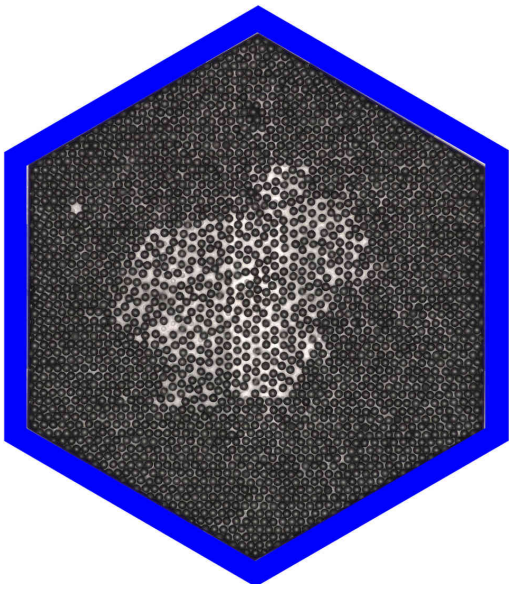

Figure 4.11: The system at an area fraction $\phi = 0.82$ after being cooled from $\Gamma \sim 2.6$ at a rate of $\dot{\Gamma} = 0.0013\,\mathrm{s}^{-1}$. The boundary used is the orderphillic boundary described in Figure 4.10 and is seen to be perfectly wetted by the crystal phase resulting in a region of disorder in the centre of the cell.

Firstly, in a granular system, there is naturally a gradient in granular temperature (mean kinetic energy of particles) from the centre to the edge of the tray near the boundaries [Smith and Smith, 2017]. The granular temperature is reduced at the edges due to inelastic collisions with the boundary which allows more energy to be dissipated at the edges of the system than in the centre. A key difference between equilibrium and non-equilibrium systems is that two coexisting phases can have different granular temperatures. The crystal phase has a lower granular temperature than the liquid phase, so one would expect this to move to the lower temperature part of the cell - near the walls. The gradient is small at high area fractions [Smith and Smith, 2017] but is also influenced by factors such as the relative size of particle:particle and particle:wall coefficients of restitution. It is therefore possible that the behaviour is a result of variations in granular temperature and particle:wall inelasticity.

Another possible explanation is that the wetting is induced by ordering imposed by the boundary i.e. it is an indication of orderphilicity (the effect I am investigating).

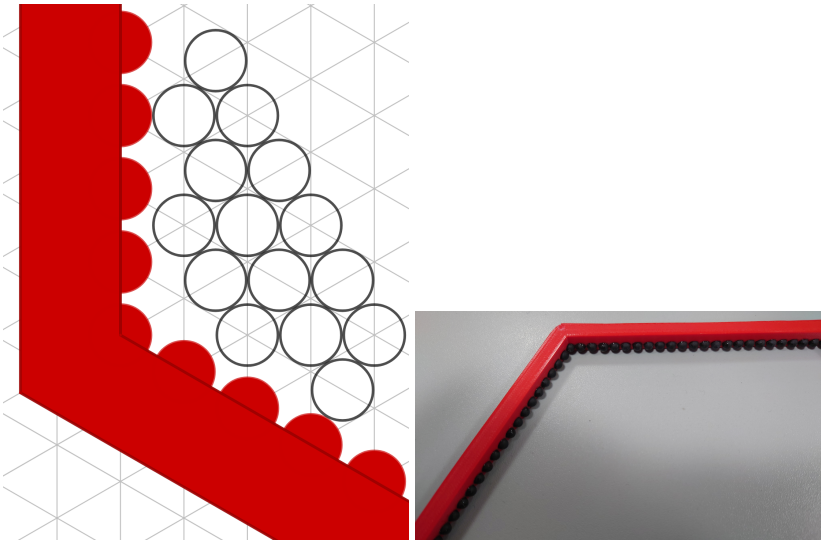

(a) (b)

Figure 4.12: (a) Diagram of the orderphobic boundary (red) showing how it doesn't mesh with the particles (black circles) in the rotated crystal phase. Dimples on the surface are located at the crossing points of the grey isometric grid. (b) A photograph of the boundary with the particles fixed in place.

4.4 Orderphobic - Wetted by the disordered phase

It was not clear whether the influence of inelasticity or the geometry of the orderphillic boundary was greater. To clarify this, we tried to use the knowledge of the geometry to create a boundary which had the opposite effect - one that "repels" the ordered phase and is wetted preferentially by the liquid phase. I will refer to this as an "orderphobic boundary". We hypothesised that geometry may be more important than inelasticity in controlling the wetting of the two phases.

To create the orderphobic boundary, the same general structure is used. However, the particles are placed to register with the positions of the dimples as these positions are not commensurate with the crystal phase that forms rotated 30° to the underlying dimple lattice. Figure 4.12 shows the geometry of the boundary and how it mismatches with the ordered phase, there is also a photo of the boundary with the particles glued in place.

To test the orderphobic boundary, the system was initialised by heating the system to $\Gamma \sim 2.6$ with $\phi = 0.82$. At this acceleration, the entire system exhibits a disordered liquid state. The system was then slowly cooled at a rate of $\dot{\Gamma} = 0.0013\,\mathrm{s}^{-1}$. At $\Gamma \sim 2.0$ a single crystalline domain surrounded by a disordered

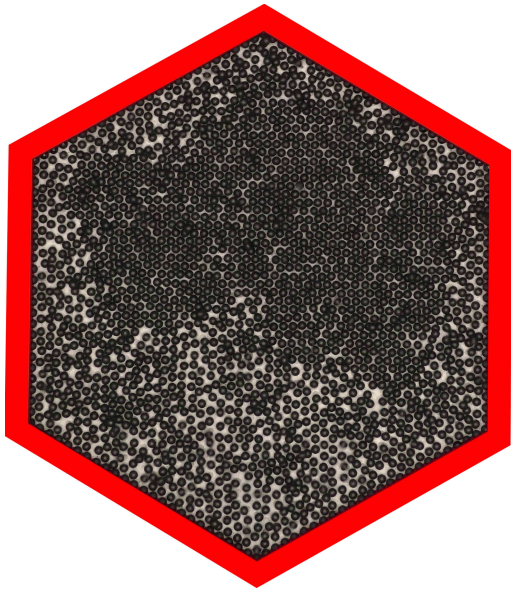

Figure 4.13: The system after cooling with an orderphobic boundary. This shows that the boundary has not been wetted by the crystal phase.

phase suddenly forms. As the system cools further, the crystal grows. Throughout the growth of the crystal, it never wets the boundary and is always separated by a significant region of the liquid phase. A snapshot of the system after it has cooled with the orderphobic boundary is shown in Figure 4.13, here the orderphobic boundary is coloured in red.

It is clear that in this case, the ordered phase prefers the centre of the tray and does not wet the edges. This orderphobic boundary has approximately the same inelasticity as the previous orderphillic boundary, so there should be the same granular temperature gradient across the tray. This confirms that it is the geometry, and not the inelasticity, of both the orderphillic and orderphobic boundaries that control the wetting of the ordered phase. Figure 4.11 and Figure 4.13 emphasise that by carefully choosing the boundary conditions we can control where the crystalline phase forms.

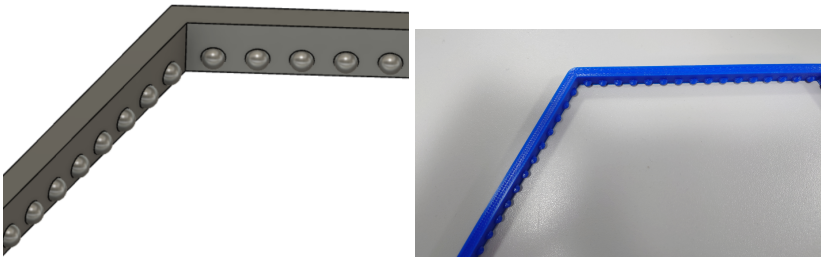

(a) (b)

Figure 4.14: The elastic version of the orderphillic boundary from Figure 4.10 using 3D-printed hemispheres instead of pockets. (a) A 3D render. (b) A photograph of the 3D print.

4.5 Elastic Orderphillic Boundary

Our results show that it is geometry and not elasticity that causes the crystal to wet the orderphillic boundary. However, does the orderphillic nature of the boundary arising from geometry also require the material to be inelastic? To test this, I recreated the final orderphillic boundary but replaced the holes with 3D-printed hemispheres, which can be seen in Figure 4.14.

This elastic orderphillic boundary was then tested using the same method as before. The system was initialised with $\phi = 0.82$ by heating the system to $\Gamma \sim 2.6$. At this acceleration, the entire system exhibits a disordered liquid state. The system was again slowly cooled at a rate of $\dot{\Gamma} = 0.0013\,\mathrm{s}^{-1}$. As the system cools the crystal phase sits next to the boundary and grows from the edges of the cell, leaving a disordered region in the centre of the cell.

The results at the experiment's lowest acceleration are shown in Figure 4.15. Here, the orderphillic boundary has been perfectly wetted by the ordered phase and looks very similar to the inelastic case in Figure 4.11. This provides additional confirmation that the geometry is more important than the inelasticity for the wetting of the boundaries.

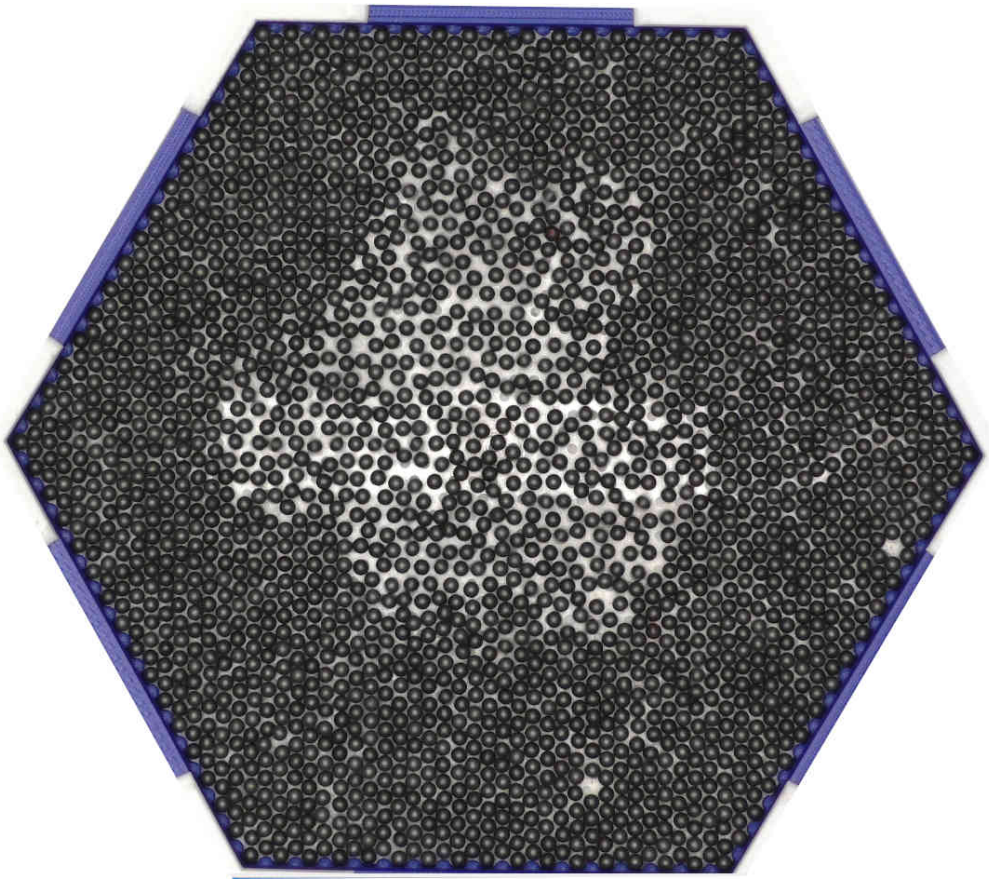

Figure 4.15: Results of cooling with the elastic orderphillic boundary showing perfect wetting by the crystal phase. This shows that for the nitrile particles, the geometry of the boundary is more important than the inelasticity.

4.6 Investigating particle elasticity

The black nitrile particles used in these experiments are extremely inelastic ($e \sim 0.1$). To further test whether the geometry or the inelasticity of the particles is having a greater effect I repeat the same experiment with some more elastic polypropylene particles ($e \sim 0.6$) but using the same orderphobic boundary. Figure 4.16 shows the results of cooling the polypropylene particles in the nitrile orderphobic ring. Upon cooling, a crystal phase with the same lattice parameters still forms. A competition is observed between the frustration of the crystal in the particle layers immediately adjacent to the boundaries and a tendency for the liquid phase to separate to the middle of the experiment. This occurs no matter how slowly the system is cooled, so is not a kinetically trapped configuration but a non-equilibrium steady state.

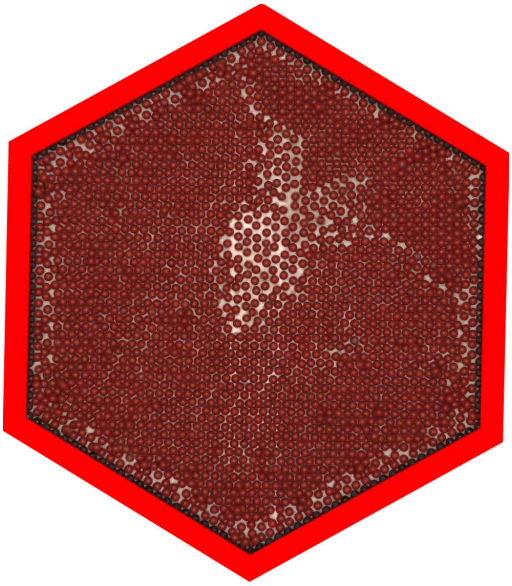

Figure 4.16: Results of cooling elastic polypropylene balls with the inelastic orderphobic boundary in place. Here, the crystal phase collects at the boundary but doesn't mesh with it. This is because the coefficient of restitution between particle and wall is much lower than between pairs of particles. This shows that for elastic particles, the inelasticity of the boundary dominates.

In a quasi-2D granular experiment, energy enters the system through particles interacting with the vibrating base. At large area fractions, energy is predominantly transferred and dissipated through interparticle (e_{pp}) and particle-wall collisions (e_{pw}), rather than advection [Smith and Smith, 2017]. In Figure 4.16 $e_{pw} \ll e_{pp}$, therefore the dissipative energy flux near the wall is larger than in the centre of the experiment, creating a gradient in the granular temperature from cold at the edges to hot in the centre. Since the higher-density crystal phase has a lower granular temperature, this forms at the edge, only frustrated in the first few layers by the structure of the system boundary.

In contrast, when using the nitrile balls the edge is preferentially wet by the liquid phase. Here, $e_{pw} \sim e_{pp}$ resulting in a more spatially uniform dissipation. This enables the boundary structure to control the location of the different phases. The orderphillic boundary in Figure 4.11 confirms this theory as both the elasticity and the structure support the wetting of the ordered phase, reversing the spatial phase separation that occurred in Figure 4.13. There is therefore a subtle interplay of the boundary geometry and the temperature gradient. If the gradient is kept small enough then the geometry can control the wetting.

4.7 Combined Orderphillic and Orderphobic

To further confirm our understanding of the role of the boundary structure, I created a hybrid boundary where three sides (red) promote disorder and the remaining sides (blue) promote order. A photograph of this boundary is shown in Figure 4.17. As the system is cooled, the crystalline phase nucleates at the orderphillic boundary and grows to fill the orderphillic half of the cell. As the system cools further such that a significant portion of the cell is crystal, the edge of the liquid-crystal interface is strongly pinned to the two points on the boundary which divides the two halves. Snapshots of the system after it had cooled are shown in Figure 4.18. Two different rotations of the boundary confirm that the behaviour is caused by the geometry of the boundary and not the level of the system.

As this boundary breaks the symmetry, it could not be used to level the system using the methods described in Chapter 2. To get around this, the system was levelled using the orderphillic boundary before the boundaries were carefully swapped. This is the procedure that I follow in any experiment which uses an asymmetric boundary.

4.8 Conclusions

In this section, I've shown that I can use the geometry of the boundaries to finely control the positions of the ordered crystal and disordered liquid phases. The main results of this chapter are summarised in Table 4.1. This control will allow me to perform better quantitative analysis that I will demonstrate in Chapter 5 as I can use the orderphobic boundary to prevent heterogeneous nucleation from skewing my results. I can also use the knowledge of how different geometries are wet to create intruders that I use to investigate an effect known as the orderphobic effect in Chapter 6.

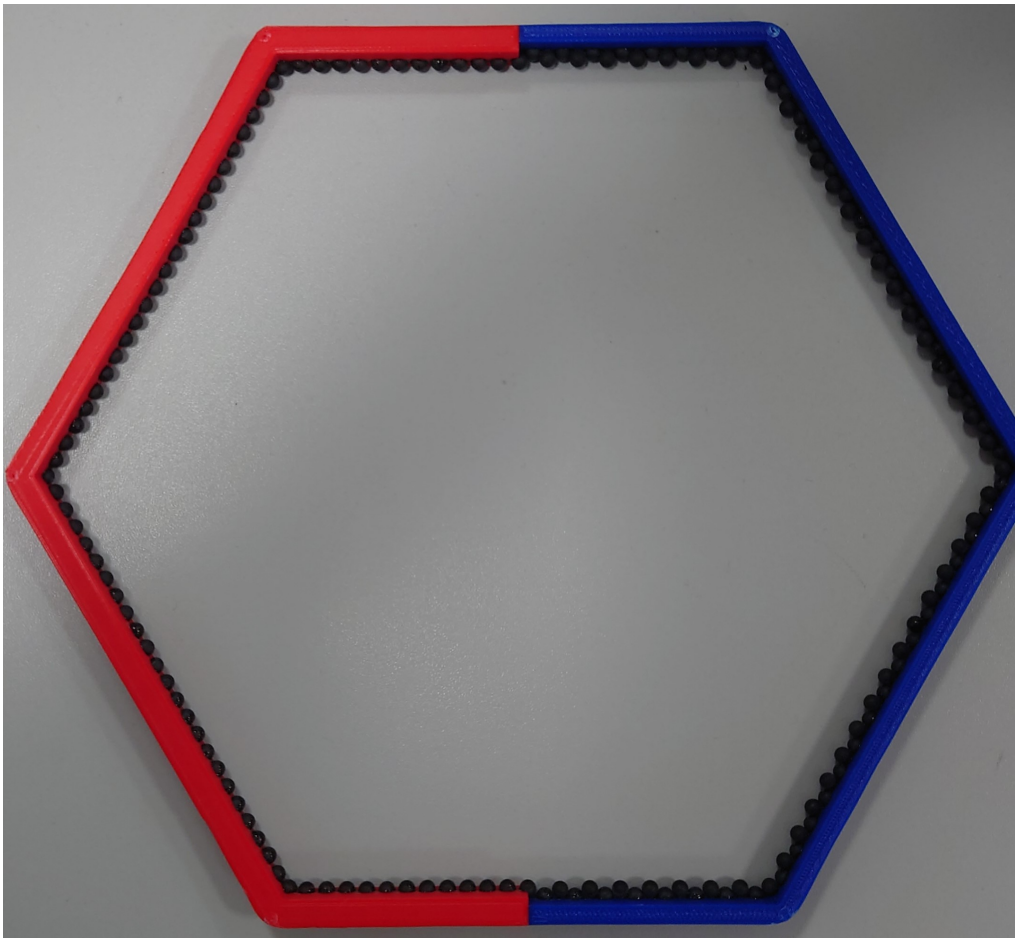

Figure 4.17: Photograph of the boundary where one half (red) is orderphobic like in Figure 4.12 and the other half (blue) is orderphillic like in Figure 4.10.

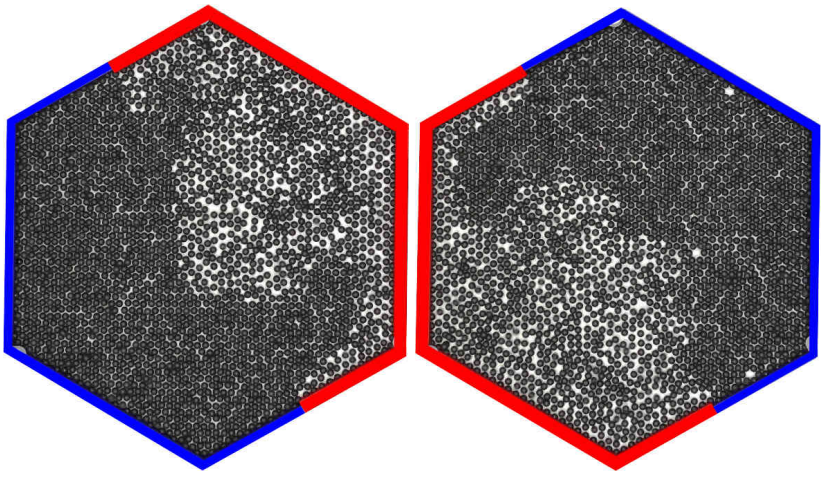

(a) (b)

Figure 4.18: Snapshots of the system after cooling with the 50/50 orderphobic/orderphillic boundary. The boundary is rotated on the system to show that the effect is caused by the geometry of the boundary and not the level of the system.

	Orderphobic Boundary	Orderphillic Boundary
Inelastic particles and inelastic boundaries.	Figure 4.13. Single crystal in the centre of the cell, surrounded by the liquid phase.	Figure 4.11. Single crystal in contact with the boundary, surrounding the liquid phase in the centre of the cell.
Inelastic particles and elastic boundaries.		Figure 4.15. Same as above.
Inelastic boundaries and elastic particles.	Figure 4.16. Crystal around the edges of the cell, but has a gap of disorder between the crystal and the boundary. The bulk of the liquid sits in the centre of the cell.	

Table 4.1: A summary of the main results in Chapter 4.

Chapter 5

Evidence of a First-order Phase Transition

In Chapter 3, I showed some initial findings that the dimpled surface with a lattice spacing of 4.80 mm ($L/D = 1.2$) produced behaviour that suggested that the liquid-to-crystal phase transition was first order. In this chapter, I will demonstrate quantitative evidence that the transition is first-order. To achieve this, I will use the knowledge of the boundaries from Chapter 4 to control the wetting of the phases to facilitate better analysis.

5.1 Coexistence

The presence of coexistence where there is a clear boundary between the liquid and crystal phases shows that the crystal phase exhibits surface tension. This surface tension is evidence that the liquid-to-crystal phase transition is first order.

I start by revisiting the qualitative observations that I introduced in Chapter 3. First, a coexistence between a liquid-like and crystal-like phase was observed in Figure 3.4. The crystal-like phase was oriented such that its lattice was rotated 30° from the underlying dimpled lattice and had a smaller spacing such that alternative particles along a single direction sat in the dimples as seen in the diagram in Figure 3.5.

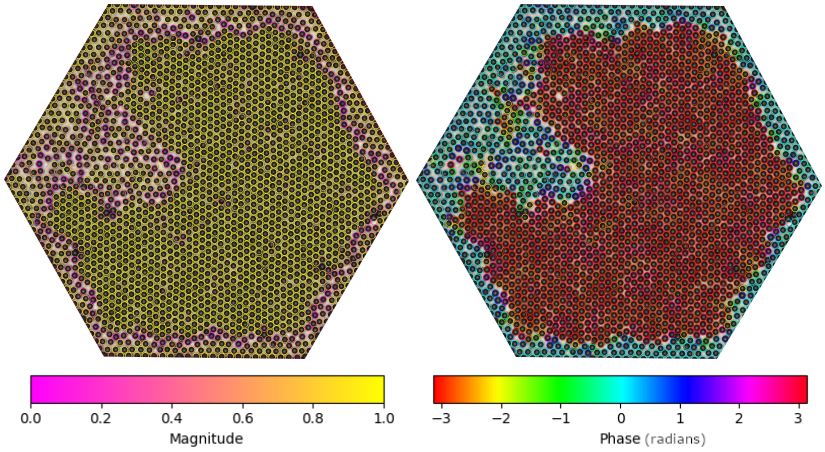

(a) (b)

Figure 5.1: An example of coexistence between a liquid and a solid at an area fraction of 0.66 and at $\Gamma = 1.3$. (a) Shows the magnitude of the hexatic order parameter. (b) Shows the phase of the hexatic order parameter.

This coexistence can be clearly seen by calculating the hexatic order parameter, ψ_6, and annotating an image with coloured circles representing the magnitude and phase of ψ_6 which is shown in Figure 5.1. By considering the phase and magnitude of ψ_6 we can clearly see that the liquid phase where individual particles have low magnitude and no phase correlations between nearby particles. The crystal phase can be clearly seen where individual particles have high magnitude and high phase correlations between nearby particles.

The coexistence between two phases with distinctly different properties is a clear sign of a first-order phase transition. If we revisit the discussion in Section 1.1 we remember that phase coexistence is only possible in a first-order phase transition, as the system can reduce its free energy by splitting into multiple phases. This is in contrast to a continuous phase transition where phase coexistence is not possible and the transition occurs through continuous changes in the system's properties.

Another concept that relates to coexistence that only exists in first-order phase transition is that of nucleation and growth. When a system in one phase is cooled in a first-order system until the other phase is more stable, it remains in the now metastable state until a region of the other phase is nucleated. Once this nucleated crystal reaches a critical size, it begins to grow. Figure 5.2 shows the nucleation of a stable crystallite that grows as the system is cooled from $\Gamma = 2.0$ to $\Gamma = 1.8$

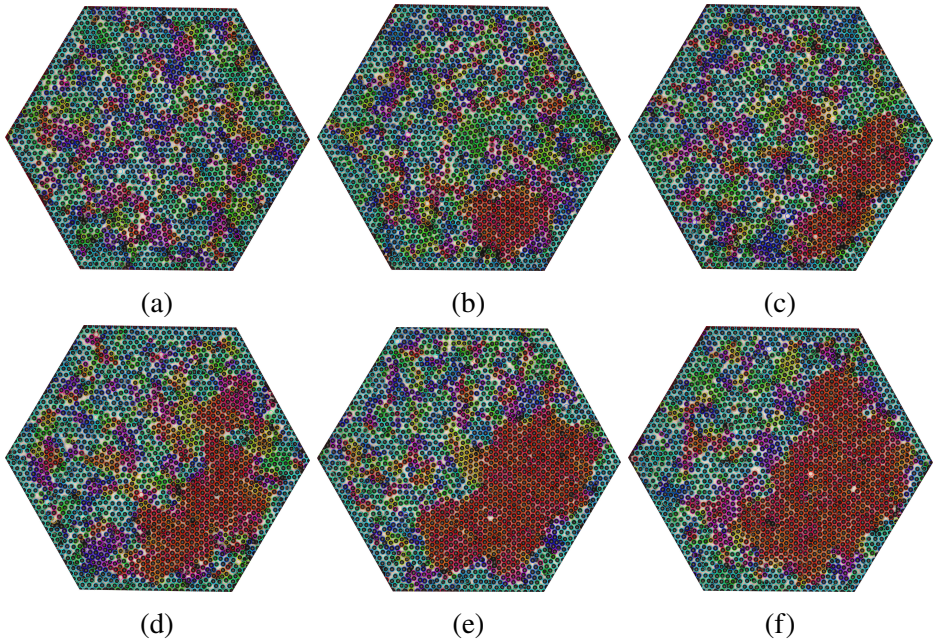

Figure 5.2: An example of the nucleation and growth of a crystal as the system cools from (a) $\Gamma = 2.0$ to (f) $\Gamma = 1.88$ at an area fraction of 0.66.

at an area fraction of 0.66. What cannot be seen in this figure is that before this crystal nucleates, smaller crystallites fluctuate into and out of existence until one forms the crystallite seen in this figure. These fluctuating crystallites can be seen more clearly in Supplemental Movie 1.

5.2 Hysteresis

Hysteresis is a phenomenon in which the change in order (melting/freezing) of a system lags behind the temperature change that causes it. A common example of hysteresis that is a close analogy to my system is the melting of ice where hysteresis can be observed in the temperature of the ice as it melts. When heat is added to the environment, the temperature of the ice does not immediately increase. Instead, the temperature of the ice remains constant while the heat energy is used to break the bonds between water molecules. Once all the bonds between water molecules have been broken and the water is completely liquid, the temperature can then rise. The energy required to melt the ice is the latent heat. Specifically, latent heat is the energy absorbed or released by a substance during a phase change without a change in temperature.

If hysteresis is present in the liquid-to-crystal transition in my system then it would show as a gap between the heating and cooling curves in plots of the global hexatic order parameter, Ψ_6. If hysteresis is observed then it would suggest that there is a latent heat required to melt the crystal, indicating a first-order phase transition [Selinger, 2015]. Latent heat is an indicator of a first-order phase transition because it represents the energy required to move through the discontinuous change that only exists in a first-order phase transition.

For an equilibrium system the hysteresis would also be expected to increase with the cooling rate. This is because there is an energy barrier associated with changing phase and the probability of a particle having the required energy to overcome this barrier is fixed by the Boltzmann factor. Therefore, the longer the system sits at a certain temperature the higher the likelihood of a particle reaching the required energy to overcome the barrier. If the cooling rate is increased, the particle sits at each temperature for less time, so has a lower probability of reaching the required energy. While this description is for an equilibrium system, it should also extend to describe non-equilibrium scenarios.

An experiment at an area fraction of 0.66 was set up using the orderphobic boundaries. These boundaries are used to prevent the nucleation of crystals at the edges of the cell, which could affect the amplitude at which the ordering starts.

The system was initialised at an amplitude of $\Gamma = 2.6$ and cooled at several different rates to $\Gamma = 1.3$ before heating back to the original amplitude at the same rates. For each cooling rate, the experiment was repeated 5 times and the average order parameter for discrete steps of duty cycle corresponding to acceleration steps, $\Delta\Gamma = 0.01$ was calculated. The average order parameter of the system was calculated by excluding a small region of particles near the edges of the cell which is annotated as the green dotted line in Figure 5.3 which shows the system at high and low accelerations. The size of the exclusion region was chosen to coincide with the edges of the liquid domain once the system was fully cooled. Excluding these particles around the edge is important as the values of their order parameters are affected by their proximity to the edge.

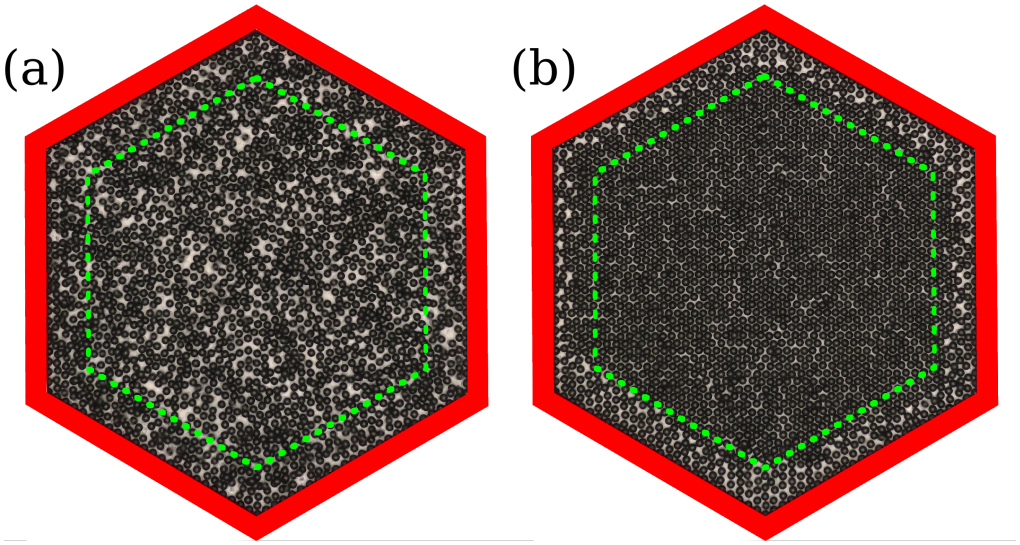

Figure 5.3: Shows the acceleration of the system used for hysteresis calculations at (a) $\Gamma = 2.4$ and (b) $\Gamma = 1.7$. Only particles inside the green dashed line were used for calculations of the global order parameter as it avoids any effects from the boundary.

The results are plotted in the graph of Figure 5.4 for rates of $\dot{\Gamma}$ = (a) 0.0013 s^{-1}, (b) 0.0026 s^{-1} and (c) 0.0052 s^{-1} showing the cooling (blue circles) and heating (red diamonds) where the shaded regions show the standard deviation of the absolute order parameter between the 5 different runs of the experiment. As one heats and cools, the curves do not sit on top of each other. This difference, or hysteresis, increases as the cooling rate increases. Faster rates were not included because they caused the system to quench.

This demonstration of hysteresis provides evidence of latent heat which is indicative of a first-order phase transition as the hysteresis increases with the cooling rate as expected.

The observation of hysteresis suggests a first-order phase transition for the particles on the dimpled plate. However, one cannot be certain based on this data alone that the origin of this first-order transition is the dimpled plate. Komatsu et al. also observed first-order behaviour in a quasi-2d granular experiment [Komatsu and Tanaka, 2015]. They concluded that the use of highly inelastic particles can create first-order behaviour. Our experiments also use inelastic particles, so this is an important consideration. Does the hysteresis arise from particle inelasticity

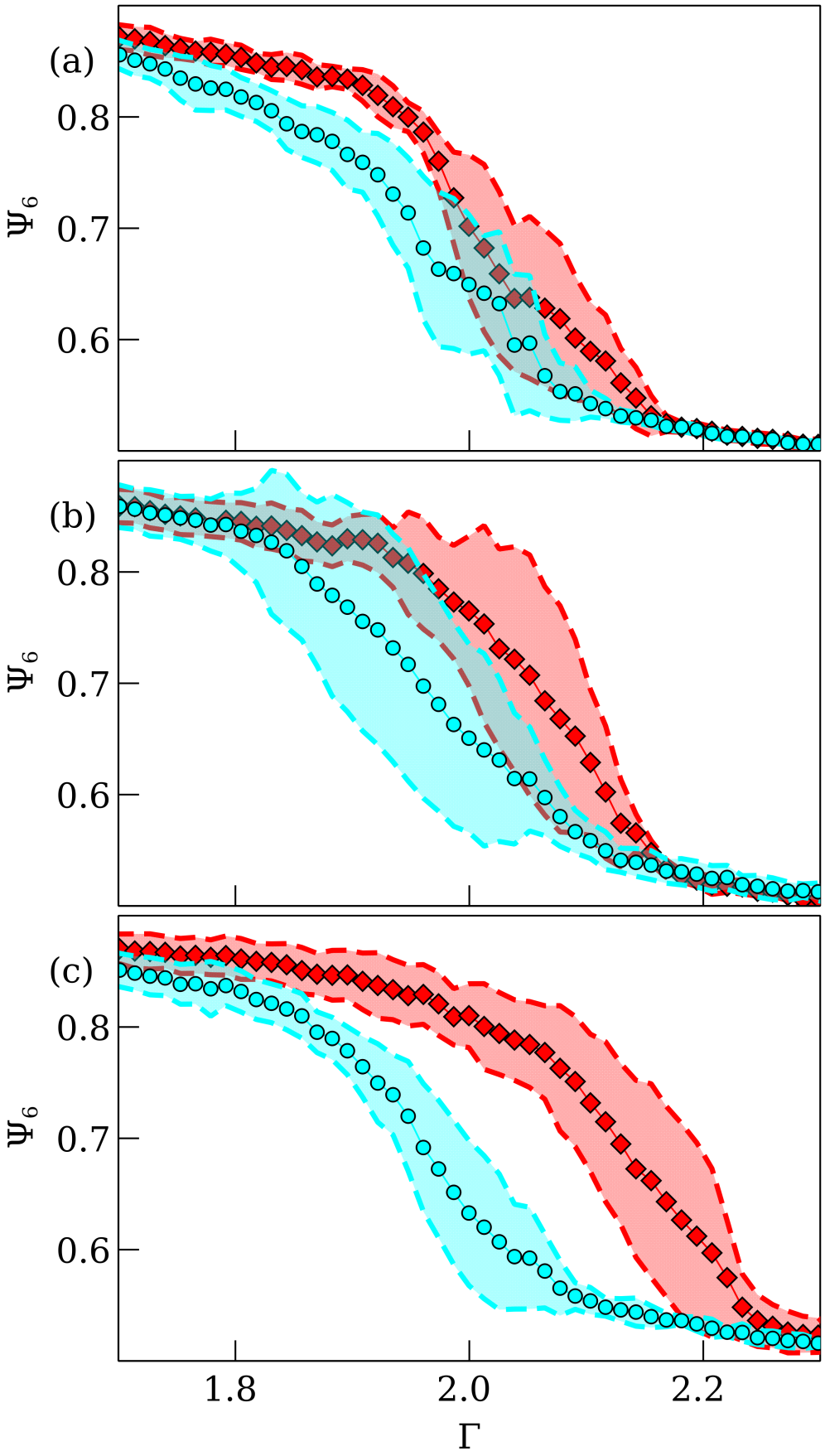

Figure 5.4: Hysteresis of the hexatic order parameter on a dimpled plate for cooling and heating rates of $\dot{\Gamma}$ = (a) 0.0013 s^{-1}, (b) 0.0026 s^{-1} and (c) 0.0052 s^{-1}. This shows an increase in the size of the hysteresis loop with an increasing cooling/heating rate.Shaded regions show the standard deviation between 5 repeat experiments.

or is it caused by the surface dimples? To answer this question we compared the behaviour of the same particles on surfaces, with and without dimples. If the hysteresis is due to the dimples it should disappear for experiments on the flat plate.

For the flat plate experiments, the plate was sandblasted to provide roughness in the same way as the dimpled plate. The roughness helps convert the vertical motion of the plate to the lateral translation of the particles. The same experiments as before were repeated for rates of $0.0026\,\mathrm{s}^{-1}$ and $0.0052\,\mathrm{s}^{-1}$. Higher rates again caused the system to quench too quickly. Figure 5.5 show images of the system at high and low amplitudes and plots of the average order parameter for the two different cooling rates. In these graphs, the red heating curve is slightly above the blue cooling curve but the errors of the curves overlap. This suggests that the hysteresis if it exists at all is very small. It clearly indicated that the first-order transition is strongly influenced by the dimples.

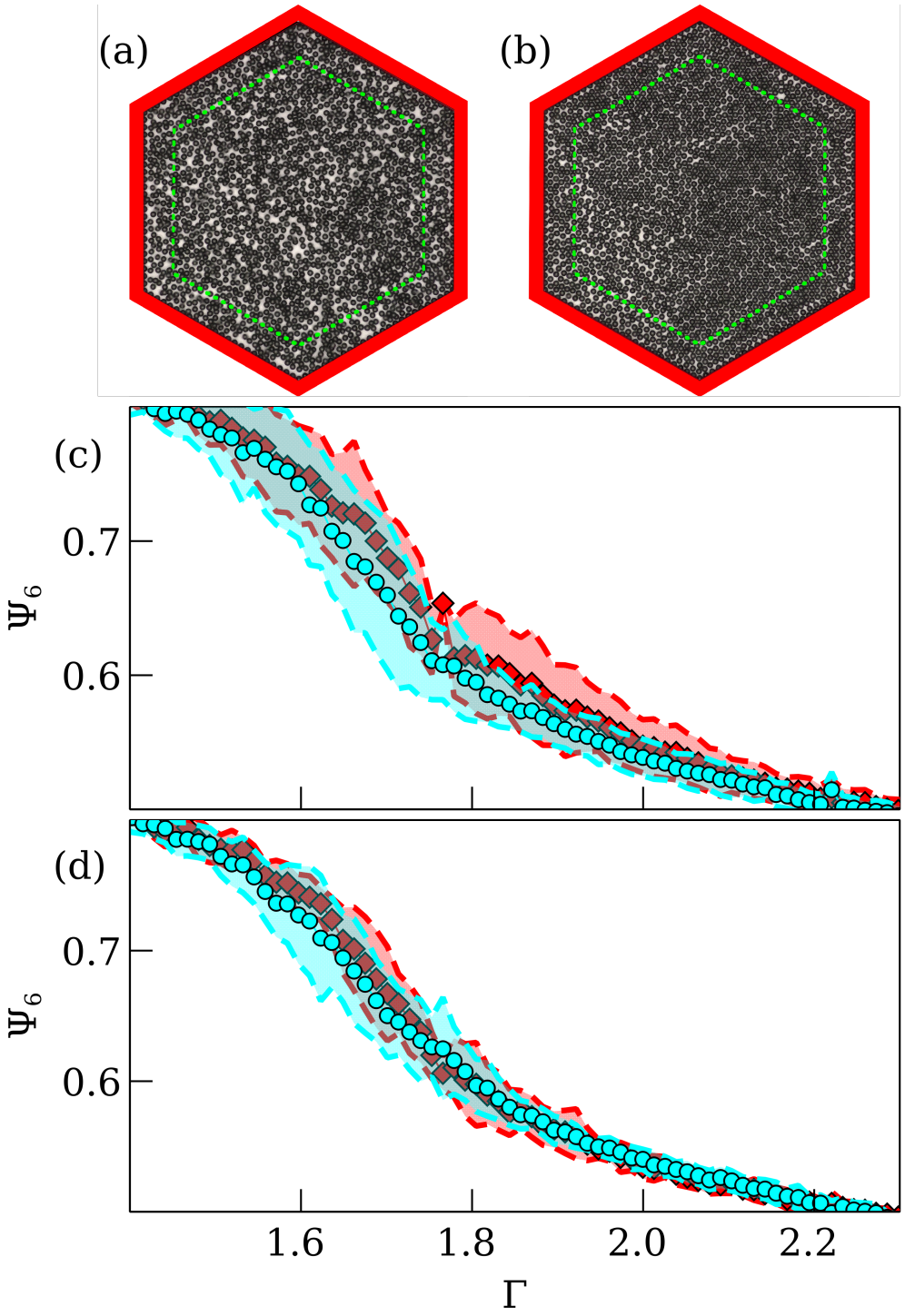

Figure 5.5: Demonstrating the absence of hysteresis while moving through the liquid-solid phase transition on a flat plate. (a) High Γ starting condition for the system. (b) Low Γ end position of the system, Only particles inside the green line are considered for analysis. (c, d) Cooling (blue circles) and heating (red diamonds) curves for a cooling rate of $\dot{\Gamma}$ = (c) 0.0026 s^{-1} and (d) 0.0052 s^{-1}. Shaded regions show the standard deviation between 5 repeat experiments.

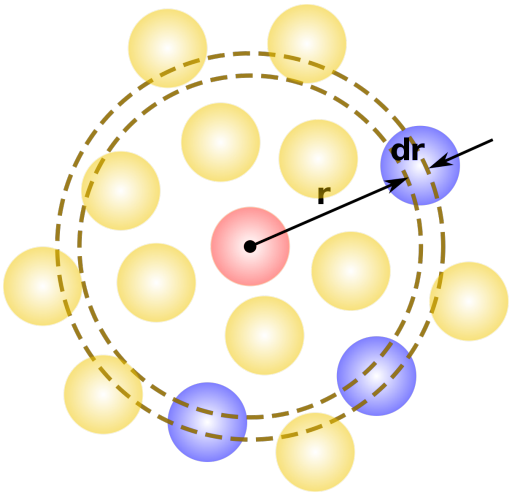

Figure 5.6: Figure from [Wiki47222, 2017]. Shows the annulus construction used to calculate $g(r)$.

5.3 Correlations

Whilst our results thus far suggest a first-order phase transition, it is still unclear whether the transition is a single first-order phase transition from liquid to solid as in three dimensions or a two-step transition through an intermediate hexatic phase with a first-order hexatic-liquid transition described by [Bernard and Krauth, 2011]. To test this we can test for the presence of the hexatic phase by measuring when the spatial correlations for orientational and positional order change from power law to exponential decay.

The spatial correlation for the position, commonly known as the pair correlation function $g(r)$ is given by

$$g(r) = \frac{A}{2\pi r \Delta r N(N-1)} \sum_{j \neq k} \delta(r - |\vec{r_{jk}}|), \tag{5.1}$$

which describes the ratio of the average number density of particles between r and $r + \Delta r$ to the average number density of the system N/A. Here N is the total number of particles and A is the area of the cell. For each value of r this function simply takes the ratio of the number of particles in the annulus $[r, r + \delta r]$ to the expected number of particles in an equivalent area. This is demonstrated in Figure 5.6 which shows the particles that are in the annulus (blue) for the reference particle (red). It is simply a measure of the probability of finding a particle at a distance r from a reference particle.

A maximum value of r is chosen r_{max} such that only particles that are r_{max} from the boundary of the system can be used as starting positions for the particles j. This maximum value needs to be chosen such that a reasonable number of particles remain in the calculation and the factor $N-1$ needs to be adjusted to the number of particles used for the calculation.

The spatial correlation for the orientational order $g_6(r)$ is calculated in much the same way but is weighted by the correlation of each pair of particles order parameters $\psi_6^j \psi_6^{k*}$ and is given by

$$g_6(r) = \frac{A}{2\pi r \Delta r N(N-1)} \sum_{j \neq k} \delta(r - |\vec{r_{jk}}|) \psi_6^j \psi_6^{k*}. \tag{5.2}$$

The type of phase transition is determined by determining how the positional and orientational orders decay. KTHNY theory predicts for a 2D liquid-to-crystal phase transition that in the solid phase, $g_6(r)/g(r)$ should decay slower than $r^{-1/4}$ and $g(r)$ should decay slower than $r^{-1/3}$. In the hexatic phase, the algebraic decay of $g_6(r)/g(r)$ should remain while the decay of $g(r)$ should become exponential. Finally, in the liquid phase, the decay of $g_6(r)$ should also become exponential. Therefore, the accelerations at which the two correlations decay represent the liquid-hexatic and the hexatic-solid transition points.

To calculate the correlations for my system, the dimpled plate was initialised at an area fraction of 85% and dimensionless acceleration $\Gamma = 2.3$. The system is then slowly cooled and data is recorded at discrete accelerations. Figure 5.7 shows the spatial and orientational correlations plotted for several different accelerations as the system is cooled. The orange lines on each graph indicate algebraic decay.

An $r_{max} = 10s$ was chosen where s is the spacing between particles in the crystal as this was deemed to be a reasonable compromise resulting in around 40% of particles being used as origin particles in the experiment. It can be seen that the correlations in Figure 5.7 for $\Gamma = 2.2$ decay faster than algebraic and the correlations for $\Gamma = 1.2$ decay slower than algebraic decay showing that both the positional and orientational correlations have changed from short-range to long-range. It can also be seen that both the correlations change from exponential to a power law decay between $\Gamma = 2.1$ and $\Gamma = 1.8$.

(a) $\Gamma = 2.2$ (b) $\Gamma = 2.1$

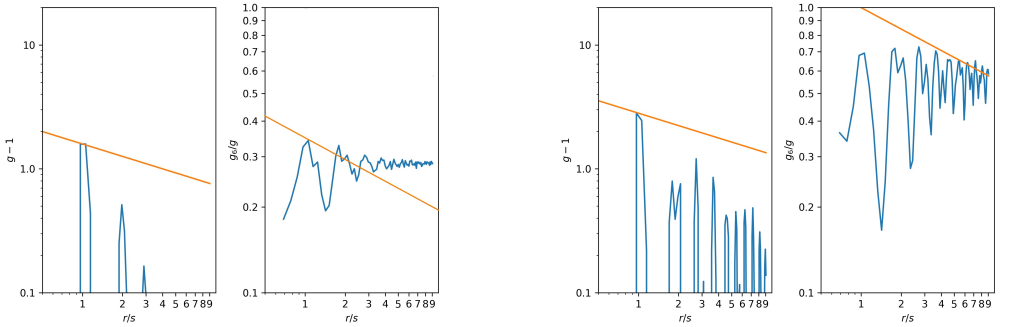

(c) $\Gamma = 1.8$ (d) $\Gamma = 1.6$

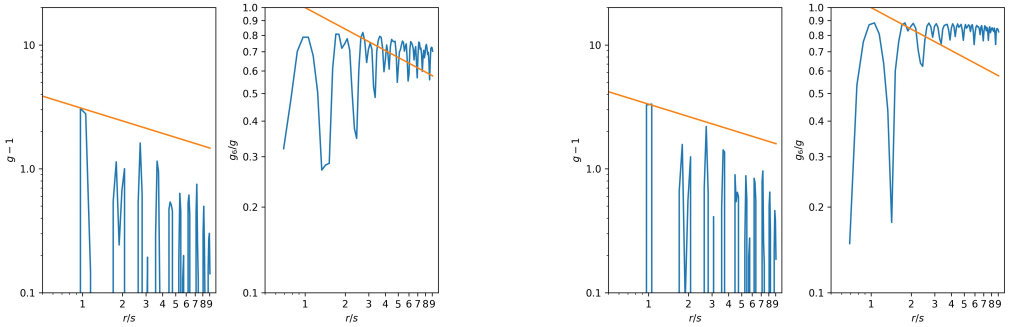

Figure 5.7: This shows correlations for the dimpled system at an area fraction of 0.85. Correlations $g(r) - 1$ and $g_6(r)/g(r)$ as a function of the distance r/s where s is the nearest neighbour spacing of particles in the crystal. The correlations are shown at 4 different accelerations as the system is cooled from $\Gamma = 2.2$ to $\Gamma = 1.2$. The orange lines are guides for the eye and in the $g(r)$ plots represents $r^{-1/3}$ and in the $g_6(r)$ plot represents $r^{-1/4}$.

With such a short value of r_{max} it is difficult to distinguish whether a power law or an exponential decay fits the peaks of the data better. If the correlations for orientational and positional order do change from power law to exponential decay at the same time then this would infer that there is no hexatic phase and the phase transition is a single step first-order from liquid to solid. However, it could still be possible that these transitions happen at different values of Γ between 1.8 and 2.1. To resolve this, it would be desirable to have a much bigger system which would allow larger values of r_{max} that would enable a much larger range of values that could be used to test the fit.

It is also debatable whether this analysis should be done in systems that exhibit coexistence despite it being a common method [Han et al., 2008]. At low accelerations, there is a large crystal surrounded by liquid. Particles near the centre of the crystal further than r_{max} from the edge will add large contributions to $g(r)$ from neighbouring particles that are also in the crystal. Whereas a particle in the crystal that is much closer to the edge will add smaller contributions to $g(r)$ from neighbouring particles in the liquid phase.

5.4 Susceptibility

In experiments, finite size and time effects can introduce ambiguities in the results from calculations of the correlations [Han et al., 2008]. Co-existing crystal and liquid phases can also result in a power-law decay that mimics a hexatic phase [Gribova et al., 2011]. To avoid these difficulties, I measured the susceptibility of the translational and orientational order parameters. It has been shown that these parameters are much less affected by finite-size effects [Sun et al., 2016].

The orientational (translational) susceptibilities are defined as

$$\chi_{6(T)} = \langle|\Psi^2_{6(T)}|\rangle - \langle|\Psi_{6(T)}|\rangle^2, \tag{5.3}$$

where

$$\Psi_{6(T)} = \sum_n \psi_{6(T))} \tag{5.4}$$

is the average orientational (translational) order parameter of the system. The susceptibility characterises the size of the fluctuations in an order parameter and exhibits a maximum at a phase transition. If our system is a one-step first-order transition then one would expect the orientational, χ_6, and translational, χ_T, susceptibilities to have a peak at the same Γ. In contrast, a two-step transition would have peaks for χ_6 and χ_T at different values of Γ. The peak for χ_6 would correspond to the hexatic-liquid transition as the orientational order is destroyed whereas the peak for χ_T would correspond to the solid-hexatic transition as the positional order is destroyed.

To test these hypotheses on the dimpled plate the system is slowly cooled from $\Gamma = 2.3$ to $\Gamma = 1.2$. Vector plots of the orientational (a, c, e) and translational (b, d, f) order parameters are plotted in Figure 5.8 as the system is cooled. The length of the vectors in the orientational order are the magnitude of the orientational order, where longer arrows represent a more ordered configuration. The angle and colour are related to the orientation of the measured hexagonal order. The length of the translational order vector is always 1, while the angle and colour represent the degree of translational order, such that $\pm\pi$ corresponds to particles positioned at the expected lattice points of the crystal. Plotting the vector field allows us to visually compare changes in the spatial correlations.

If we consider the system at high amplitude ($\Gamma = 2.0$) then we can see that the system is in a liquid state as there are no obvious spatial correlations in either the orientational order or translational order Figure 5.8e,f. As the system is cooled further a large area of the orientational and translational vector fields suddenly become spatially correlated, indicating a formation of a crystalline nucleus which can be seen at $\Gamma = 1.9$ in Figure 5.8c,d. This nucleus remains stable and fluctuations in its shape and size remain synchronised both spatially and temporally in both order parameters (see Supplementary Movie 1). This synchronisation between the orientational and positional order persists as the crystal grows which suggests that the two types of order are strongly tied together. This is compelling evidence that the dimpled surface results in a first-order transition from liquid-solid without an intervening hexatic phase as the hexatic phase requires the two types of order to become disconnected.

These results are confirmed by analysing the susceptibilities which characterise the size of fluctuations in an order parameter and exhibit a maximum at a phase transition. These are plotted in Figure 5.8g for orientational (cyan) and translational (magenta) order and both exhibit a maximum at $\Gamma \sim 1.9$. This corresponds to the critical nucleus discussed and indicates that the system moves from long-range to short-range orientational and positional order at the same acceleration. This is a confirmation that the transition on the dimpled plate is a single-step first-order transition.

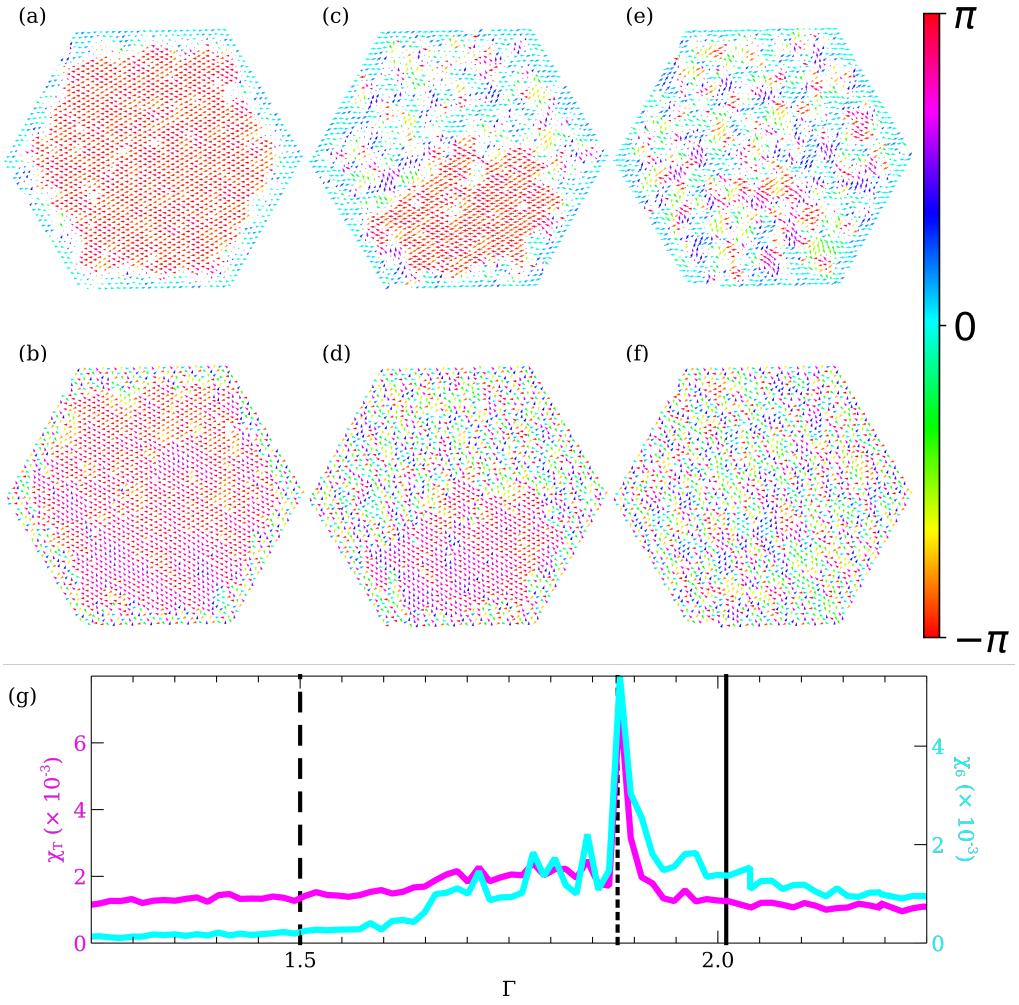

Figure 5.8: First-order phase transition with decreasing Γ on a dimpled plate. The upper panels show a vector representation of the complex order parameters (a, c, e) orientational - ψ_6 and (b, d, f) translational - ψ_T at (a, b) Γ = 1.5, (c, d) Γ = 1.9, and (e, f) Γ = 2.0. Cooled at a rate of $\dot{\Gamma} \sim 2.2 \times 10^{-4}\text{s}^{-1}$. The presence of a single-ordered domain separated from a liquid phase is clearly visible. (g) The susceptibility χ characterises the size of fluctuations in each order parameter. The maximum in χ_6 (magenta) and χ_T (cyan) occur at the same value of Γ indicating a first-order phase transition.

Performing the same experiment using the flat plate, the maximum fluctuations of each order parameter occur separately, indicating two separate transitions for the orientational ($\Gamma \sim 1.78$) and the translational susceptibility ($\Gamma \sim 1.57$) Figure 5.9g. As the system cools through these transitions, one observes a gradual increase in the length scale of spatial correlations in the orientational order parameter Figure 5.9 e->c->a. The spatial length scale of the translational order parameter (Figure 5.9 f->d->b) also gradually grows as the system is cooled. However, unlike the dimpled plate, the changes of both order parameters are continuous and there are no clear spatial correlations between the two which suggests the two are not tightly linked. These observations are much clearer when watching Supplementary Movie 2 which shows the orientational and translational vector fields changing as the acceleration is reduced.

I've shown that the flat plate reproduces the results of equilibrium hard spheres where the transition undergoes a two-step transition. Despite using very inelastic particles this disagrees with [Komatsu and Tanaka, 2015] who saw a first-order phase transition with inelastic particles. This shows that the first-order phase transition is driven by the surface structure of the dimpled plates.

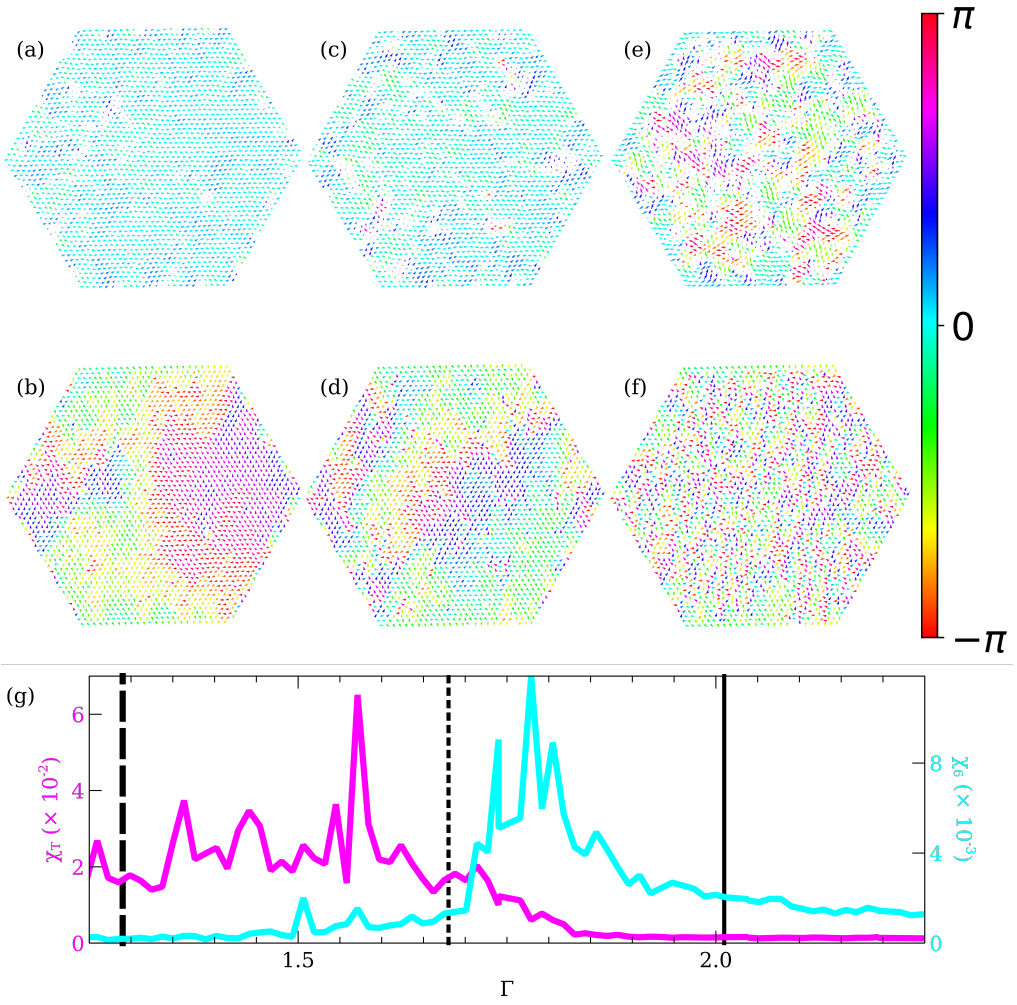

Figure 5.9: Two-step phase transition with decreasing Γ on a flat plate. The upper panels show a representation of the complex order parameters (a, c, e) orientational - ψ_6 and (b, d, f) translational - ψ_T at (a, b) Γ = 1.3, (c, d) Γ = 1.68 and (e, f) Γ = 2.0. Cooled at a rate of $\dot{\Gamma} \sim 2.2 \times 10^{-4} \mathrm{s}^{-1}$. No correlations are observed between the two vector fields. (g) The susceptibility χ characterises the size of fluctuations in each order parameter. The maximums in χ_6 (magenta) and χ_T (cyan) occur at different values of Γ indicating a two-step transition with an intervening hexatic phase.

5.5 Capillary Scaling of Interfaces

In equilibrium, interfaces between two different phases are not smooth. Instead, thermal motion gives rise to statistical fluctuations that make the interface rough. This roughness has been quantitatively described in terms of thermally excited capillary waves [Mandelstam, 1913].

Capillary fluctuations have been observed in many equilibrium systems such as at the interface of glycerol measured using x-ray scattering [Seydel et al., 2001]. Colloidal systems have also shown evidence of capillary fluctuations at liquid-gas interfaces where individual particles can be seen [Aarts et al., 2004]. Here, the surface tension scales with k_BT/d^2, where d is the particle size and k_BT is the thermal energy.

In simulations of model lipid bilayers, the presence of capillary scaling was used to confirm that the liquid-solid phase transition was first-order [Katira et al., 2015]. To achieve this, they measured the interface using a two-dimensional version of the three-dimensional construction found in [Willard and Chandler, 2010] which measures the interface using atomic coordinates of particles along the interface. To determine the position of the interface they used a coarse-grained field which characterises the orientational order in the system. It is calculated by

$$\bar{\psi}(\vec{r},t) = \sum_l f(\vec{r}-\vec{r}_l;\xi)\psi_l, \tag{5.5}$$

where $\vec{r}_l$ is the position of the lth particle, and $f(\vec{r}-\vec{r}_l,\xi)$ is a delta-like function defined as

$$f(\vec{r}-\vec{r}_l,\xi) = (1/2\pi\xi^2)\exp(-|\vec{r}-\vec{r}_l|^2/2\xi^2). \tag{5.6}$$

The coarse-graining width, ξ, was chosen to be the average spacing of particles in the ordered phase. The interface between the two phases was then defined as the field positions in which the orientational order is intermediate between the ordered and disordered phases. They then found that the Fourier spectrum of the height fluctuations, $\langle|\delta h_k|^2\rangle$ scales with $k_BT/L\gamma k^2$ where γ is the surface

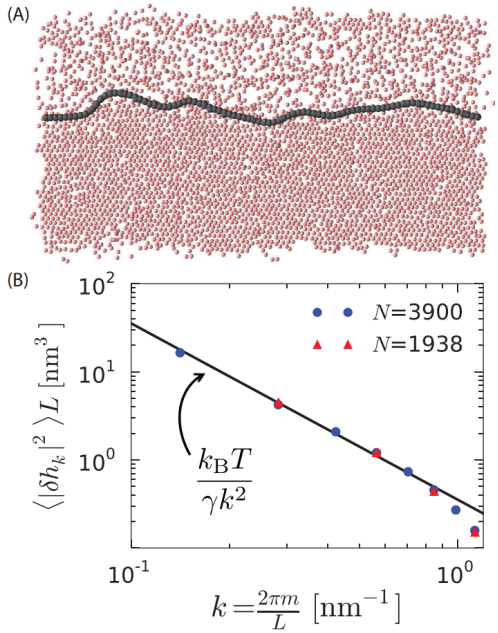

Figure 5.10: Figure from [Katira et al., 2015]. (A) Snapshot of their system showing the ordered and disordered phases with the calculated interface marked in grey. (B) The Fourier spectrum of the height fluctuations which shows the expected small-k scaling from capillarity theory.

tension, $k_B T$ is the thermal energy and k is the wave number. Figure 5.10 shows (A) a snapshot of their system showing the ordered and disordered phases with the interface marked in grey and (B) the Fourier spectrum of the height fluctuations showing small-k scaling.

Whether this theory can be used to confirm the nature of the phase transition in our non-equilibrium granular system is not clear. Many of the assumptions that are essential to the theory are not satisfied when the a-thermal nature of granular systems is considered. Despite this, in other cases, granular systems have been shown to mimic equilibrium behaviour. In fact, [Luu et al., 2013] showed that in a granular system, the interface between the liquid phase and an exotic square crystal phase was consistent with capillary scaling.

Here, I present an experiment in my granular system that attempts to measure the capillary scaling of the solid-liquid interface. I use the boundary, introduced in Chapter 4, which consists of 50% orderphobic and 50% orderphillic edges. This boundary acts to contain the ordered phase to one-half of the cell and pins the ends of the order-disorder interface at the division between orderphobic and orderphillic.

As the system is asymmetrical, the system could not be levelled with this boundary in place. Instead, the system was levelled using a completely orderphillic boundary before the boundaries were carefully replaced with the 50:50 boundary. This methodology was shown to be valid in Figure 4.18.

The cell was filled to an area fraction of 0.65 such that at an acceleration of $\Gamma = 1.81$ the ordered phase filled around half of the cell but with enough energy to cause the interface to fluctuate. Pictures of the experiment were then calculated at intervals of 6 minutes for 12 hours. The interval was chosen to be long enough that the interface had fluctuated by a significant amount visually.

The interface was found by calculating Equation 5.5 for our system. This is done by tiling the cell with a fine square lattice and calculating the average orientational order parameter $\bar{\psi}(\vec{r})$ at each site. If ψ_d and ψ_o are the average hexatic order parameter of the disordered and ordered phases then the order-disorder interface is identified by interpolating between lattice sites to find the set of points $\vec{s}$ such that $\psi(\vec{s}, t) = (\psi_d + \psi_o)/2$. Figure 5.11 shows an example of the interface calculated at a single time for my system.

Using the calculated interface the Fourier spectrum of the height fluctuations, $\langle|\delta h_k|^2\rangle$, are calculated. The Fourier component δh_k is calculated using

$$\delta h(x) = \sum_k \delta h_k \exp(ikx) \tag{5.7}$$

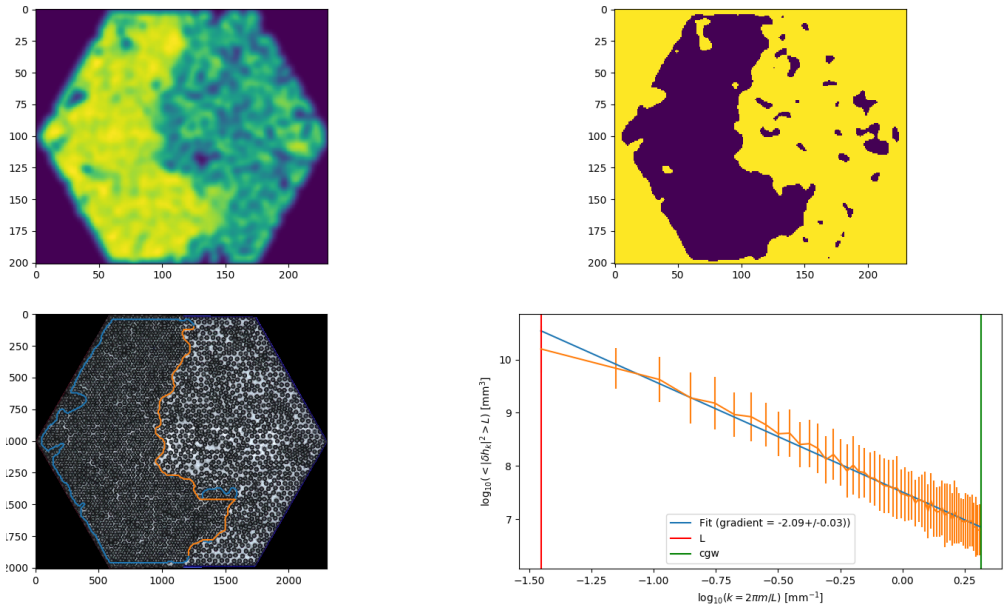

Figure 5.11: Top left: A snapshot of the system showing the coarse-grained field as a heatmap. Top right: The coarse-grained field is thresholded such that the boundary shows the liquid-solid interface. Bottom left: The calculated interface (orange) is shown which takes the nearest x coordinate of the interface at each y coordinate. Bottom right: The Fourier component of the height fluctuations for a coarse-graining width of 3 mm.

where $\delta h(x)$ is the height fluctuation measured from the line dividing the orderphobic and orderphillic halves of the cell and x is a point along this line. Normally this is calculated on systems with periodic boundary conditions which isn't the case in my system. However, since the interface is pinned at $x = 0$ at both ends, the analysis is performed such that $k = 2\pi m/L$ where L is the width of the cell along the interface and m is an integer.

According to capillarity theory, $\langle|\delta h_k|^2\rangle \sim k_B T/L\gamma k^2$ for small k where k_B is Boltzmann's constant [Safran, 2018]. Figure 5.11 shows the time-averaged capillary fluctuations calculated for the dimpled system at an area fraction of 0.65 and acceleration $\Gamma = 1.8$. The error bars are propagated from the standard deviation of $|\delta h_k|^2$ over time. The best-fit line was calculated between wavenumbers corresponding to the coarse-graining width and the length of the system. These bounds were chosen as they define the minimum and maximum resolution of the process.

If the system were at equilibrium we would expect the gradient of the line to be -2. This behaviour was confirmed for a granular experiment in [Luu et al., 2013]. The gradient in our experiment, however, shows a dependence on the choice of the coarse-graining width. Suggested coarse-graining widths are similar to the spacing between particles in a crystal. I calculated the gradient with coarse-graining widths between 1 mm and 24 mm which correspond to particles between 1/4 and 6× the diameter of the particles. This results in exponents varying from 2.15 ± 0.03 to 1.65 ± 0.03.

This dependency on a chosen variable means that I am hesitant to claim that our system exhibits capillary scaling like that observed in systems close to equilibrium. However, whatever the choice of the coarse-graining width, the resulting gradient always has a very small error so perhaps this methodology is correct and the coarse-graining width needs to be chosen so that the gradient is -2. This would then allow us to calculate the intercept of the graph which is proportional to $k_B T/\gamma$ where k_B is Boltzmann's constant, T is the temperature and γ is the surface tension. However, there are some difficulties in calculating these parameters for our system. Can the granular temperature T_g be used in place of the equilibrium temperature T? What is the equivalent of k_B for our system? The granular temperature is the average kinetic energy of the system, so, perhaps the total kinetic energy of the system could replace the $k_B T$ term.

I've shown that capillary fluctuations can be measured in the 50:50 system which is further evidence of a first-order phase transition. However, more work is needed to apply this theory to calculations of the surface tension. One possible route could be to film the system with a high speed camera, so the total kinetic energy of the system could be calculated which would allow us to calculate the surface tension.

5.6 Conclusions

The presence of two distinct susceptibility peaks on the flat plate suggests it undergoes a two-step transition consistent with other quasi-2D granular studies [Olafsen and Urbach, 2005, Reis et al., 2006, Sun et al., 2016]. In addition, we were unable to find evidence of a finite surface tension or the presence of coexistence in this system. This suggests that in our experiments on the flat plate, contrary to recent equilibrium results on colloids [Thorneywork et al., 2017], the liquid-hexatic transition is a continuous two-step transition.

For the dimpled plate, the presence of coexistence, a hysteresis loop and a single susceptibility peak suggest the dimpled plate undergoes a first-order transition. This contrast confirms that the first-order phase transition observed with the dimples does not merely strengthen a first-order liquid-solid phase transition, that ultimately arises from particle inelasticity, but fundamentally alters the nature of the transition.

In our experiments using a flat plate, highly inelastic particles ($e \sim 0.1$) resulted in a two-step phase transition. This is different from the results of [Komatsu and Tanaka, 2015] who found that the inelasticity of their particles ($e \sim 0.1$) resulted in a first-order phase transition. Subtle differences in granular experiments can radically alter observed phase behaviour, such as small changes in the height of a lid [Castillo et al., 2012]. Indeed, the Komatsu experiment differs from ours in having a confining lid. However, our work casts doubt on whether inelasticity alone is sufficient to change the order of the transition.

The introduction of a dimpled surface breaks both the orientational and translational symmetry of the 2D particle fluid. However, this is only significant if the kinetic energy at which particles undergo a liquid-solid transition is sufficiently small to be influenced by the underlying topography. This situation is like equilibrium scenarios involving noble gases on an underlying graphite lattice. There the hexatic intermediate is not observed if the liquid-solid transition occurs at thermal energies comparable to the substrate potential [Aeppli and Bruinsma, 1984]. If the dimples are significant, both orientational and translational ordering

are affected together resulting in a single transition. One might also think that the creation of pentagonal/heptagonal disclinations, essential to the KTHNY scenario, would be much more difficult in the presence of a surface that encourages hexagonal ordering.

The additional results provided by the study of correlations and capillary scaling were inconclusive in determining the order of the phase transition but importantly, do not contradict a first-order phase transition. Finally, this together with the conclusive evidence is confirmation that our system with the dimpled plate is first-order and not continuous.

In the next chapter, I will present an investigation of the orderphobic effect which relies on the first-order phase transition demonstrated in this chapter and the knowledge of creating orderphobic surfaces from Chapter 4.

Chapter 6

The Orderphobic Effect

I have shown in the previous chapter that our system exhibits a first-order liquid-to-crystal phase transition. In Chapter 4, I showed that I can use geometry to create orderphobic surfaces which cannot be wetted by the ordered phase. Together these findings allow us to investigate the orderphobic effect which I present in this chapter.

6.1 Introduction

Some molecules when placed in water are not readily dissolved. These molecules are hydrophobic. When multiple hydrophobic molecules are placed into water they tend to aggregate. This can be explained by considering how changes to both the entropy, S, and the internal energy, U, of the system effect the total free energy, F of the system at a constant temperature T which is given by

$$F = U - TS. \tag{6.1}$$

In water there is no long-range ordering, so the entropy is high. When hydrophobic molecules are introduced to the water, the ordering of the water molecules surrounding the hydrophobic intruders is increased [Chandler, 2005]. This decreases the entropy of the system. When hydrophobic molecules then aggregate,

the amount of increased ordering in the system decreases which in turn increases the entropy. An increase in the entropy decreases the free energy of the system (Equation 6.1) which results in an effective attractive force between hydrophobic molecules.

Additionally, the intruding hydrophobic molecule adds an interface in the water with a surface tension which increases the internal energy of the system. This increases the free energy of the system, so is unfavourable. When intruding molecules aggregate the total length of interfaces in the water is reduced. This reduces the internal energy and therefore reduces the free energy penalty due to interfaces. The reduction in free energy acts as an effective attractive force between hydrophobic molecules.

Katira et al. presented a theory for a powerful force of assembly in simulations between transmembrane proteins in lipid bilayers [Katira et al., 2016]. The force was a consequence of the first-order phase transition that exists between ordered and disordered phases in their lipid membrane [Katira et al., 2015]. Since this force of assembly is analogous to the attractive force between hydrophobic molecules in water, they refer to this effect as the "Orderphobic Effect".

While Katira et al. observed the orderphobic effect in a particular system they proposed that the effect is general and should exist in any system which has an underlying first-order order-disorder transition [Katira et al., 2016].

6.2 Theory

Katira et al. studied a system that consisted of a simulation of a lipid bilayer that exhibited coexistence between a disordered liquid phase and an ordered solid phase with a first-order phase transition between them. They found that inserting a transmembrane protein into the ordered phase of the bilayer induced a pre-melting-like effect [Katira et al., 2016]. A pre-melting effect refers to a disordered structure surrounding an interface (here, the transmembrane protein) in an otherwise ordered phase [Limmer and Chandler, 2014].

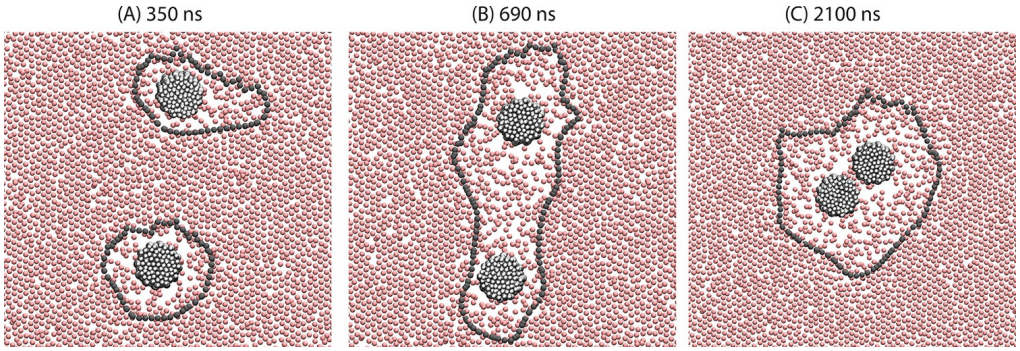

Figure 6.1: Figure from [Katira et al., 2016]. Series of snapshots as two model atransmembrane proteins are pulled together by an attractive orderphobic force. In (A) the two transmembrane proteins have created a region of disorder around themselves separated by an interface to the ordered bulk. The positions of the proteins fluctuate until the interfaces join in (B). Once the interfaces have joined, the surface tension of the interface acts to pull the particles together to reduce the length of the unfavourable interface which results in (C).

The boundary of the disordered domain forms a stable fluctuating interface between the ordered and disordered phases. Since the boundary is fluctuating, this allows the protein to diffuse around the system as the boundary fluctuates. As the order-disorder phase transition is first-order, the order-disorder boundary exhibits surface tension. Therefore, neighbouring proteins can experience an effective force of attraction by minimising the size of the order-disorder interface and hence the total interfacial energy. This effective force is the "orderphobic force".

Katira showed that their proteins nucleate a fluctuating order-disorder interface due to a geometric mismatch between the protein and crystal lipid phase. Checking that the interface followed the capillary wave theory explained in the previous section also showed that the order-disorder transition was first-order. Simulations were then used to observe the force of assembly. Fluctuations in the interfaces caused the two interfaces to combine such that a single disordered phase surrounded the two proteins. The finite interfacial tension of the interface then caused the two proteins to be pulled together allowing the length of the interface to decrease therefore reducing the free energy of the system. Figure 6.1 shows a series of snapshots that show two transmembrane proteins experiencing attraction from the orderphobic force.

Most importantly they showed that the length scale of the force was larger than the diameter of the particles in the lipid bilayer. This is important as it distinguishes the orderphobic force from other shorter-range forces that can cause assembly such as the depletion force. They find that the length scale of the force is equal to roughly double the average radius of the disordered region around their proteins.

6.3 Motivation

Two of the key principles of the orderphobic effect are the presence of a first-order order-disorder phase transition and the orderphobic intruders which prefer the disordered phase. I have shown these two principles in my system. In Chapter 5 I showed that the order-disorder phase transition in my system is first-order. In Chapter 4 I showed boundaries that preferred one phase or the other. Since our system has these properties, if intruding objects with the same properties as the boundary can be created, then they should display orderphilicity. This would then allow us to demonstrate that the orderphobic effect is generally true for the first time.

6.4 Designing Intruders

To start my investigations to determine whether the orderphobic effect can be observed in my first-order granular system I first needed to find a suitable intruder that is analogous to the transmembrane protein. The requirements for this intruder are as follows: (1) It must induce a region of disorder around itself that has a stable fluctuating interface with the ordered phase. (2) The size of this region must be large enough that other forces of assembly with smaller length scales can be discounted. (3) The intruder must be allowed to diffuse around the experimental cell so that the forces of attraction can be observed.

Unlike in equilibrium systems, collisions between granular particles are always somewhat inelastic, so energy is always lost during a collision. This means that the energy of objects in granular experiments is a balance between the energy input (collisions with the vibrating baseplate) and energy loss (collisions and friction with other objects). This has an unfortunate consequence for testing intruders as objects that differ in size and material from the rest of the particles can end up with vastly different energies.

This is important, as intruders need to have enough energy to diffuse around when placed in the ordered phase. However, if the intruders have too much energy they would bounce higher than the diameter of the other particles, allowing them to move underneath and push the intruder on top of the ordered phase.

Another way that our system differs from an equilibrium system is that the amount of order/disorder in the system is fixed at a certain amplitude and packing fraction. Inserting intruders into the system would increase the packing fraction and increase the amount of order in the system. Therefore, when intruders are added to the system the equivalent area of particles is removed from the system to ensure the order/disorder ratio remains the same.

To induce a region of disorder the shape of the intruders was designed with a structure similar to the orderphobic boundary described in Chapter 4. Firstly, a triangular lattice of circles with a diameter matching the particles is generated with spacing equal to the dimple spacing. Then, to create the bulk of the intruder, circles of different radii are placed on this pattern centred on one of the particles. The final shape of the intruder is selected from the union of this large circle with the smaller circles in the lattice. An example of the final shape is presented as the grey shape in Figure 6.2 which has an intruder radius $R_i = 2.5L$ where L is the dimple spacing of the baseplate.

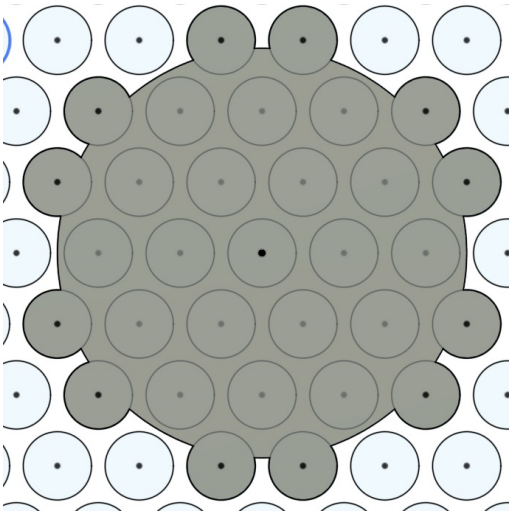

Figure 6.2: Example of the basic intruder shape designed to promote disorder by matching the shape of the underlying lattice. The intruder has a radius $R_I = 2.5L$ where L is the dimple spacing of the baseplate. The intruder shape is generated by taking the union of the blue circles and a circle of arbitrary size to form the grey shape.

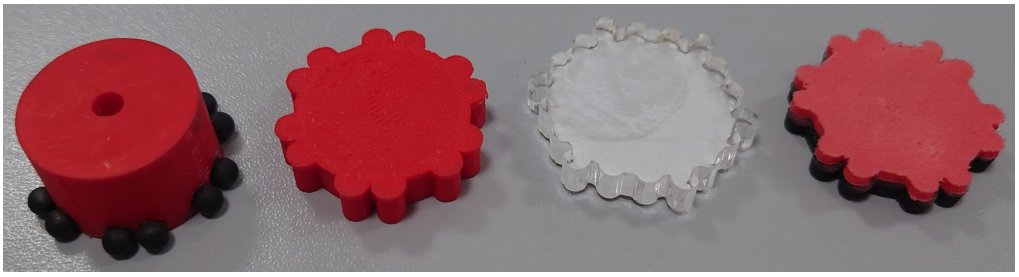

Figure 6.3: Photographs of 4 different orderphobic intruders used in experiments. (1) 3-D printed PLA cylinder with nitrile balls glued in pockets. (2) 3-D printed PLA shape. (3) Laser-cut acrylic. (4) Two layers of foam with a thin acrylic disk sandwiched between.

Creating Intruders

In this section, I introduce a selection from the various iterations of intruders that were used and discuss what I learned from each design. Figure 6.3 shows the four intruders discussed in this section. Many more intruders were designed, but these intruders were chosen for discussion as they explain most of the lessons learned.

The first intruder in Figure 6.3 was produced by 3D printing it in solid PLA, a material much stiffer than the nitrile balls used as particles. Nitrile balls were glued into pockets around the perimeter of the intruder so that its shape matches the style of Figure 6.2. If the intruder was fixed in place then it was successful in inducing a region of disorder around its perimeter which can be seen in Figure 6.4.

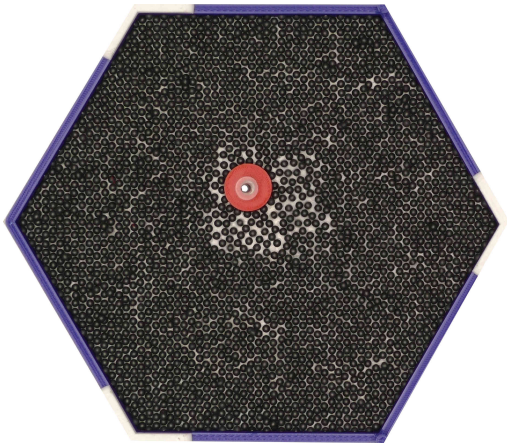

Figure 6.4: Disorder forming around a fixed intruder after the system has been cooled.

However, if the intruder is placed in the system such that it is free to move it very quickly receives a 'kick' from the shaker which causes it to tip; particles in the monolayer then quickly fill the space below the intruder and push it above the rest of the monolayer.

Several attempts were made to prevent this from happening which weren't successful. The stability of the intruder was increased to prevent tipping both by increasing the diameter and making the intruder cone-shaped but neither of these prevented the issue. The elasticity of the intruder was reduced to reduce the effect of 'kicks' from the base. This was done by introducing thin layers of foam beneath the intruder, while this did reduce the effect of kicks from the base it raised the height of the balls around the edge of the intruder making it easier for particles in the surrounding liquid to work their way under the intruder. Ultimately, it was decided that the balls stuck around the edge of the intruder made it easier for this to occur as their shape makes it easier for a particle to strike the intruder with an upwards force at one edge which causes it to tip.

The second intruder aimed to fix this issue by using 3D-printed cylinders instead of fixing the balls to the edges. Without the particles fixed around the edge, the intruders were far too elastic and would instantly jump above the monolayer at any reasonable acceleration. This shape was tested with several materials. Laser-cut

acrylic intruders were used which initially looked very positive as they moved around the system at reasonable speeds without leaving the surface. However, this meant that these intruders seemed to ignore the effects of the particles and moved based on imperfections in the vibrations that were otherwise unmeasurable.

The final intruder in Figure 6.3 showed the most promise. It was made from two layers of 2 mm polyethylene foam with a 0.5 mm thick disc of acrylic glued between them to provide stiffness. These intruders were much less likely to jump above the monolayer of particles and were successful in inducing disorder around themselves.

6.5 Testing the Orderphobic Effect

The orderphobic effect was tested with these intruders. The system was set up with the orderphillic boundary so that the only edges that wet disorder are the intruders. The system was started with $\phi \sim 0.85$ at $\Gamma \sim 2.6$. An equivalent area of particles to 2 intruders was removed from the system before the intruders were placed in the cell far apart from each other. The particles were held in place by hand while the system was cooled slowly to $\Gamma \sim 2.0$. The particles were then released. At this amplitude, most of the cell is filled with the ordered phase while each intruder is surrounded by a small region of disorder which can be seen in Figure 6.5a. At this amplitude, the intruders diffuse very slowly but eventually (roughly five minutes) the interfaces surrounding each of the intruders join together (Figure 6.5b). After a long time (10 minutes) the order-disorder interface still surrounds both intruders (Figure 6.5c). However, before the intruders had time to move together within the interface one of the intruders hopped out of the monolayer. The experiment was repeated many times. In some experiments, the interfaces successfully merged before an intruder escaped the monolayer but the joining of the intruders never occurred.

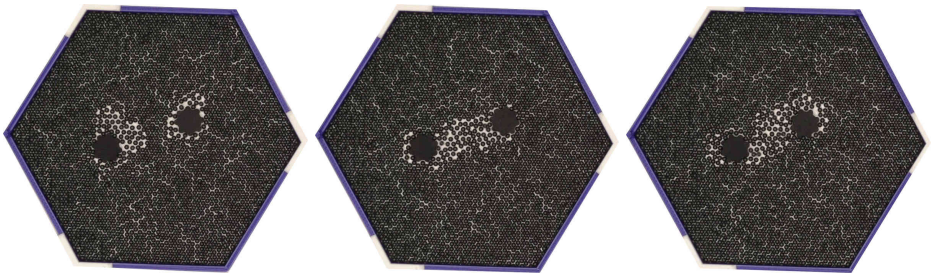

(a) (b) (c)

Figure 6.5: Testing the orderphobic force with two intruders at $\phi = 0.85$ and $\Gamma = 2.6$. Snapshots show the time evolution of the system which shows the interfaces of the intruders joining together.

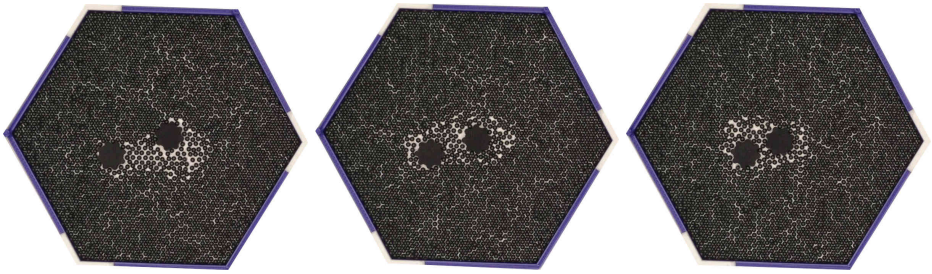

(a) (b) (c)

Figure 6.6: Testing the orderphobic force with two intruders at $\phi = 0.85$ and $\Gamma = 2.6$. Snapshots show the time evolution of the system which shows the intruders moving together in their joined interface.

For the sake of my sanity, the experiment was adapted such that the intruders were held apart but close enough that the interface surrounded both intruders. The experiment was then continued from this intermediate point. Figure 6.6 shows the most successful of many experiments where the intruders moved together and reduced the length of the order-disorder interface. This experiment took around 5 minutes.

While together Figure 6.5 and Figure 6.6 appear to show similar behaviour to the work by Katira et al. [Katira et al., 2016], it was difficult to be sure as over 90% of roughly 50 experiments ended prematurely.

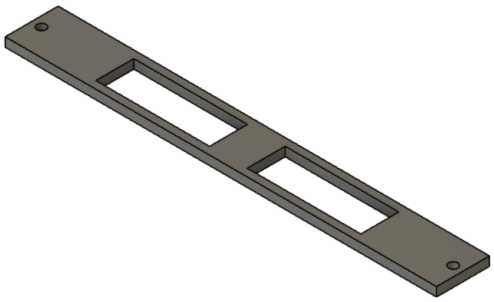

Figure 6.7: A 3D model of the slotted rail used to hold the intruders in restricted paths.

Using Rails

The lack of repeatability in the previous experiments caused by the intruders jumping out of the monolayer was highly problematic. To confirm the presence of the orderphobic force I would need to show the effects over many repeats. To achieve this a variety of techniques involving rails were used which would allow the intruders to move in one direction without jumping out of the layer.

Several types of rail were trialled before the final version described was settled on. The final design was created from two long straight sheets of clear acrylic fixed on top of each other. The bottom sheet (see Figure 6.7) consists of two large rectangular holes which act as slots that the intruder can move inside. The top sheet has no holes and acts as a lid for the slots. The rail is fixed in place across the cell such that the top of the slot is 16 mm above the surface. Any intruder placed in the slots has a height of 15 mm so that it is free to bounce off the surface without leaving enough gap for the 4mm diameter particles to move underneath. This height is simply the lowest height that could be used which cleared the height of the boundaries.

The gap between the slots was set to 24 mm. Smaller gaps were trialled but, if the gap between the intruders is too small then the intruders could be held together by other forces such as the pressure of particles in the liquid phase pushing the intruders together. This gap was chosen such that a reasonable number of particles could come between the intruders while being small enough that their interfaces can join together.

The intruders in these experiments used a 3D printed PLA core like the first intruder in Figure 6.3 but with polyethylene foam added to the top and bottom to dampen the vibrations. The experiment was run at a constant amplitude so that the energy received by the intruder remained the same. The cell was then filled to two different area fractions, the first at 0.6, so that the whole system is in the liquid phase and the second at 0.85, so that most of the system is in the solid phase, but there is a region of liquid around each intruder. The positions of the intruders were then tracked for several hours.

Figure 6.8 shows the results of this experiment. The top panel shows the probability density of the intruders' positions in the solid (blue) and liquid (red) scenarios, the mean positions in each scenario are noted by the dashed vertical lines. The central panel shows an example of the intruders where their liquid-solid interfaces have joined together in the solid phase scenario. The bottom panel shows position-time plots of each intruder in the translucent lines, and the opaque lines show the one-minute time averaged positions.

The position-time graph shows that the intruders often move quite quickly from one end to the other of their slot. If one were to watch the particles, one would see the particles randomly walking for a while before suddenly moving to one end or the other of the slot. We believe this may be due to a ratcheting effect between the intruder and the rail which occurs randomly. The speed at which this happens gives the intruders in the same liquid bubble the momentum to escape despite the surface tension of the interface. This behaviour is why we opted to track the probability density of the position instead of just looking for single occurrences of the phenomena like in [Katira et al., 2016].

The probability density plots show that the average positions of the particles are closer together for the solid scenario than for the liquid scenario. It also shows a peak in the positions at the centre for both scenarios, although it is much higher for the solid scenario. This may be evidence that the orderphobic effect is present and creating an attractive force between the two intruders when their interfaces are combined. However, the peak in probability density for the liquid scenario suggests that there may be other mechanisms pushing the intruders together. I

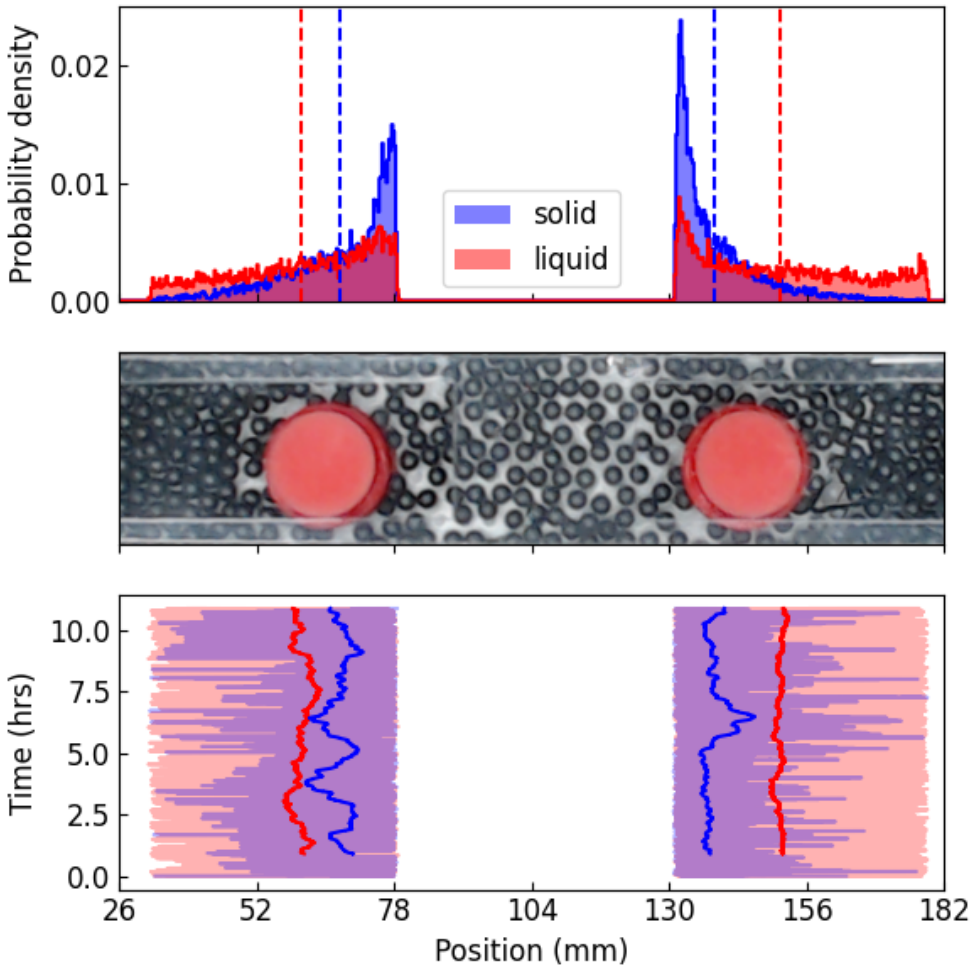

Figure 6.8: Testing the orderphobic effect with rails in a liquid (red) and a solid (blue). Top panel: Histogram of the position of each intruder over time. Dashed lines show the mean position of each intruder. Middle panel: A snapshot of the intruders at a single time. Bottom panel: A plot of the intruders' positions over time.

have a few suggestions for mechanisms that may cause this. First, the rail holding the intruder down might not be stiff enough which would cause non-uniform vibrations along its length. It might therefore be favourable for the intruders to sit in the middle of the rail. Secondly, if the intruders are randomly walking around and both reach the middle together, there may be a force holding them together that is not the orderphobic force. This could arise from a reduction in the pressure from particles between the intruders so that more collisions are pushing the intruders together than pushing them apart.

6.6 Conclusions

The experiments presented above are a subset of a larger set. These are just the most successful ones. Overall, after performing these experiments, I'm confident that the orderphobic effect does exist in our system. This is not surprising given the orderphilicity of the boundaries in Chapter 4 and the first-order nature of the order-disorder phase transition.

Ultimately, however, our results were inconclusive and were unable to rule out other effects. This is because there were a few fundamental problems with our approach.

The first came from how energy is inputted into our system. Unlike equilibrium systems, the steady state is created from a careful balance of the energy in from vibrations and the energy out from dissipation. This works fine for the particles as they are all the same however, the intruders receive and dissipate energy in a very different manner from the particles so will always be at a different granular temperature.

The other major issue was the intruders jumping out of the monolayer. Our experiment is kept quasi-2d by limiting the height that particles jump by limiting the maximum acceleration. If the odd particle does jump above the monolayer it easily finds its way back to the monolayer which is not the case for the intruders. Adding methods to control the height of the intruders only acted to change the interactions of the intruder and caused other problems.

I believe that if one were able to create an experiment that removes these two fundamental problems then one would be able to show conclusive evidence of the orderphobic effect however, the exact nature of this experiment eludes me. I would have liked to continue working on this project, but after many months of work we decided to move on to the study presented in Chapter 7.

Chapter 7

Phase Behaviour at Several Values of L/D

In Chapter 3, I showed observations from experiments using three different dimple lattice spacings. For chapters 4 - 6, I then focussed on a single lattice spacing. In this chapter, I present a more thorough investigation of how changing the dimple spacing changes the phase behaviour of our system.

7.1 Introduction

Significant research on granular systems has studied the various phases that can be observed when the properties of the system change. One area of focus is the effect of confinement by a lid on phase behaviour, which has been shown to exhibit a variety of behaviours. Prevost et al. found that when the height of the lid is set to 1.75 ball diameters, increasing the amplitude of vibrations beyond a critical value leads to crystallisation in a square lattice [Prevost et al., 2004].

Reyes and Urbach also studied the effect of confinement by a lid, but they varied the area fraction and driving acceleration of the system and observed several different phases, including motionless hexagonal close-packed spheres, fluctuating hexagonally ordered single-layer crystals, and a homogeneous liquid. [Reyes and Urbach, 2008] Another avenue is exploring how changing the elasticity of the particles can change the nature of the phases. Reyes and Urbach also varied the material of the particles used, using both steel and brass ball bearings

with coefficients of restitutions of 0.95 and 0.77 respectively [Reyes and Urbach, 2008]. They found that some of the phases that were observed for stainless steel were not present for the brass balls. Komatsu and Tanaka further explored the effect of the coefficient of restitution by comparing steel and nitrile rubber balls [Komatsu and Tanaka, 2015].

In equilibrium physics, one common system where the properties of the substrate have a very important role in the resulting phase behaviour is systems of adsorbed gases on molecular substrates. Instead of considering the diameter of the atom in these systems we instead consider the substrate-free lattice spacing. The substrate-free lattice spacing is the spacing of atoms in a crystal that forms in the absence of a substrate. This spacing is then compared to the lattice spacing of the underlying substrate. Depending on how the ratios of these two length scales differ, several types of structure can form [Bak, 1982]. These structures can be either commensurate or incommensurate. Commensurate lattices have a crystal spacing that is some simple fraction or simple multiple of a periodic spacing that exists in the underlying lattice. In incommensurate lattices, the crystal spacing cannot be represented by some simple fraction of a lattice spacing.

In the case of adsorbed gases on molecular substrates the potential from the underlying substrate is relevant. When a commensurate lattice forms, the underlying potential means that it is energetically favourable for the natural spacing of the atoms to be slightly stretched or compressed to mesh with the underlying lattice. In an incommensurate case, the underlying potential is not strong enough to significantly alter the crystal spacing enough to be commensurate. However, the adsorbed gas will be locked to the substrate in such a way as to minimise its energy.

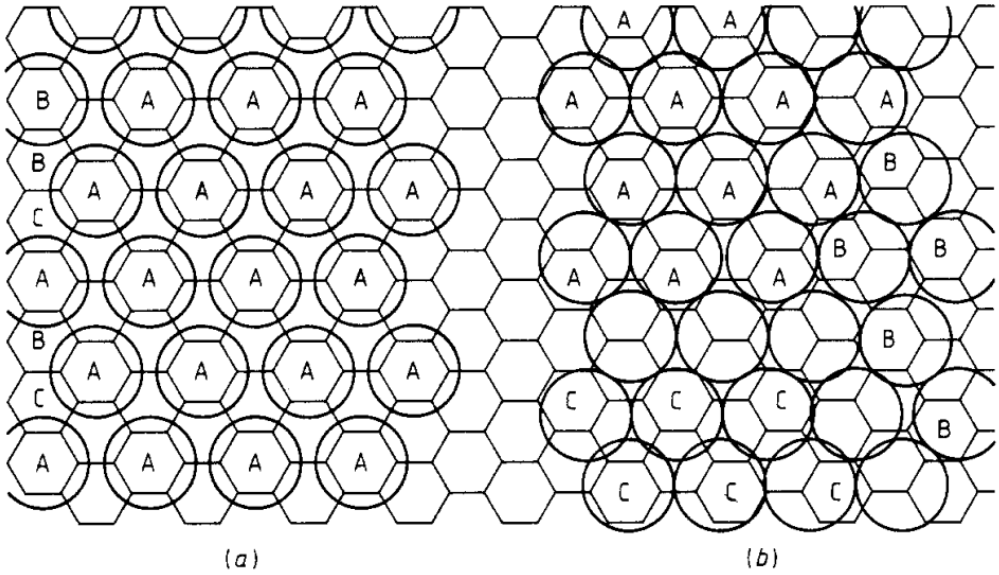

Figure 7.1: Figure from [Bak, 1982]. Shows the structures of the krypton monolayer adsorbed on graphite. (a) Commensurate $\sqrt{3}$ structure. (b) Incommensurate structure.

A simple example of an adsorbed gas is krypton on graphite. The area fraction (monolayer coverage) is increased by increasing the pressure of the gas in the chamber above the monolayer. At low area fractions, it forms a commensurate $\sqrt{3}$ structure where one out of three honeycomb lattice cells is occupied by a krypton atom. As the area fraction is increased, however, the phase becomes incommensurate [Bak, 1982]. Demonstrations of these two phases are shown in Figure 7.1.

Argon which has a smaller natural lattice spacing than krypton produces different behaviour. It always produces incommensurate structures and investigations into the nature of its melting transition suggest that the transition is continuous [McTague et al., 1982]. Xenon has a larger natural lattice spacing than krypton and forms incommensurate triangular structures. Investigations into the nature of the melting transition suggested that the transition is strongly first-order for submonolayer densities [Litzinger and Stewart, 1980], but as the density increases the transition becomes continuous [Specht et al., 1984].

Previous chapters showed that close analogies between hard sphere models and granular systems do exist. Since they only explored one spacing it is desirable to explore different spacings in some more detail to further explore how granular systems can be used as analogies to equilibrium systems such as adsorbed gases. Previous chapters implied that the dimple pattern lowers the energy associated with a particular crystal configuration. This is controlled by two factors - interaction strength with the dimples and the possible geometric packing of particles.

In the previous chapters, I showed that a dimple spacing of 4.8 mm caused a system of 4 mm balls to undergo a first-order liquid-to-solid phase transition. The spacing of dimples was such that the apothem distance of 4.156 mm is close to the ball diameter along which direction the crystal of the solid formed. An equivalent flat plate exhibited a continuous two-step phase transition. This begs the question of how other dimple spacings can affect the behaviour of solid phases and the nature of their liquid-to-solid phase transitions.

7.2 Methods

The dimpled plates created for the previous chapters were difficult to make precisely and very time-consuming to make, requiring large amounts of workshop time that wasn't available. Much of this difficulty came from creating consistently sized dimples across the surface of the plate. The dimples were milled using a very precise CNC mill which should have been able to reliably mill the dimples to the same depth after the surface had been lapped. However, due to the large radius of the ball cutter, very small deviations in height create a very large difference in the diameter of the dimple. Due to the manufacturing process of the aluminium plates that were bought to create the dimpled plates, milling hundreds of dimples into the plates releases the plate's tension causing them to warp creating inconsistencies in the size of the dimples. The likelihood of this

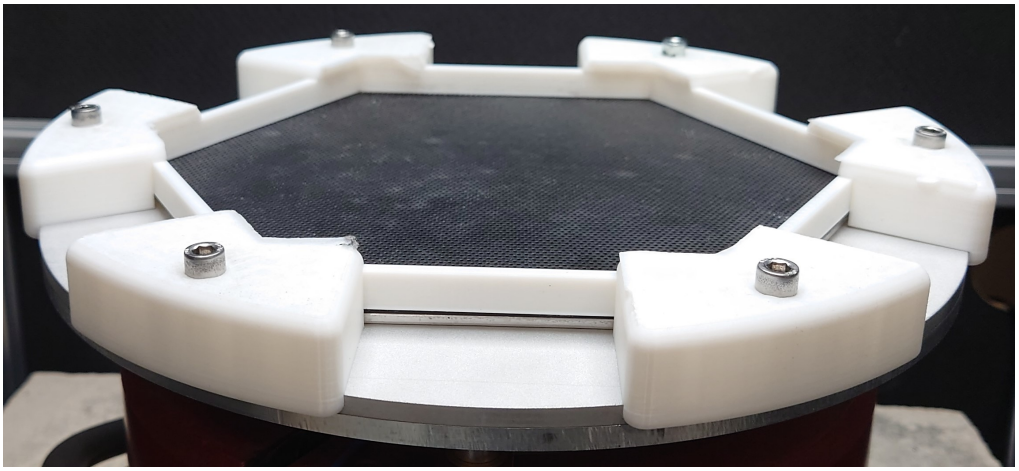

Figure 7.2: Photograph of the dimpled HIPS plate showing how it is fixed to the shaker.

happening could be reduced by increasing the thickness of the plates however, this could only be done so much, as there was a weight limit on the shaker above which the vibrations became unstable. Due to this many attempts were required to create a plate with acceptable deviations in dimple sizes.

This required me to develop a new, quicker method of creating the dimpled plates. The method for creating the new dimpled plates involved cutting a lattice of holes in sheets of HIPS (high-impact polystyrene) using a CO_2 laser cutter. The sheets of HIPS were then glued to an aluminium hexagonal plate (5mm thick) to keep the thin sheet of plastic flat and maintain uniform vibrations. This plate was then secured to the shaker by clamping around the edges with a 3D-printed boundary. Figure 7.2 shows a photograph of the dimpled plates and their mounting mechanism.

While changing the material and design of the baseplate I also took the opportunity to change the balls used in the experiments. The 4 mm diameter nitrile balls were replaced with 2 mm stainless steel ball bearings. Changing so many parameters in an experiment would normally be a concern, but I describe our reasoning below.

Firstly, the reduction in size allows us to dramatically increase the number of particles in our experiments which should reduce finite-size effects that can influence phase transitions. Furthermore, it will increase the size of a sample of the system which is ‘far’ from the boundary which improves the results of some

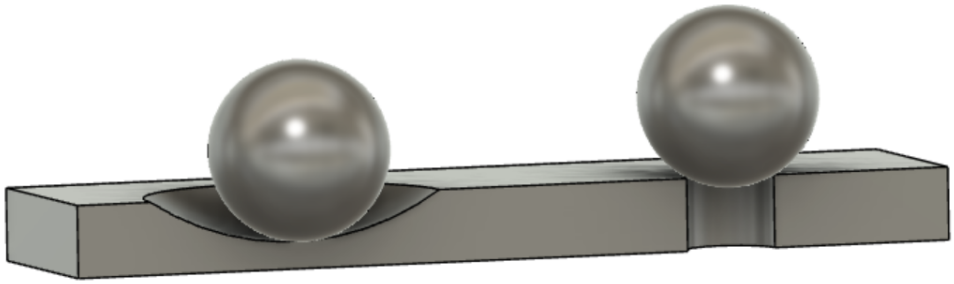

Figure 7.3: (Left) A ball sat in a dimple, where the ball only makes contact in one place at the bottom of the ball. For easier viewing, the dimple has been significantly increased in size. (Right) A ball sat in a hole, where the ball makes contact with the base in a ring.

analysis as it is found that the boundaries of a system produce a velocity gradient as you move towards the edges [Smith and Smith, 2017]. The accuracy of the tracking should not be altered as stainless steel balls are much easier to image than the nitrile balls.

The second significant change is that of the particle's elasticity. We showed in chapter 4 that when changing from the inelastic nitrile balls to the much stiffer polypropylene balls the nature of the transition was not altered. The interactions with the orderphobic/orderphillic boundaries were changed, however, the boundaries will be ignored in this chapter as creating boundaries for each spacing was not reasonable.

Balls don't necessarily interact with the holes in the same way that they would interact with the dimples from the previous chapters. Figure 7.3 shows diagrams of a ball sitting in a dimple and a ball sitting in a hole. In the first case where the ball sits in a dimple, the ball only touches the base at a single spot and is free to roll around as the radius of curvature of the dimples is much greater than that of the ball. However, in the second case where the ball sits in a hole, the ball contacts the edges of the hole and is not as free to roll around without leaving the hole. This suggests that there may be differences in how the particles interact with the different types of dimples. A quasi-one-dimensional system designed such that it can be filmed from the side with a high-speed camera has been built to study how exactly the dimples affect the particles which will be the subject of future research.

To choose the size of the holes that would be appropriate for the 2 mm diameter balls I first had to find the upper bound for the diameter of the holes so that when sat in a hole the balls cannot touch the surface beneath. For a sheet of thickness T, a ball of radius R, the maximum radius of the hole, r, is $r < \sqrt{T(2R - T)}$. So for $T = 1.5\,\text{mm}$ and $R = 1.00\,\text{mm}$, the maximum radius of the hole is 0.86 mm.

As the focus of this chapter is to investigate how changing the spacing between holes affects the behaviour of different phases I performed a very crude investigation into the diameter of the holes as deeply investigating another dimension of the phase space was not practicable. To select the size of the holes, plates were made with a hole spacing of 2.42 mm and hole radii of 0.37, 0.57 and 0.77 mm. The system was set up with a dilute liquid of particles and cooled at a rate of $0.1\,\text{s}^{-1}$ comparable to the slow rates used in Chapter 3 on the three different plates to observe their behaviour. In the case of the smallest holes, as the system cooled the holes seemed to have little effect with balls ceasing to move and ending in random positions rather than being trapped by the holes. When the largest holes were used, the particles were trapped even at very high amplitudes such that the difference in energy between particles in and out of a hole was huge. The hole radius of 0.57 mm provided a balance between these conditions and was selected going forwards.

Using this hole size I decided on several hole separations to investigate. The first two spacings I will report on are both perfectly commensurate. These spacings are 2.00 mm and 2.31 mm which are compatible with two different types of commensurate crystal.

Next, I will show what happens to the phase behaviour as the spacings are stretched from their perfect spacings. This should provide some space between the particles and be more representative of the system in Chapter 5. These two spacings are 2.15 and 2.42 mm and I will refer to them as stretched commensurate surfaces. This 2.42 mm lattice spacing has an equivalent spacing to diameter ratio as the system in Chapter 5 so will be used to compare the differences between the two systems.

The final set of spacings that I will discuss are when the spacings are smaller than the diameter of the particles. Here, there are several spacings between 1.87 and 1.99 mm which produce clusters of crystals of varying size.

Furthermore, I'll show two different spacings where some of the phases I've previously discussed coexist in competition with each other. The first of these spacings is 2.25 mm which produces both evidence of a commensurate crystal similar to that in the 2.15 mm spacing and evidence of clusters that are present in spacings less than 2 mm. The second is 1.91 mm which produces the clusters that all the spacings below 2 mm produce but also a commensurate crystal similar but not identical to that of the 2.31 mm spacing.

7.3 Perfect Commensurate Crystals

The simplest way to form a commensurate crystal on a triangular lattice is to place one ball in every single hole. This is referred to as a 1×1 commensurate lattice. This is shown in Figure 7.4a where the grey circles represent the lattice sites and the blue circles represent the particles in the crystal. The smallest spacing that this is possible for is when the lattice spacing perfectly matches the particle diameter of 2.00 mm.

The next simplest way is to tile particles such that 1 in every 2 lattice sites is occupied. To achieve this the crystal is rotated by 30°. This is referred to as a $\frac{\sqrt{3}}{2} \times \frac{\sqrt{3}}{2} R30°$ crystal as the distance between particles is $\frac{\sqrt{3}}{2}L$ where L is the lattice spacing and the crystal is rotated by 30° with respect to the underlying lattice. This is shown in Figure 7.4b where the grey circles represent the lattice sites and the red circles represent the particles in the crystal. The smallest spacing, L that this is possible for is when $L\frac{\sqrt{3}}{2} = D$ which for a particle diameter D of 2.00 mm results in $L = 2.31$ mm.

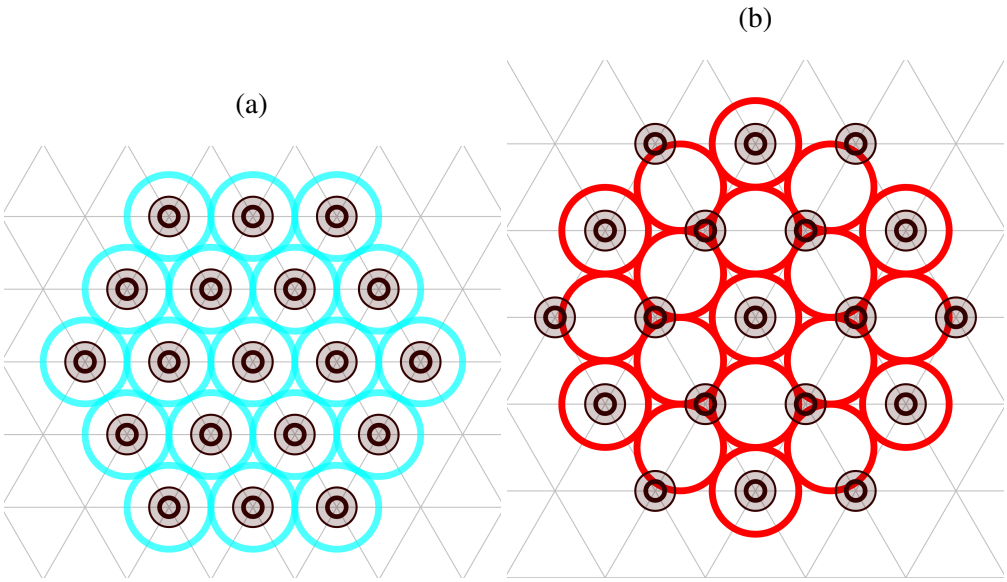

Figure 7.4: Diagrams showing how a commensurate crystal made of 2 mm diameter particles can sit on top of a (a) 2.00 mm and (b) 2.31 mm spaced lattice. The black and grey circles represent the dimples and the large coloured circles represent the particles. The colour represents the angle of the hexatic order parameter on the same colour map that will be used in future figures.

2.00 mm spacing

The first spacing to explore is when the hole spacing perfectly matches the diameter of the balls. The plate with a hole spacing of 2 mm was filled with 2 mm diameter ball bearings to area fractions of 0.65, 0.75 and 0.85. The system was cooled from a dimensionless acceleration of 3.4 to 2.0 at a rate of $0.02\,s^{-1}$. Snapshots of the hexatic order of the system are shown in Figure 7.5 at different area fractions and accelerations as the system cools. Each particle is represented by an arrow where its size represents the magnitude of the hexatic order parameter and its direction/colour represents the phase. Here, the growing amount of cyan arrows represent the amount of crystal increasing as the system is cooled. The red arrows represent particles that have jumped on top of other particles and formed crystals in the second layer.

In Figure 7.5 the amount of crystal, shown by the cyan particles with phase ≈ 0 rad, increases as the dimensionless acceleration is reduced. The red particles with phase $\approx \pm\pi$ rad are particles that have jumped on top of the first layer and formed crystals in the second layer.

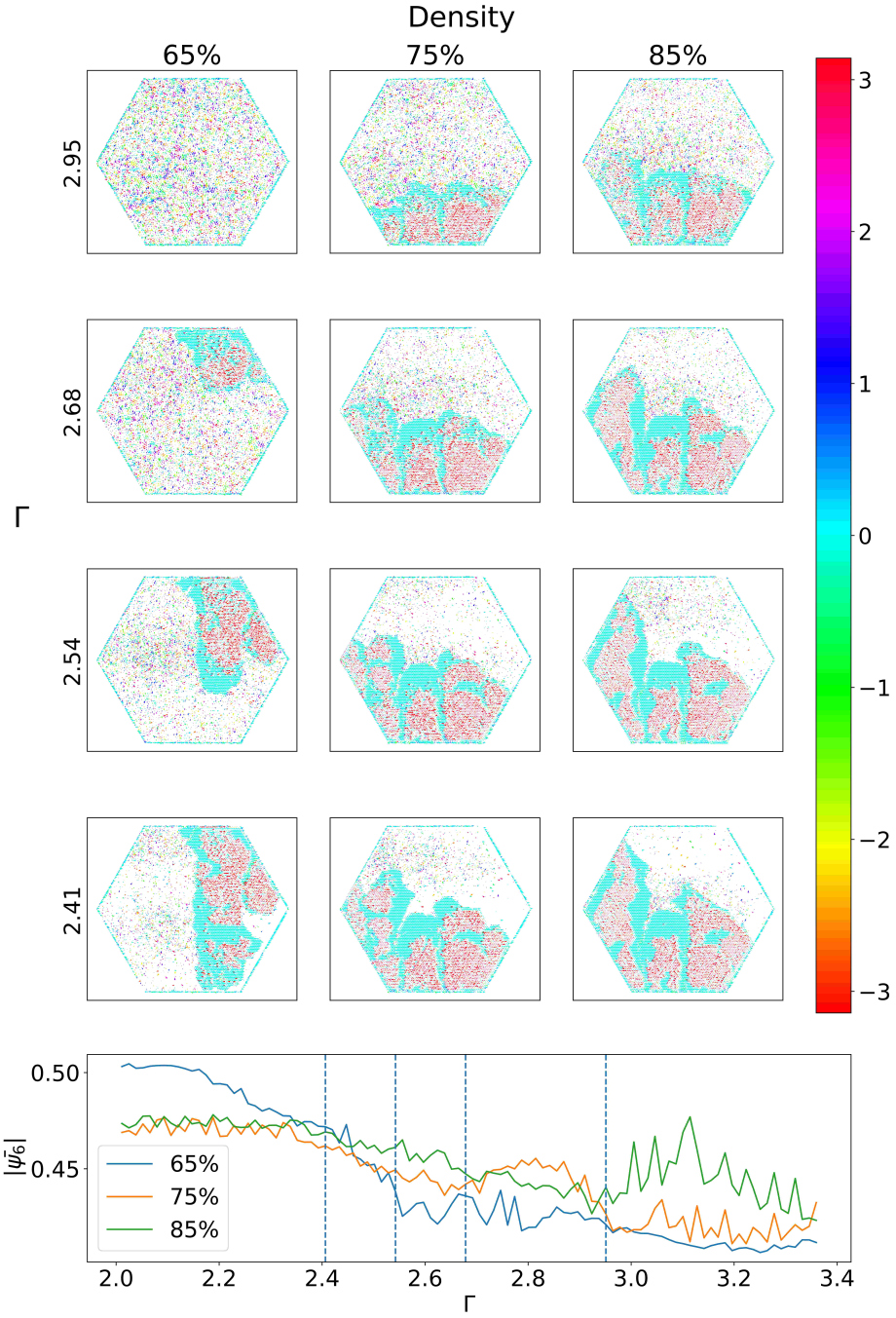

Figure 7.5: $\boldsymbol{L}$ **= 2.00 mm.** Top: Snapshots of the system at different area fractions and dimensionless accelerations. Each particle is represented by an arrow where its size and direction indicate the magnitude and phase of the particle's hexatic order parameter. The colour of the arrow also indicates the phase in radians. In this case, the particle with a red hexatic order are particles on top of a crystal with a cyan hexatic order. Bottom: The average hexatic order parameter of the system as it is cooled at area fractions of 0.65, 0.75 and 0.85 at a rate of 0.02 g/s. There is a lot of noise in these plots that arises from the particles in the top layer effecting the calculation of the hexatic order parameter.

The particles crystallise in the second layer because the crystal in the bottom layer differs from the crystals seen in Chapter 5. Particles in the bottom layer move around until they collide with the crystal, when they do the particles seem to lose all of their energy and join the crystal. The crystal doesn't fluctuate like it did before but seems to be completely stationary. The behaviour is similar to the inelastic collapse observed in [Olafsen and Urbach, 1998]. Inelastic collapse occurs when inelastic particles undergo collisions at a very high rate so that all the kinetic energy of the particles is dissipated [McNamara and Young, 1994]. The energy loss is greater than the energy provided by the vibrating baseplate, so the particles are completely stationary.

Consequently, the stationary behaviour of the crystal meant that any particle that jumped above the crystal rather than joining it would randomly walk around on the surface of the crystal. Once enough of these particles joined the second layer they could also form crystals themselves.

Unfortunately, this behaviour means it is difficult to study this system quantitatively as the particles in the top layer obscure the tracking of the particles in the bottom layer. This can be seen in the bottom panel of Figure 7.5 which shows the average hexatic order parameter for each area fraction as the system cools. The plots are extremely noisy as the particles on the top layer obscure the particles on the bottom layer, affecting the results. One possible means to solve this would be to add a lid to the system to prevent particles from jumping high enough to stack on top of one another. However, as discussed before, introducing a lid can significantly change the phase behaviour of the system[Prevost et al., 2004].

2.31 mm spacing

Next, I look at a different spacing where particles form a perfectly commensurate $\frac{\sqrt{3}}{2} \times \frac{\sqrt{3}}{2} R30^\circ$ crystal. The system was started with the same area fraction of particles at the same acceleration of 3.4 and cooled to 2.0.

Figure 7.6 shows snapshots of the system for different area fractions and accelerations as the system cools. Each arrow represents a particle's hexatic order parameter. As the system cools it can be seen that the crystal that nucleates from a point continues to grow as the system cools. The phase of the hexatic order parameter is $\approx \pm\pi$ which is consistent with the expected direction of the crystal.

Again the crystal seems to undergo inelastic collapse such that particles in the crystal seem to be completely motionless while particles in the surrounding liquid seem to have quite a high energy. However, in this case, the particles don't stack on top of each other forming a second layer. Perhaps while the crystal doesn't seem to move it may still have more energy than the crystal in the 2.00 mm case, ejecting particles from the top layer or allowing them to fall into the bottom layer by pushing other particles aside.

Like the rotated system in Chapter 5, when the area fraction of the system is sufficiently low enough that the number of particles is less than the number of holes we cease to see any crystallisation. This is because each particle becomes trapped by its hole which holds the particles far enough apart that they cannot interact - only becoming ordered once the temperature is low that all the balls become trapped by the holes.

The bottom panel in Figure 7.6 shows the average hexatic order parameter for the three different systems of different area fractions as the system is cooled. Here, we can see that as the area fraction is increased the start of the transition point moves towards higher accelerations.

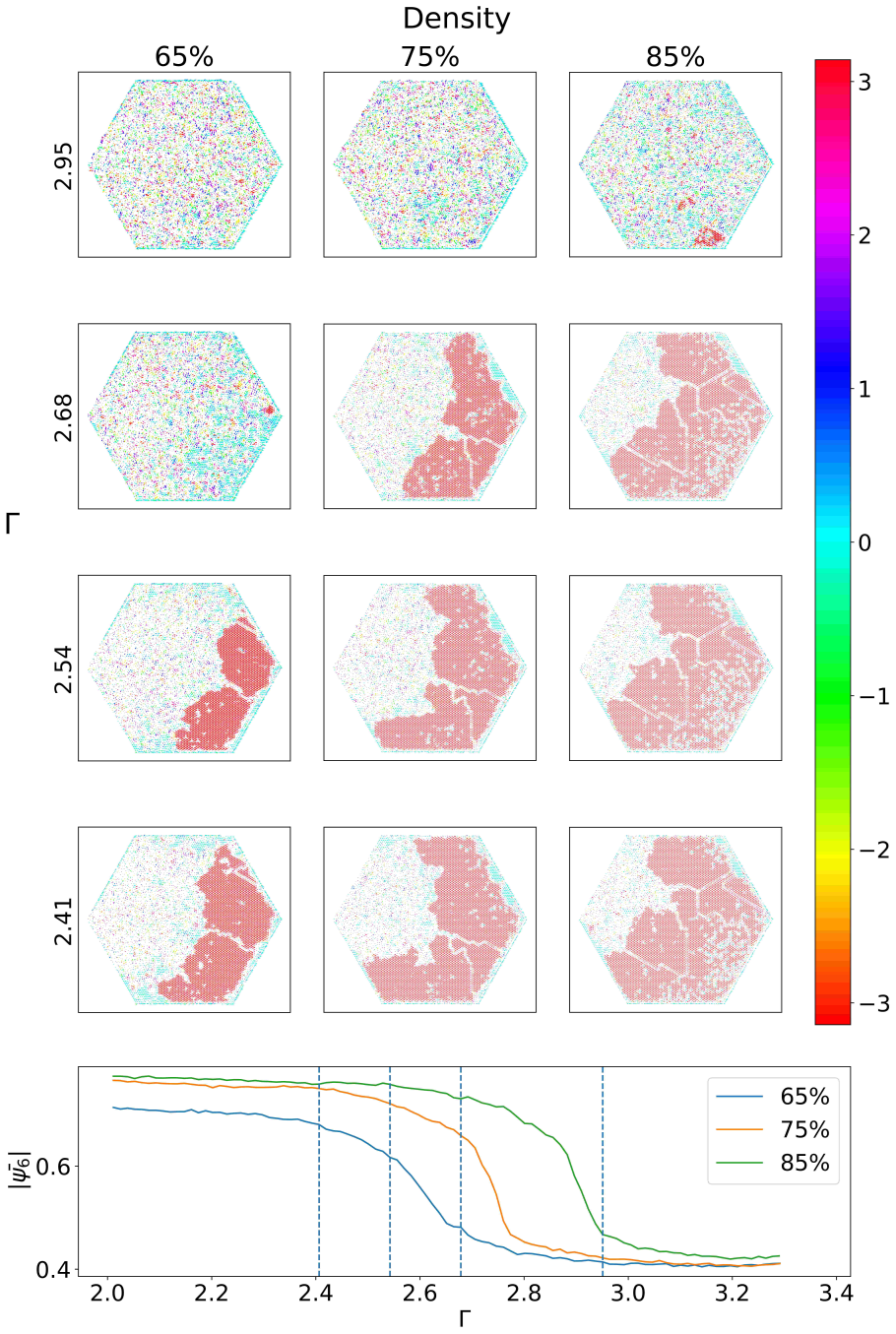

Figure 7.6: $L = 2.31$ **mm.** Top: Snapshots of the system at different area fractions and dimensionless accelerations. Each particle is represented by an arrow where its size and direction indicate the magnitude and phase of the particle's hexatic order parameter. The colour of the arrow also indicates the phase in radians. Bottom: The average hexatic order parameter of the system as it is cooled at area fractions of 0.65, 0.75 and 0.85 at a rate of 0.02 g/s.

7.4 Stretched Commensurate Crystals

2.10 mm

Since spacings of 2.00 mm cause the system to undergo inelastic collapse which prohibits numerical analysis my next step was to stretch the spacing slightly to create space in the crystal and prevent the inelastic collapse. By stretching the spacing by only 5% to 2.1 mm we observe a change in behaviour - a similar plot of the hexatic order parameter is shown in Figure 7.7. Here we see the system transitioning from liquid to solid without undergoing inelastic collapse. However, unlike the systems where the crystals form along the apothem, the solid does not seem to have any surface tension - small clusters of crystal fluctuate as the solid grows and do not appear to be stable. This behaviour is very similar to the system that is shown in Supplementary Movie 2 and can be seen as the 65% system moves from accelerations of 2.54 to 2.41 where some of the crystals that have formed then disappear again. This behaviour suggests that this system may be undergoing a continuous phase transition as it lacks the critical surface tension indicative of a first-order phase transition.

2.42 mm

The second spacing that is stretched is the 2.31 mm spacing that produces $\sqrt{3} \times \sqrt{3}R30^\circ$ crystals. By stretching it by the same 5% we reach 2.42 mm which has an equivalent spacing to particle diameter ratio as the experiments in Chapter 5. This should allow comparisons to be made between the different systems.

The plate with a hole spacing of 2.42 mm was filled with 2 mm ball bearings to the same three area fractions. The system was cooled from a dimensionless acceleration of 3.4 to 2.0 at a rate of $0.02\,\mathrm{s}^{-1}$. Figure 7.8 shows the system at different duty cycles and area fractions where each arrow represents the hexatic order parameter of each particle. Here the crystal (in red) is seen to grow from a

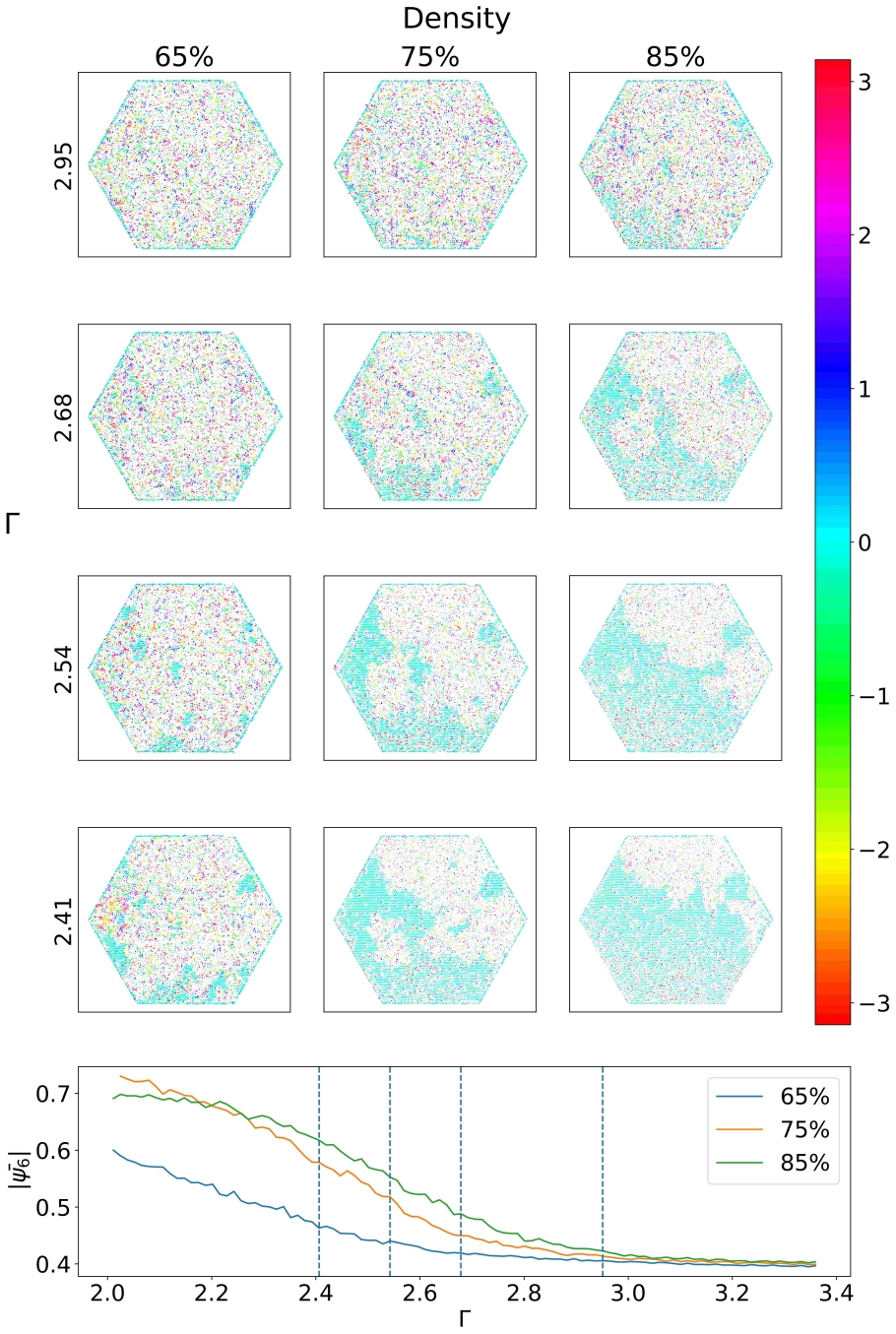

Figure 7.7: ***L* = 2.10 mm.** Top: Snapshots of the system at different area fractions and dimensionless accelerations. Each particle is represented by an arrow where its size and direction indicate the magnitude and phase of the particle's hexatic order parameter. The colour of the arrow also indicates the phase in radians. Bottom: The average hexatic order parameter of the system as it is cooled at area fractions of 0.65, 0.75 and 0.85 at a rate of 0.02 g/s.

nucleation point that remains stable once the crystal begins to grow. The crystal is oriented along the apothem direction as expected. This behaviour matches that of the system in Chapter 5 and suggests that the liquid-to-solid transition may be first-order.

However, if we compare the plots of the hexatic order, the transitions are much more gradual for this system than they are for the 2.31 mm system. This may be due to the increased space between particles that results in a lower rate of collisions between particles. The lower rate of collisions means that particles in the crystal will lose less energy and the granular temperature difference between the crystal and liquid phases will be lower.

Nature of the phase transitions

The orders of the transitions for the two types of spacing greater than 2.00 mm can be investigated by considering the hysteresis of the hexatic order parameter as the system is cooled and heated. This is performed on lattice spacings of 2.42 mm and 2.10 mm. The system is cooled from a high acceleration cycle to a low acceleration at a rate $\dot{\Gamma} = 0.02\,\mathrm{s}^{-1}$ and heated again at the same rate. The experiment is repeated 5 times for each spacing and the average order parameter at each duty cycle is found. This is shown in Figure 7.9 where the crosses and circles represent the 2.10 mm and 2.42 mm experiments respectively and the colours blue and red represent cooling and heating. Here, there is little difference between the two different experiments and while neither system seems to show the amount of hysteresis that was present in the nitrile ball system, the 2.42 mm system could have a small hysteresis loop as the heating curve sits above the cooling curve. This suggests that the phase transitions may not be first-order.

However, the coexistence between liquid and crystal which has a clear phase boundary between them suggests a first-order phase transition. Perhaps hysteresis does exist but is simply too weak to measure in our system.

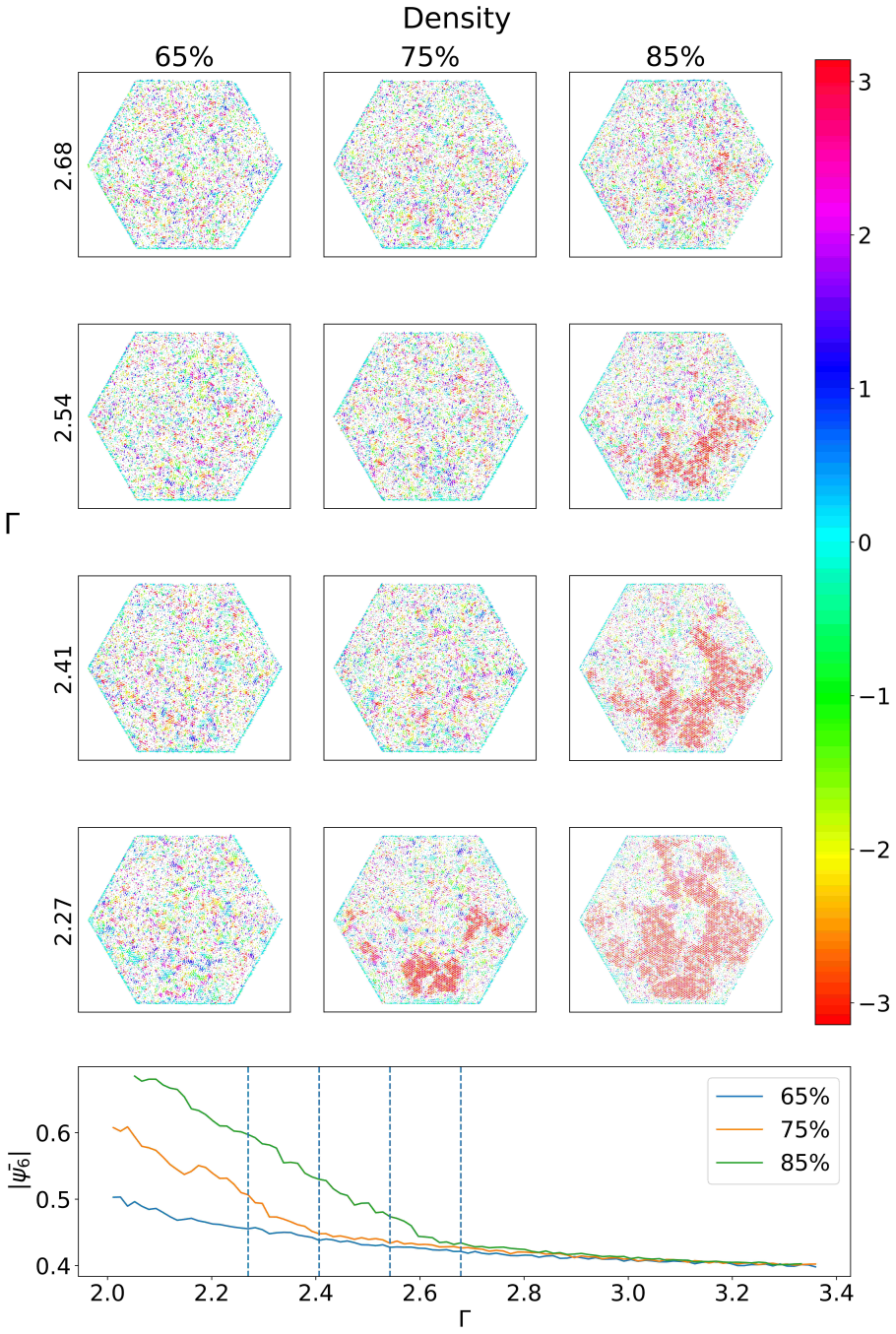

Figure 7.8: ***L* = 2.42 mm.** Top: Snapshots of the system at different area fractions and dimensionless accelerations. Each particle is represented by an arrow where its size and direction indicate the magnitude and phase of the particle's hexatic order parameter. The colour of the arrow also indicates the phase in radians. Bottom: The average hexatic order parameter of the system as it is cooled at area fractions of 0.65, 0.75 and 0.85 at a rate of 0.02 g/s.

Comparison to the previous system

Since the lattice spacing to ball diameter ratio is the same in the 2.42 mm system as it is in Chapter 5 it provides a convenient point to compare the systems. While the 2.42 mm spacing in this system doesn't provide evidence for a first-order transition, the system in Chapter 5 was very strongly first-order. This could be due to the transition to more elastic particles as this has been shown before to change a transition from first-order to continuous [Komatsu and Tanaka, 2015]. Since the evidence for first-order phase transitions was so strong for the nitrile ball system this implies it is either the different way the new dimples are made or how the more elastic ball bearings interact with the surface.

One downside of this new system is the lack of structured boundaries. The boundaries from Chapter 4 were time-consuming to create for a single spacing so creating a new geometric boundary for every spacing wasn't possible in the time available. This has many consequences that arise from not being able to control wetting at the edges of the cell. For example, not being able to prevent the ordered phase from wetting the edges makes analysing the order of the phase transition unreliable as nucleation at the edges may cause crystallisation using a different mechanism than the crystallisation at the centre of the cell.

It would be desirable to compare the energy levels that different transition points that occur in the two systems, but the accelerations cannot be easily compared as the experimental cells are of different weights and the different size balls react differently to equivalent vibrations. The smaller, more elastic ball bearings in this system required a much lower power from the shaker than the inelastic nitrile balls used in the previous chapters.

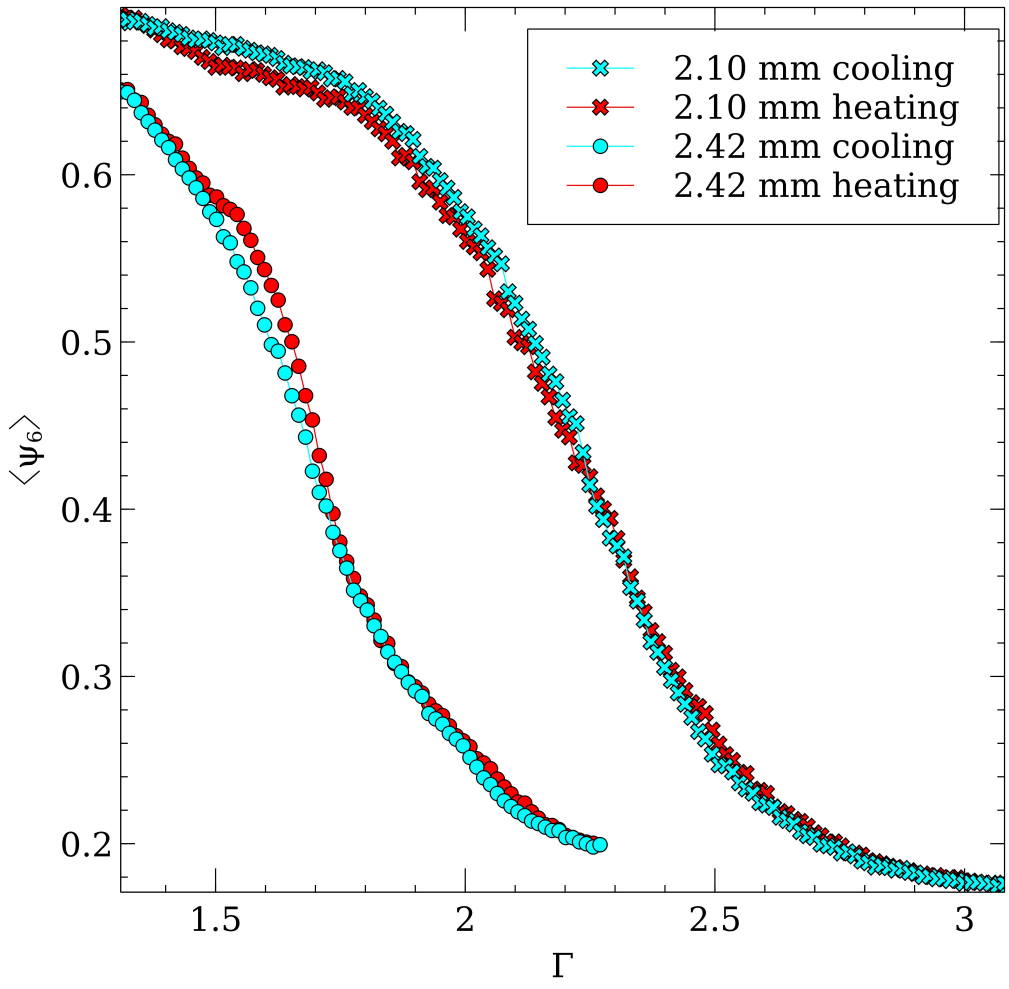

Figure 7.9: Testing for hysteresis on the 2.42 mm and 2.15 mm surfaces. Neither spacing shows much evidence of hysteresis.

7.5 Incommensurate Crystals

It has been shown above that as the lattice spacing is stretched from perfectly commensurate spacings systems still form commensurate lattices, just with greater spacing. One method of creating incommensurate crystals is to use spacings smaller than the ball's diameter. Spacings between 1.87 mm and 1.98 mm were investigated. The systems were cooled from $\Gamma = 3.4$ to $\Gamma = 2.0$ at a rate of $0.2\,\mathrm{s}^{-1}$.

Figure 7.10 shows these systems at their coldest ($\Gamma = 2.0$). Instead of forming large bulk crystals like the spacing above 2 mm, the system cools to form a structure of clusters that vary in size as the spacing changes. For most of the spacings, there are reasonable amounts of the system that are completely void of particles. This is an important observation as it shows that this behaviour is not just an effect of the optimal packing of the system but must have some aspect favouring cluster formation such as the dissipation achieved by particles in a cluster. If cluster formation wasn't favourable, particles would be expected to spread out and occupy holes uniformly across the whole system that are far enough apart.

An example of a cluster on a spacing of $L = 1.93$ mm is shown in Figure 7.11 which shows a photo of a cluster with the holes below annotated as coloured circles so that the registry between particles and dimples can be investigated. It is seen here that the central particle in a cluster sits in the centre of a hole. As you go further from the centre of the cluster, particles sit further from the centre of holes until the particle is no longer in a hole and no longer in the cluster. Figure 7.12 shows a diagram of a cluster on top of a set of holes. I use this diagram to derive a theory for the maximum size of the clusters for a given hole spacing.

For a cluster with N particles from the centre to the edge, if the central particle sits perfectly in the centre of a hole and the Nth particle sits at the outermost edge of the Nth hole then it is given that

$$(N-1)D = (N-1)L + r_{hole}, \tag{7.1}$$

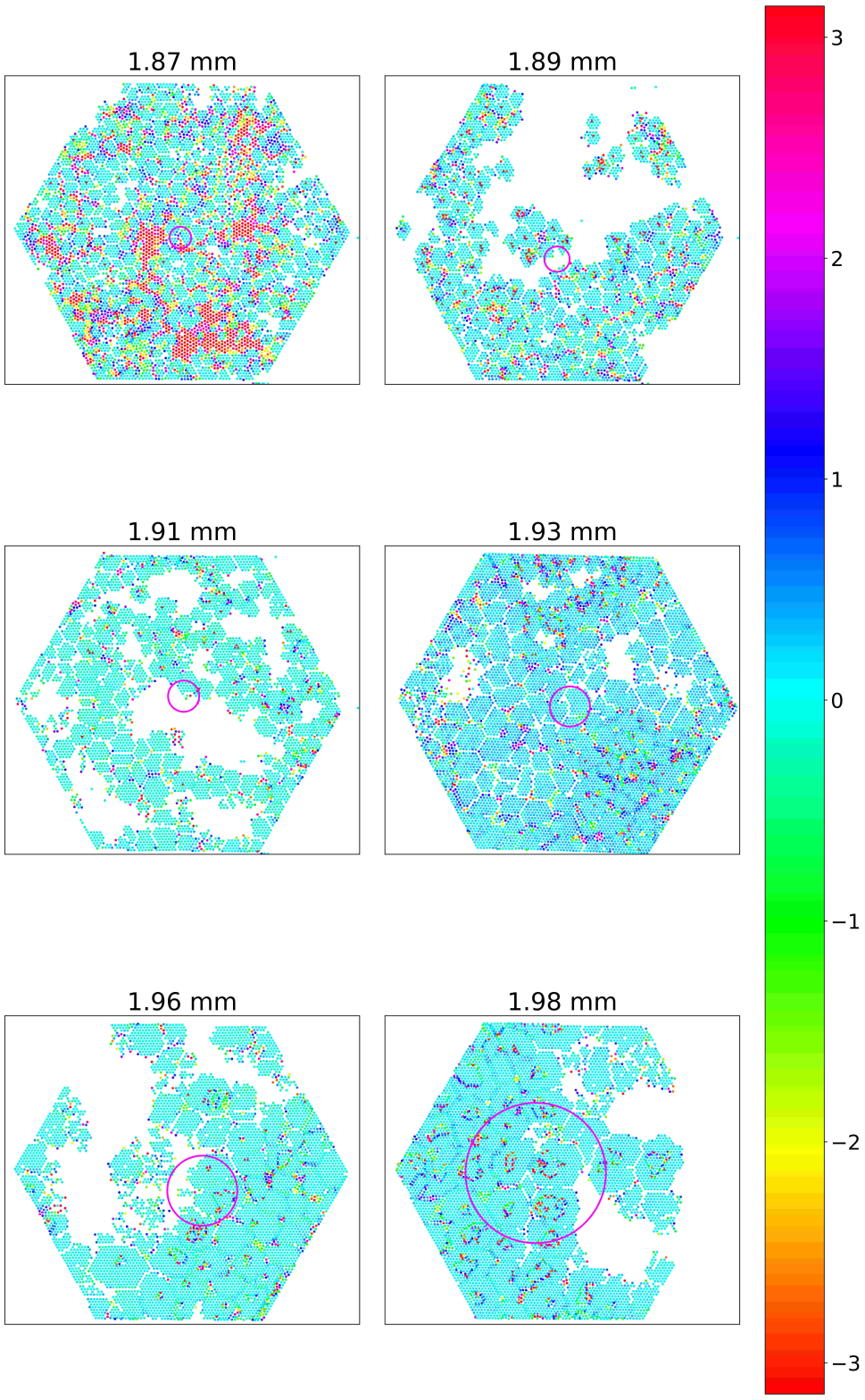

Figure 7.10: The inset panels show six systems at $\Gamma = 2.0$ after being cooled from $\Gamma = 3.4$ at a rate of $0.2\,s^{-1}$. Each circle represents a particle where is colour represents the angle of the hexatic order parameter given by the colourbar. The circles represent the expected size of a cluster predicted from the model described in Equation 7.3.

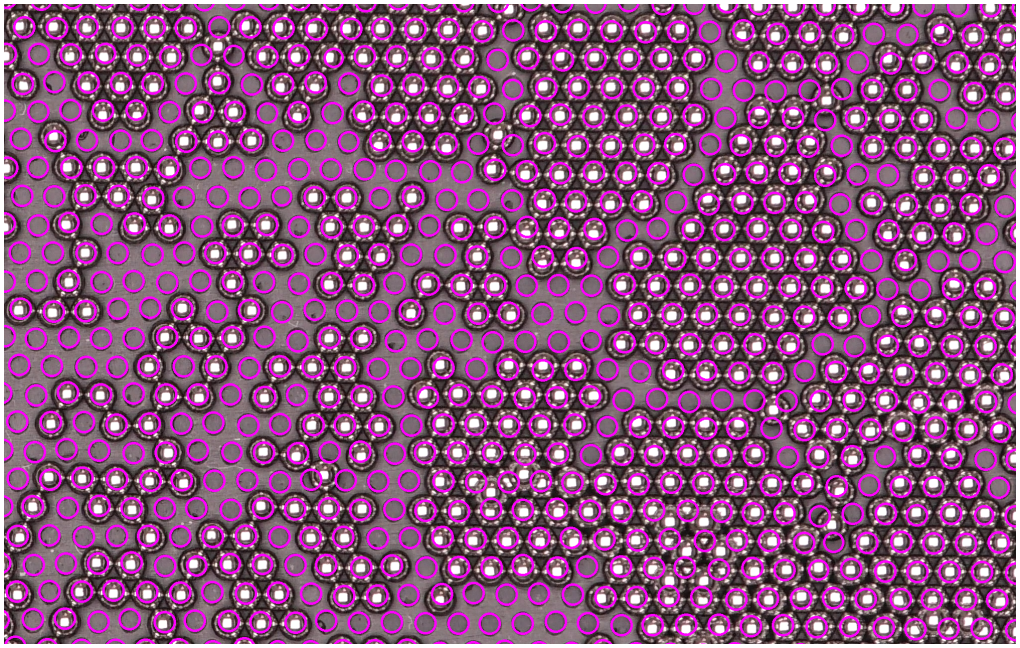

Figure 7.11: Photograph of a system of clustering particles with $L = 1.93$ mm. The positions of the holes were found using an empty system and then annotated onto the image. This shows support for the theory described in this section where a central particle sits in the centre of a hole and particles further from the centre of a cluster sit progressively closer to the outermost edge of their respective hole in a 1:1 ratio.

where D is the diameter of a ball, L is the hole spacing and r_{hole} is the radius of a hole. Rearranging this formula gives us an estimate for the maximum radius of the cluster such that

$$N = \frac{D - L + r_{hole}}{D - L}. \tag{7.2}$$

This can be rearranged to

$$N = \frac{1 - \frac{L}{D} + \frac{r_{hole}}{D}}{1 - \frac{L}{D}} \tag{7.3}$$

which makes it easier to see that the size of the cluster N increases as $L/D \to 1$.

Attempts were made to calculate the average size of a cluster in the experiments however, several different methods that were tried returned flat, noisy distributions of sizes that couldn't be reliably used to calculate an average. Each method has its own errors adding to the distribution of cluster sizes that can be seen by eye. Instead, Equation 7.3 was used to annotate Figure 7.10 with a pink circle

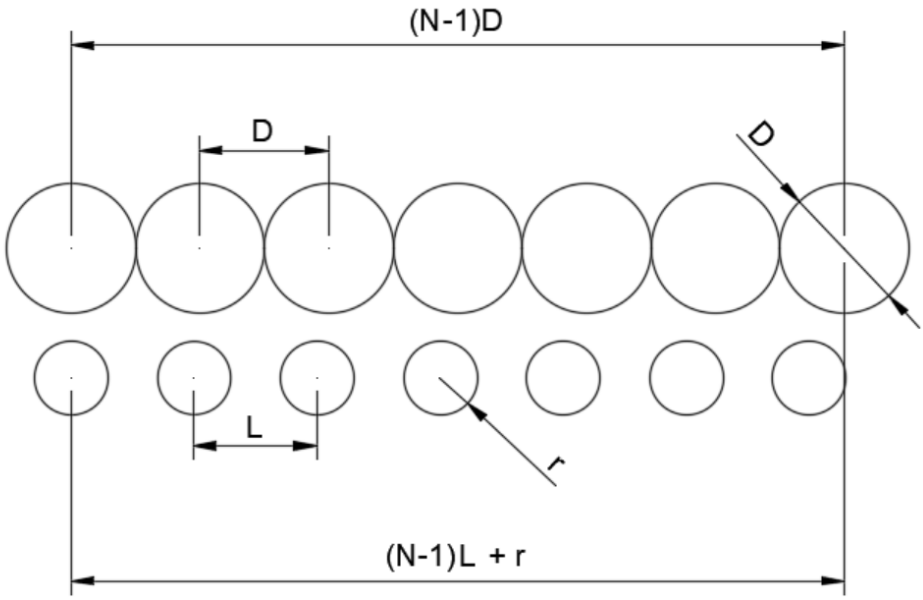

Figure 7.12: A one-dimensional diagram of the suggested model of cluster formation. The bottom row of circles represents the holes spaced L apart. The top row represents the particles forming the cluster where the leftmost particle is the central particle in a cluster and the rightmost particle is the Nth particle at the edge of the cluster which lines up with the edge of Nth hole from the centre. The left-hand side of the cluster is omitted. The dimensions at the top and bottom of the diagram represent the left and right-hand sides of Equation 7.1.

representing the size of a cluster calculated from the theory and this is used to compare. The theory fits the experiments fairly well for the spacings from 1.87 mm to 1.93 mm but as the spacing approaches 2 mm the size of the clusters is overestimated.

This overestimation might not be a problem with the model. Instead, the proximity of other clusters could prevent clusters from growing to their maximum size. Adjacent clusters will always be incommensurate with each other so cannot combine once they have nucleated separately. This can be seen in the 1.98 mm plot in Figure 7.10 where grain boundaries separate large clusters.

There could also be problems with testing the model that arise from errors in creating the surfaces. The error in the hole radius was calculated to be 0.03 mm. This was measured by photographing several small regions of one of the patterned surfaces against a backlight. A threshold was then applied to the image using the high contrast of the light through the holes to the black plastic to create

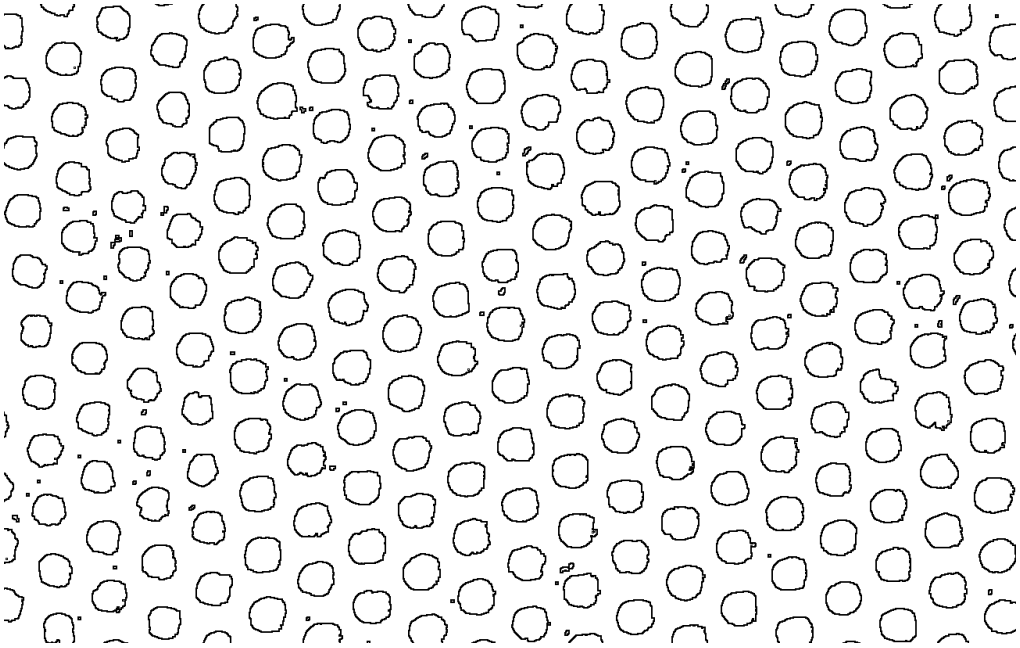

Figure 7.13: The contours representing the holes used to measure the error on the hole radius r_{hole}. This shows the variety in how much holes differ from a perfect circle which may explain the variation in cluster sizes that are produced in experiments.

a binary image. Contours for each hole were then calculated and for each contour, the minimum enclosing circle was used to get the radius of each hole. The error quoted above is the standard deviation of these radii. Figure 7.13 shows examples of the contours found where it can be clearly seen that the holes are not perfectly round. This may be another reason why the system doesn't follow the predicted theory perfectly. It could also explain why attempts to calculate the average size of clusters for each spacing failed.

Figure 7.14 shows how the size of the cluster varies with the hole spacings with the error bars calculated using the error on the hole radius. It can be seen that the error is fairly small for the smaller spacings but increases rapidly as the hole spacing approaches 2.00 mm. This suggests that the theory derived above could be valid but that the experiment is not precise enough to test this theory rigorously as the hole spacing approaches 2.00 mm.

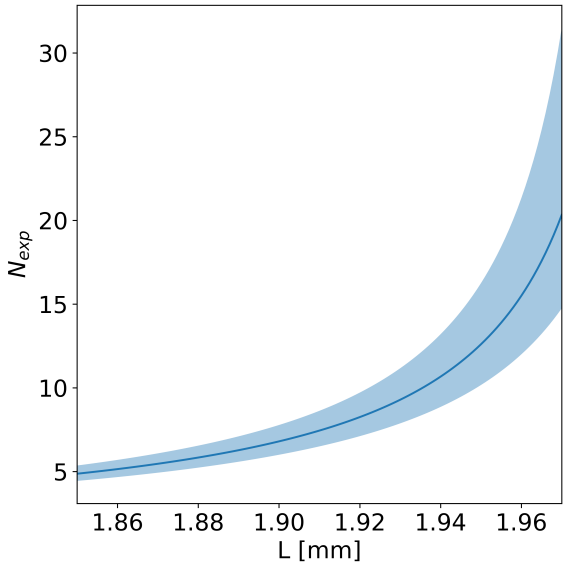

Figure 7.14: Expected cluster size N_{exp} as a function of the hole spacing L described by Equation 7.3 for $D = 2$ mm, $r_{hole} = 0.58 \pm 0.03$ mm and $\delta L = 0.01$ mm. The shaded region shows the error in the model calculated by considering the error in the hole spacing and the hole radius.

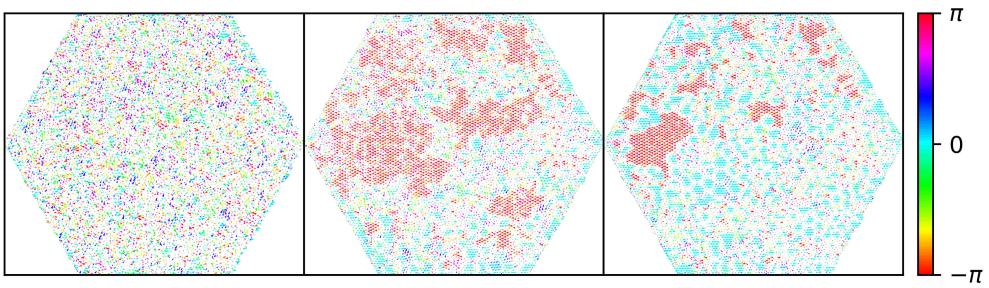

Figure 7.15: Snapshots of cooling on the 1.91 mm surface at an area fraction of 0.85. Arrows show the hexatic order parameter of individual particles. The length and direction represent the magnitude and phase of the hexatic order parameter. The colour also represents the phase.

7.6 Competing Phases

There are a few more particularly interesting lattice spacings that I have not yet discussed where two different crystal phases are present at the same time. These two crystal phases are the clusters (when the spacing was less than 2.00 mm) and the rotated commensurate crystal (when the spacing is 2.31 mm and 2.42 mm). The two spacings that show these competing phases are $L = 1.91$ mm and $L = 2.25$ mm. Here, I show an in-depth analysis of the $L = 1.91$ mm surface and compare it briefly to the system with the $L = 2.25$ mm surface.

1.91 mm

The system with the $L = 1.91$ mm surface is filled with the previously used 2.00 mm steel ball bearings to an area fraction of 0.85. Figure 7.15 shows snapshots of the system as it cools from $\Gamma = 2.95$ to $\Gamma = 1.85$ at a rate of $4 \times 10^{-4}\,\mathrm{s}^{-1}$. The arrows represent the hexatic order parameter, ψ_6, of each of the particles, where the length represents the magnitude and the angle represents the phase. The colour of the arrow also describes the phase (see colour bar). The two distinct phases can be seen once the system has cooled.

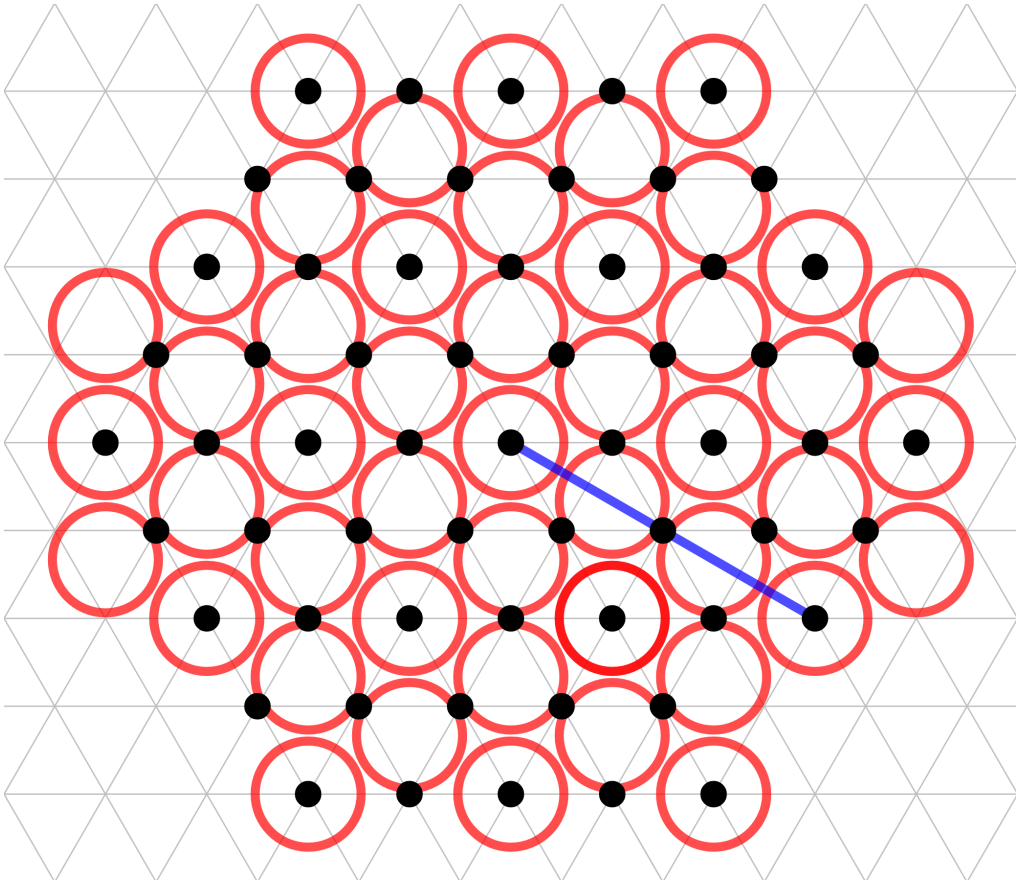

Figure 7.16: Sketch of how the particles in a crystal (red circles) sit on top of the holes (black dots) when $L = 1.91$ mm. The crystal is rotated such that one in every three particles along the apothem sits in a dimple. The blue line has a length of $2\sqrt{3}L$.

In red, a bulk crystal phase forms. The particles in this phase have a hexatic phase of $\pm\pi$ which means they are rotated 30° with respect to the dimple lattice. This is similar to what we saw for the crystal phase that appeared for the 2.31 mm spacing. However, instead of there being one particle between particles sitting in dimples there are now two particles. Figure 7.16 shows a diagram of how these particles (red circles) are located with respect to the dimples (black dots). On this diagram, the blue line has a length of $2\sqrt{3}L$, where L is the dimple spacing.

In blue, a clustered crystal forms. The particles in this phase have a hexatic phase of 0 which means they are oriented in the same direction as the dimple lattice. They are incommensurate with the dimple lattice. This is the same as the clusters that formed in Section 7.5.

If we revisit Figure 7.15 we see that the bulk phase grows first before the clusters begin to dominate as the system cools further. This raises many questions about which phase is the most stable at each temperature. To help answer these questions, I repeated this experiment at three different rates. The particles were classified based on the phase and magnitude of their hexatic order. Cluster particles required a magnitude greater than 0.8 and a phase between $\pm\frac{\pi}{4}$. Bulk crystal particles required a magnitude greater than 0.8 and a phase less than $-\frac{3\pi}{4}$ or greater than $\frac{4\pi}{4}$.

The results of cooling are shown in Figure 7.17 for cooling rates of (a) $4\times10^{-3}\,\mathrm{s}^{-1}$, (b) $4\times10^{-4}\,\mathrm{s}^{-1}$ and (c) $4\times10^{-5}\,\mathrm{s}^{-1}$. For each rate, there is a graph and three snapshots of the system. The graph shows how the percentage of particles in the bulk crystal phase (red) and clusters phase (blue) changes as the system is cooled. The three vertical lines represent the accelerations of the three snapshots drawn below. In each of the snapshots, the particles are coloured based on their classification. Cluster particles are in blue, bulk crystal particles are in red, and all other particles are in black. The accelerations of the snapshots are intentionally different between cooling rates and show points of key behaviour. The highest acceleration snapshots are placed near the point in which regions of crystal/cluster start appearing. The middle snapshot is placed near the peaks of the graphs. The lowest snapshot is placed where the system stops evolving.

Figure 7.17 shows that the cooling rate clearly affects the formation of the two different crystal phases. If we look at the left-hand snapshots (the lowest acceleration) and corresponding positions on the graphs we can see that the clusters are always the dominant phase regardless of the cooling rate. This suggests that at these low accelerations, the clusters belong to the more stable phase. We can also see that as the cooling rate decreases the amount of bulk crystal in the lowest amplitude snapshot reduces. This suggests that the bulk crystal phase is metastable at these low accelerations as more of the particles remain in this phase as the system is undercooled.

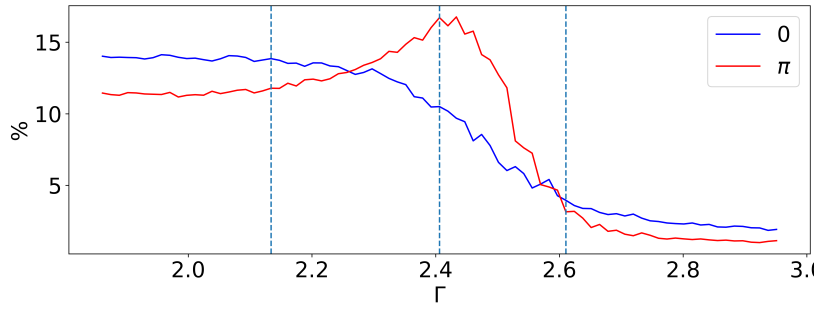

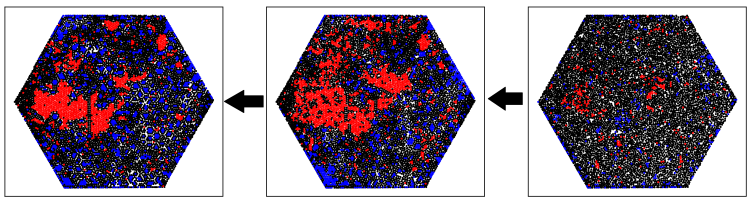

(a)

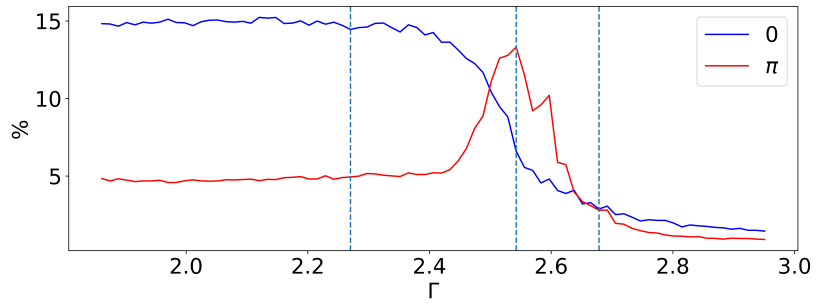

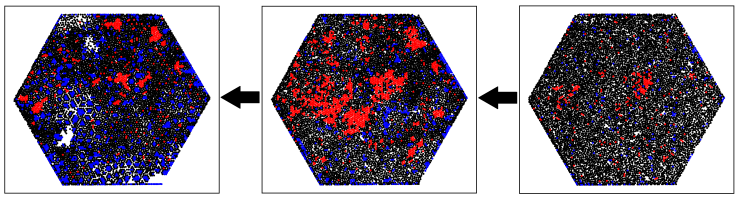

(b)

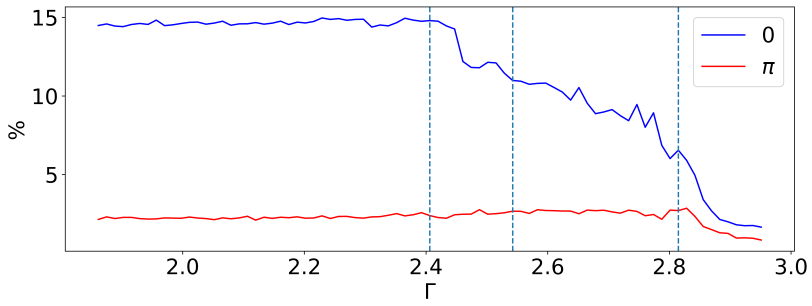

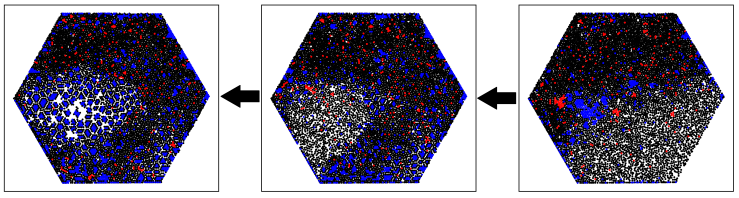

(c)

Figure 7.17: For a hole spacing of $L = 1.91$ mm the three panels show how the two distinct phases, crystal (red) and cluster (blue), form as the system cools at rates, $\dot{\Gamma}$ of (a): 4×10^{-3} s^{-1}, (b): 4×10^{-4} s^{-1} and (c): 4×10^{-5} s^{-1}. The vertical dashed lines represent the values of dimensionless acceleration the snapshots below are taken. The arrows show the time evolution of the system from high to low Γ.

For the fastest cooling rates, there is a peak in the bulk crystal phase where the percentage of particles in the bulk crystal phase is greater than those in the cluster phase. Since this peak is not visible for the slowest rate, it suggests that the crystal phase is always metastable. At the faster cooling rates, particles have similar probabilities of moving from the liquid into either the bulk crystal or cluster phases, so similar amounts of the two phases form initially. This might still be the case for the slowest rate, but particles that move into the bulk crystal phase have time to overcome the energy barrier to move into the cluster phase.

The vertical lines representing the onset of crystal phases show evidence of an undercooled liquid for all rates. At the highest accelerations, the stable phase is the liquid. As the system is cooled, the liquid phase is no longer stable. The faster the system cools, the lower the acceleration of the onset of crystal phases. This is evidence that the liquid has been undercooled and remains in a metastable phase.

Why might the clustered phase be the more stable phase? In the clusters, inelastic collapse is possible as all the particles in the cluster are in contact with each other. Whereas, in the bulk crystal phase, the particles have tiny gaps between them. That means that particles in the cluster phase lose much more energy than particles in the bulk crystal phase to collisions. Therefore, the cluster phase will have lower energy for a given acceleration.

Why does the bulk crystal form more readily at faster cooling rates? Firstly, the bulk crystal is a more stable phase than the liquid phase as its closer spacing allows for more dissipation. I suggest that this can be explained by considering the timescales associated with converting between the different phases. If the timescale associated with converting from liquid to cluster is t_{LC}, from liquid to bulk crystal is t_{LB} and from bulk crystal to cluster is t_{BC}. If the timescales are such that $t_{LB} + t_{BC} < t_{LC}$ then at faster rates when the experiment timescale $t_{exp} < t_{LC}$, the system can move to the most stable state by first moving through the bulk crystal phase. The experiment timescale t_{exp} is the time taken for the

system to move from the Γ where the liquid is most favourable to the Γ where the crystal is most favourable. At slower rates when the experiment timescale $t_{exp} > t_{LC}$ the system can move directly into the more stable cluster phase without first going through the bulk crystal phase.

2.25 mm

In the 2.25 mm spacing, the behaviour is reversed. The bulk crystal lattice now has the same orientation as the dimpled lattice below it. Whereas, the clusters lattice is now rotated 30° with respect to the dimpled lattice. Along this rotated direction, dimples are located 3.90 mm apart which is 1.95 mm when halved. This allows clusters to form using the same mechanism as for the 1.95 mm surface with a simple rotation of the clusters.

The same experiment as before was performed on this surface at a rate, $\dot{\Gamma}$ of $8 \times 10^{-4}\ \mathrm{s}^{-1}$ and the results are shown in Figure 7.18. As the hexatic phase of the two different crystal phases is reversed, red now represents the clusters and blue represents the bulk crystal. The behaviour is almost identical to the 1.91 mm spacing. Upon cooling, similar amounts of the clusters and bulk crystal form (middle snapshot) before the amount of bulk crystal reduces to make way for the more stable cluster phase.

A large aspect of work in this field has been showing that ideas from equilibrium statistical mechanics can be used to describe behaviours in these far-from-equilibrium systems. The results from this section take this further and show evidence of equilibrium ideas such as undercooling and metastability.

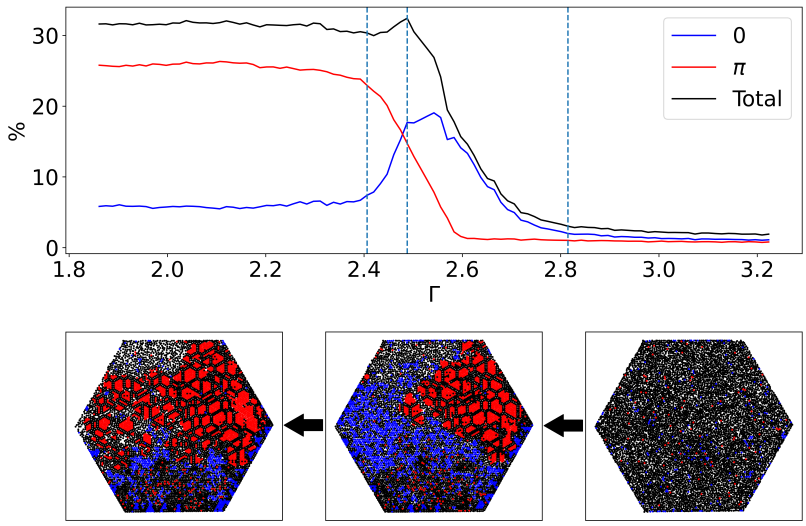

Figure 7.18: For a hole spacing of $L = 2.25$ mm the three panels show how the two distinct phases, crystal (blue) and cluster(red), form as the system cools at a rate of $\dot{\Gamma} = 8 \times 10^{-4}\,\mathrm{s}^{-1}$. The vertical dashed lines represent the values of dimensionless acceleration the snapshots below are taken.

7.7 Conclusions

I've shown that for the spacings I have investigated three distinct crystal types are observed. Commensurate crystals form that are aligned with the underlying dimple lattice for spacings 2.00 mm and 2.10 mm. For the 2.31 and 2.42 mm dimple spacings, commensurate crystals also form that are rotated 30° with respect to the dimple lattice and have two particles per dimple in this direction. For spacings less than 2.00 mm, incommensurate crystals form in clusters which increase in size as the ball diameter to dimple spacing ratio approaches 1. There were also two spacings, 1.91 mm and 2.25 mm, that showed a combination of these phases.

Inelastic collapse was also observed for the 2.00 mm, 2.31 mm and all spacings less than 2.00 mm. As the spacing gets closer to the diameter of the particles for a given energy input, the frequency of the collisions increases, dissipating more energy. For these spacings, all the particles in the crystals are always in contact, so the frequency of collisions effectively goes to infinity. These effective infinite collisions act to destroy all the kinetic energy for these particles as the whole crystal can dissipate the vibrational energy. For other spacings, particles in their mean crystal positions are not in contact with their neighbours, so the frequency of collisions is much lower and the energy of the crystal is higher.

Table 7.1 shows a summary of the phases that occur at different dimple spacings.

Spacing, L (mm)	L/D	Crystal	Inelastic Collapse
< 2.00	< 1	Clusters	✓
2.00	1	1×1	✓
2.10	1.05	1×1	×
2.31	$\frac{2}{\sqrt{3}} = 1.15$	$\frac{\sqrt{3}}{2} \times \frac{\sqrt{3}}{2} R30°$	✓
2.42	1.21	$\frac{\sqrt{3}}{2} \times \frac{\sqrt{3}}{2} R30°$	×
1.91	0.96	Clusters and $\frac{2\sqrt{3}}{3} \times \frac{2\sqrt{3}}{3} R30°$	✓clusters, × crystal
2.25	1.125	$R30°$ clusters and 1×1	✓clusters, × crystal

Table 7.1: A summary of the crystal structures that form at different dimple spacings. L/D is the lattice spacing to particle diameter ratio.

Through using the dimple spacings that showed both the bulk crystal and clustered crystal phases we were also able to show evidence of metastability and undercooling which suggests that the phase transitions in these systems are first-order.

Chapter 8

Conclusions and Future Work

8.1 Conclusions

In this thesis I have shown that by changing the topography of the surface we successfully changed the nature of the phase transition for our system from continuous to first-order. This first-order phase transition allowed us to investigate to what extent ideas from equilibrium statistical mechanics can be applied to our system.

Our initial investigations in Chapter 3 showed that using dimpled lattices with three different spacings produced three distinct behaviours. These three behaviours were: small clusters of crystal, crystals with no clear coexistence and crystals with a clear coexistence with liquid. The final behaviour showed first-order behaviour, so was focussed on for much of the thesis.

Using this first-order system, we investigated, in Chapter 4, how we could alter the geometry and elasticity of the boundaries to control which phase they were wetted by. Controlling the wetting consequently allowed us to tightly control where the liquid and solid phases appeared. This is similar to the way wetting can be used to control equilibrium systems and could have some applications in the manufacturing of 2D materials.

What we learned about controlling the spatial configuration of the phases facilitated the investigations into the nature of the phase transition in Chapter 5. We showed that the dimples changed the nature of the transition from continuous to first-order by considering coexistence, the presence of hysteresis and a single peak in the orientational and positional susceptibilities. In addition, we showed that the equilibrium ideas of capillary scaling at interfaces could be applied to our non-equilibrium system, however, how this is used to calculate the surface tension remains unclear.

Together the work in Chapter 4 and Chapter 5 showed that by altering the geometry of the surface and boundaries we can carefully control the liquid-to-solid phase transitions. A selection of results from these chapters were published in Physical Review Letters [Downs et al., 2021] and was well received, featuring in Physics as an editor's suggestion.

It was proposed that the orderphobic effect discovered in [Katira et al., 2016] should be generic to any system with a first-order order-disorder phase transition. We aimed to test whether this generality extended to our non-equilibrium system. The results I presented in Chapter 6 showed behaviour which could be explained by the orderphobic effect. Unfortunately, we were unable to design an experiment that would allow enough repeatability of results to confirm the effect.

Finally, in Chapter 7, we reduced our focus on the single dimple spacing and investigated more generally how changing the dimple spacing changes the phase behaviour of our system. We showed a variety of different phases for different spacings. A few specific spacings showed a combination of different phases which were used to investigate the relative stability of the different phases.

Throughout this thesis, I have shown time and again that despite the non-equilibrium nature of our experiment that many of the classic equilibrium results hold. I've shown that our system can exhibit hysteresis, surface tension with capillary wave fluctuations and an equilibrium-like first-order phase transition. This is very surprising as non-equilibrium systems break many of the assumptions of equilibrium statistical mechanics. We have shown that these ideas hold for

our system which should provide insight for theorists to investigate how this is the case. However, it would be interesting to know if these ideas still hold as we move from our steady-state system to one that is even further from equilibrium? For example, for systems that do not form steady states at fixed temperatures.

Another success of this work was the development of our open-source particle tracking software. The software allows for tracking and analysis of objects in any two-dimensional experiments that produces videos or images. This has significantly improved our own workflow and has successfully been used by undergraduates with limited coding skills to perform better physics experiments. We published this work in the Journal of Open Source Software [Smith and Downs, 2021] to allow others to make use of our tool.

8.2 Future Work

The experiments presented in this thesis have generated several new questions. Here I present a few of the questions that I would like to see answered.

Firstly, it would be great to finish off the work in Chapter 6 investigating the orderphobic effect. If an experiment could be created that allows a repeatable investigation then it would hopefully confirm the generality of the orderphobic effect proposed in [Katira et al., 2016]. This would be exciting as it would be yet another equilibrium behaviour that can be extended to a non-equilibrium system.

The work investigating the different spacings in Chapter 7 used a new system of ball bearings on a laser-cut sheet. This produced behaviour that appeared first-order when considering the coexistence of phases but didn't exhibit the large hysteresis loops that were observed for the nitrile system. This behaviour is different and must have been caused by either changing the particles from nitrile to stainless steel or changing the material and nature of the surface. It would be desirable to investigate why this was the case, perhaps repeating the investigations from Chapter 5 with stainless steel balls or the investigations from Chapter 7 with nitrile balls would provide some insight.

It would also be interesting to investigate how the dimples interact with the particles in the system. Specifically, the difference between interactions of the milled dimples and laser cut holes. At very low Γ, it is clear that the dimples just trap the particles due to gravity. However, at higher Γ it is not so clear. We are particularly interested in how the horizontal motion of the particles is changed by the dimples. To investigate this, we have developed a small apparatus using a quasi-1D cell which combined with a high-speed camera should allow us to answer these questions.

It is not possible to compare the transition points between different experiments by comparing the values of Γ that they occur at. This is because changing the dimple spacing seems to change the energy of the particles. One parameter that could be used to compare the systems is the granular temperature, T_g. Unfortunately, we could not calculate an accurate value for T_g given the slow frame rate of our camera. An investigation into how the dimple spacing affects the granular temperature of the different phases in our system could therefore be insightful. It would also be useful to perform simulations at different sampling rates to work out what frame rate a camera would need to calculate T_g as a high frame rate camera at a high enough resolution would be very expensive.

Bibliography

[Aarts et al., 2004] Aarts, D. G. A. L., Schmidt, M., and Lekkerkerker, H. N. W. (2004). Direct visual observation of thermal capillary waves. *Science*, 304(5672):847–850.

[Aeppli and Bruinsma, 1984] Aeppli, G. and Bruinsma, R. (1984). Hexatic order and liquid density fluctuations. *Physical Review Letters*, 53(22):2133–2136.

[Alder and Wainwright, 1957] Alder, B. J. and Wainwright, T. E. (1957). Phase transition for a hard sphere system. *The Journal of Chemical Physics*, 27(5):1208–1209.

[Alder and Wainwright, 1962] Alder, B. J. and Wainwright, T. E. (1962). Phase transition in elastic disks. *Physical Review*, 127(2):359–361.

[Allan et al., 2014] Allan, D., Caswell, T. A., Keim, N., Boulogne, F., Perry, R. W., and Uieda, L. (2014). *Trackpy: Trackpy v0.2.4*.

[Anderson et al., 2017] Anderson, J. A., Antonaglia, J., Millan, J. A., Engel, M., and Glotzer, S. C. (2017). Shape and symmetry determine two-dimensional melting transitions of hard regular polygons. *Physical Review X*, 7(2):021001.

[Archer and Malijevský, 2016] Archer, A. J. and Malijevský, A. (2016). Crystallization of soft matter under confinement at interfaces and in wedges. *Journal of Physics: Condensed Matter*, 28(24):244017.

[Armstrong et al., 1989] Armstrong, A. J., Mockler, R. C., and O'Sullivan, W. J. (1989). Isothermal-expansion melting of two-dimensional colloidal monolayers on the surface of water. *Journal of Physics: Condensed Matter*, 1(9):1707–1730.

[Bak, 1982] Bak, P. (1982). Commensurate phases, incommensurate phases and the devil's staircase. *Reports on Progress in Physics*, 45(6):587–629.

[Bernard, 2011] Bernard, E. (2011). *Algorithms and applications of the Monte Carlo method : Two-dimensional melting and perfect sampling*. Theses, Université Pierre et Marie Curie - Paris VI.

[Bernard and Krauth, 2011] Bernard, E. P. and Krauth, W. (2011). Two-step melting in two dimensions: First-order liquid-hexatic transition. *Physical Review Letters*, 107(15).

[Bernard et al., 2009] Bernard, E. P., Krauth, W., and Wilson, D. B. (2009). Event-chain monte carlo algorithms for hard-sphere systems. *Physical Review E*, 80(5):056704.

[Birgeneau et al., 1981] Birgeneau, R. J., Brown, G. S., Horn, P. M., and Moncton, D. E. (1981). Synchrotron x-ray study of monolayer krypton melting. *Journal of Physics C: Solid State Physics*, 14(3):L49–L54.

[Castillo et al., 2012] Castillo, G., Mujica, N., and Soto, R. (2012). Fluctuations and criticality of a granular solid-liquid-like phase transition. *Physical Review Letters*, 109(9):095701.

[Chandler, 2005] Chandler, D. (2005). Interfaces and the driving force of hydrophobic assembly. *Nature*, 437(7059):640–647.

[Crocker and Grier, 1996] Crocker, J. C. and Grier, D. G. (1996). Methods of Digital Video Microscopy for Colloidal Studies. *Journal of Colloid and Interface Science*, 179(1):298–310.

[Dash et al., 1995] Dash, J. G., Fu, H., and Wettlaufer, J. S. (1995). The premelting of ice and its environmental consequences. *Reports on Progress in Physics*, 58(1):115–167.

[Davey et al., 1984] Davey, S. C., Budai, J., Goodby, J. W., Pindak, R., and Moncton, D. E. (1984). X-ray study of the hexatic-phase transition in liquid-crystal films. *Physical Review Letters*, 53(22):2129–2132.

[Downs et al., 2021] Downs, J., Smith, N., Mandadapu, K., Garrahan, J., and Smith, M. (2021). Topographic control of order in quasi-2d granular phase transitions. *Physical Review Letters*, 127(26):268002.

[Engel et al., 2013] Engel, M., Anderson, J. A., Glotzer, S. C., Isobe, M., Bernard, E. P., and Krauth, W. (2013). Hard-disk equation of state: First-order liquid-hexatic transition in two dimensions with three simulation methods. *Physical Review E*, 87(4).

[Forterre and Pouliquen, 2008] Forterre, Y. and Pouliquen, O. (2008). Flows of dense granular media. *Annual Review of Fluid Mechanics*, 40(1):1–24.

[Ganapathy et al., 2010] Ganapathy, R., Buckley, M. R., Gerbode, S. J., and Cohen, I. (2010). Direct measurements of island growth and step-edge barriers in colloidal epitaxy. *Science*, 327(5964):445–448.

[Geim and Novoselov, 2007] Geim, A. K. and Novoselov, K. S. (2007). The rise of graphene. *Nature Materials*, 6(3):183–191.

[Gribova et al., 2011] Gribova, N., Arnold, A., Schilling, T., and Holm, C. (2011). How close to two dimensions does a lennard-jones system need to be to produce a hexatic phase? *The Journal of Chemical Physics*, 135(5):054514.

[Grimes and Adams, 1979] Grimes, C. C. and Adams, G. (1979). Evidence for a liquid-to-crystal phase transition in a classical, two-dimensional sheet of electrons. *Physical Review Letters*, 42(12):795–798.

[Halperin and Nelson, 1978] Halperin, B. I. and Nelson, D. R. (1978). Theory of Two-Dimensional Melting. *Physical Review Letters*, 41(2):121–124.

[Han et al., 2008] Han, Y., Ha, N. Y., Alsayed, A. M., and Yodh, A. G. (2008). Melting of two-dimensional tunable-diameter colloidal crystals. *Physical Review E*, 77(4):041406.

[Hoover and Ree, 1968] Hoover, W. G. and Ree, F. H. (1968). Melting transition and communal entropy for hard spheres. *The Journal of Chemical Physics*, 49(8):3609–3617.

[Jaster, 2004] Jaster, A. (2004). The hexatic phase of the two-dimensional hard disk system. *Physics Letters A*, 330(1-2):120–125.

[Kapfer and Krauth, 2015] Kapfer, S. C. and Krauth, W. (2015). Two-dimensional melting: From liquid-hexatic coexistence to continuous transitions. *Physical Review Letters*, 114(3).

[Katira et al., 2015] Katira, S., Mandadapu, K. K., Vaikuntanathan, S., Smit, B., and Chandler, D. (2015). The order-disorder transition in model lipid bilayers is a first-order hexatic to liquid phase transition.

[Katira et al., 2016] Katira, S., Mandadapu, K. K., Vaikuntanathan, S., Smit, B., and Chandler, D. (2016). Pre-transition effects mediate forces of assembly between transmembrane proteins. *eLife*, 5.

[Komatsu and Tanaka, 2015] Komatsu, Y. and Tanaka, H. (2015). Roles of energy dissipation in a liquid-solid transition of out-of-equilibrium systems. *Physical Review X*, 5(3):031025.

[Kosterlitz and Thouless, 1973] Kosterlitz, J. M. and Thouless, D. J. (1973). Ordering, metastability and phase transitions in two-dimensional systems. *Journal of Physics C: Solid State Physics*, 6(7):1181.

[Lee and Strandburg, 1992] Lee, J. and Strandburg, K. J. (1992). First-order melting transition of the hard-disk system. *Physical Review B*, 46(17):11190–11193.

[Li and Ciamarra, 2020] Li, Y.-W. and Ciamarra, M. P. (2020). Attraction tames two-dimensional melting: From continuous to discontinuous transitions. *Physical Review Letters*, 124(21):218002.

[Limmer and Chandler, 2014] Limmer, D. T. and Chandler, D. (2014). Premelting, fluctuations, and coarse-graining of water-ice interfaces. *The Journal of Chemical Physics*, 141(18):18C505.

[Litzinger and Stewart, 1980] Litzinger, J. and Stewart, G. (1980). *Ordering in Two Dimensions*. Elsevier.

[Luu et al., 2013] Luu, L.-H., Castillo, G., Mujica, N., and Soto, R. (2013). Capillarylike fluctuations of a solid-liquid interface in a noncohesive granular system. *Physical Review E*, 87(4):040202.

[Mak, 2006] Mak, C. H. (2006). Large-scale simulations of the two-dimensional melting of hard disks. *Physical Review E*, 73(6):065104.

[Mandelstam, 1913] Mandelstam, L. (1913). Über die rauhigkeit freier flüssigkeitsoberflächen. *Annalen der Physik*, 346(8):609–624.

[Matvija et al., 2017] Matvija, P., Rozbořil, F., Sobotík, P., Ošťádal, I., Pieczyrak, B., Jurczyszyn, L., and Kocán, P. (2017). Electric-field-controlled phase transition in a 2d molecular layer. *Scientific Reports*, 7(1).

[McNamara and Young, 1994] McNamara, S. and Young, W. R. (1994). Inelastic collapse in two dimensions. *Physical Review E*, 50(1):R28–R31.

[McTague et al., 1982] McTague, J. P., Als-Nielsen, J., Bohr, J., and Nielsen, M. (1982). Synchrotron x-ray study of melting in submonolayer ar and other rare-gas films on graphite. *Physical Review B*, 25(12):7765–7772.

[Mermin, 1968] Mermin, N. D. (1968). Crystalline order in two dimensions. *Physical Review*, 176(1):250–254.

[Mermin and Wagner, 1966] Mermin, N. D. and Wagner, H. (1966). Absence of ferromagnetism or antiferromagnetism in one- or two-dimensional isotropic heisenberg models. *Physical Review Letters*, 17(22):1133–1136.

[Miserev et al., 2021] Miserev, D., Klinovaja, J., and Loss, D. (2021). Magnetic phase transitions in two-dimensional two-valley semiconductors with in-plane magnetic field. *Physical Review B*, 103(2):024401.

[Mishra et al., 2016] Mishra, C. K., Sood, A. K., and Ganapathy, R. (2016). Site-specific colloidal crystal nucleation by template-enhanced particle transport. *Proceedings of the National Academy of Sciences*, 113(43):12094–12098.

[Motteler, 1985] Motteler, F. C. (1985). PhD thesis, The University of Washington.

[Narayan et al., 2007] Narayan, V., Ramaswamy, S., and Menon, N. (2007). Long-lived giant number fluctuations in a swarming granular nematic. *Science*, 317(5834):105–108.

[Olafsen and Urbach, 1998] Olafsen, J. S. and Urbach, J. S. (1998). Clustering, order, and collapse in a driven granular monolayer. *Physical Review Letters*, 81(20):4369–4372.

[Olafsen and Urbach, 1999] Olafsen, J. S. and Urbach, J. S. (1999). Velocity distributions and density fluctuations in a granular gas. *Physical Review E*, 60(3):R2468–R2471.

[Olafsen and Urbach, 2005] Olafsen, J. S. and Urbach, J. S. (2005). Two-dimensional melting far from equilibrium in a granular monolayer. *Physical Review Letters*, 95(9):098002.

[Peierls, 1935] Peierls, R. (1935). Quelques propriétés typiques des corps solides. *Annales de l'institut Henri Poincaré*, 5(3):177–222.

[Peng et al., 2010] Peng, Y., Wang, Z., Alsayed, A. M., Yodh, A. G., and Han, Y. (2010). Melting of colloidal crystal films. *Physical Review Letters*, 104(20):205703.

[Pindak et al., 1981] Pindak, R., Moncton, D. E., Davey, S. C., and Goodby, J. W. (1981). X-ray observation of a stacked hexatic liquid-crystal phase. *Physical Review Letters*, 46(17):1135–1138.

[Prevost et al., 2004] Prevost, A., Melby, P., Egolf, D. A., and Urbach, J. S. (2004). Nonequilibrium two-phase coexistence in a confined granular layer. *Physical Review E*, 70(5):050301.

[Pusey and van Megen, 1986] Pusey, P. N. and van Megen, W. (1986). Phase behaviour of concentrated suspensions of nearly hard colloidal spheres. *Nature*, 320(6060):340–342.

[Qi and Dijkstra, 2015] Qi, W. and Dijkstra, M. (2015). Destabilisation of the hexatic phase in systems of hard disks by quenched disorder due to pinning on a lattice. *Soft Matter*, 11(14):2852–2856.

[Rao et al., 2015] Rao, C. N. R., Gopalakrishnan, K., and Maitra, U. (2015). Comparative study of potential applications of graphene, mos2, and other two-dimensional materials in energy devices, sensors, and related areas. *ACS Applied Materials & Interfaces*, 7(15):7809–7832.

[Reichhardt and Reichhardt, 2021] Reichhardt, C. and Reichhardt, C. J. O. (2021). Active matter commensuration and frustration effects on periodic substrates. *Physical Review E*, 103(2):022602.

[Reis et al., 2006] Reis, P. M., Ingale, R. A., and Shattuck, M. D. (2006). Crystallization of a quasi-two-dimensional granular fluid. *Physical Review Letters*, 96(25):258001.

[Reyes and Urbach, 2008] Reyes, F. V. and Urbach, J. S. (2008). Effect of inelasticity on the phase transitions of a thin vibrated granular layer. *Physical Review E*, 78(5):051301.

[Russo and Wilding, 2017] Russo, J. and Wilding, N. B. (2017). Disappearance of the hexatic phase in a binary mixture of hard disks. *Physical Review Letters*, 119(11):115702.

[Rysti et al., 2021] Rysti, J., Mäkinen, J., Autti, S., Kamppinen, T., Volovik, G., and Eltsov, V. (2021). Suppressing the kibble-zurek mechanism by a symmetry-violating bias. *Physical Review Letters*, 127(11):115702.

[Safran, 2018] Safran, S. A. (2018). *Statistical Thermodynamics of Surfaces, Interfaces, and Membranes*. CRC Press.

[Scott and Kilgour, 1969] Scott, G. D. and Kilgour, D. M. (1969). The density of random close packing of spheres. *Journal of Physics D: Applied Physics*, 2(6):863–866.

[Selinger, 2015] Selinger, J. V. (2015). *Introduction to the Theory of Soft Matter From Ideal Gases to Liquid Crystals*. Springer.

[Seydel et al., 2001] Seydel, T., Madsen, A., Tolan, M., Grübel, G., and Press, W. (2001). Capillary waves in slow motion. *Physical Review B*, 63(7):073409.

[Smith and Downs, 2021] Smith, M. I. and Downs, J. G. (2021). Particletracker: a gui based particle tracking software. *Journal of Open Source Software*, 6(66):3611.

[Smith, 2019] Smith, N. D. (2019). *Boundary Effects in a Quasi-2d Granular Mono-layer*. PhD thesis, University of Nottingham.

[Smith and Smith, 2017] Smith, N. D. and Smith, M. I. (2017). Boundary effects in a quasi-two-dimensional driven granular fluid. *Physical Review E*, 96(6):062910.

[Specht et al., 1984] Specht, E. D., Sutton, M., Birgeneau, R. J., Moncton, D. E., and Horn, P. M. (1984). Phase diagram and phase transitions of krypton on graphite in the one-to-two-layer regime. *Physical Review B*, 30(3):1589–1592.

[Strandburg, 1988] Strandburg, K. J. (1988). Two-dimensional melting. *Reviews of Modern Physics*, 60(1):161–207.

[Sun et al., 2016] Sun, X., Li, Y., Ma, Y., and Zhang, Z. (2016). Direct observation of melting in a two-dimensional driven granular system. *Scientific Reports*, 6(1).

[Thorneywork et al., 2017] Thorneywork, A. L., Abbott, J. L., Aarts, D. G., and Dullens, R. P. (2017). Two-dimensional melting of colloidal hard spheres. *Physical Review Letters*, 118(15):158001.

[van Zon et al., 2004] van Zon, J. S., Kreft, J., Goldman, D. I., Miracle, D., Swift, J. B., and Swinney, H. L. (2004). Crucial role of sidewalls in velocity distributions in quasi-two-dimensional granular gases. *Physical Review E*, 70(4):040301.

[van Zon and MacKintosh, 2004] van Zon, J. S. and MacKintosh, F. C. (2004). Velocity distributions in dissipative granular gases. *Physical Review Letters*, 93(3):038001.

[Virtanen et al., 2020] Virtanen, P., Gommers, R., Oliphant, T. E., Haberland, M., Reddy, T., Cournapeau, D., Burovski, E., Peterson, P., Weckesser, W., Bright, J., van der Walt, S. J., Brett, M., Wilson, J., Millman, K. J., Mayorov, N., Nelson, A. R. J., Jones, E., Kern, R., Larson, E., Carey, C. J., Polat, İ., Feng, Y., Moore, E. W., VanderPlas, J., Laxalde, D., Perktold, J., Cimrman, R., Henriksen, I., Quintero, E. A., Harris, C. R., Archibald, A. M., Ribeiro, A. H., Pedregosa, F., van Mulbregt, P., and SciPy 1.0 Contributors (2020). SciPy 1.0: Fundamental Algorithms for Scientific Computing in Python. *Nature Methods*, 17:261–272.

[Weber et al., 1995] Weber, H., Marx, D., and Binder, K. (1995). Melting transition in two dimensions: A finite-size scaling analysis of bond-orientational order in hard disks. *Physical Review B*, 51(20):14636–14651.

[Wiki47222, 2017] Wiki47222 (2017). Rdf schematic. Online.

[Willard and Chandler, 2010] Willard, A. P. and Chandler, D. (2010). Instantaneous liquid interfaces. *The Journal of Physical Chemistry B*, 114(5):1954–1958.

[Young, 1979] Young, A. P. (1979). Melting and the vector Coulomb gas in two dimensions. *Physical Review B*, 19(4):1855–1866.

[Zollweg and Chester, 1992] Zollweg, J. A. and Chester, G. V. (1992). Melting in two dimensions. *Physical Review B*, 46(17):11186–11189.